DEVELOPING AN EXPERIMENTAL SETUP FOR THUNDER BAY WASTE POLLUTION CONTROL PLANT (WPCP) TO EVALUATE UV LAMP PERFORMANCE

by

MRUNMAYEE NIKAM

B. Eng., Shivaji University, India, 2015

A THESIS SUBMITTED IN PARTIAL FULFILMENT OF
THE REQUIREMENTS FOR THE DEGREE OF
MASTER OF SCIENCE IN ENVIRONMENTAL ENGINEERING

Lakehead University
Thunder Bay

July 2019

Abstract

An automated experimental setup was developed to measure the spectral irradiance of new low pressure (LP) ultraviolet lamp (UV). The experimental analysis was performed by the measurement of the UV intensity along the length of the lamp to evaluate the variation in UV output during preliminary 5% lifespan of the UV lamp. The automation of the experimental setup has executed with the Arduino-LabVIEW interfaced computer program to maintain sequential collaboration among the setup components. The new LP UV lamp had a non-uniform output with the unexpected rise and drop in the UV intensity at certain locations along the length.

The lamp showed predominant ageing signs at the electrode, which was confirmed by the visual observation after the appearance of the darken quartz sleeve near the electrode and further reduction in UV output was verified by the experimental analysis as a result of the obstructed transmittance of the UV radiation through the quartz sleeve. Initially, UV output of the new lamp was uniform; however, as the lamp was aged analysis noticed non-uniform output along the length of the lamp though the lamp was operated for same working conditions throughout the entire experimental phase. The non-uniform temperature profile of the UV lamp was studied with the implementation of the thermal imaging IR camera to confirm variable temperature gradient inside the quartz sleeve and at the surface of the quartz sleeve. The thermal analysis recognized the overheating of the lamp electrode. Further, as amp aged the temperature profile at the lamp electrode raised significantly.

The experimental analysis proved that the lamp ageing was more noticeable at lamp ends than the middle part of the lamp, which was confirmed after evaluation of the UV intensity along the length of the lamp as well as after performing the output stability test at electrode for corresponding lamp operating cycle.

Table of Contents

Abstract ..... **ii**
Table of Contents ..... **iv**
List of Tables ..... **ix**
List of Figures ..... **x**
List of Equations ..... **xiii**
Nomenclature ..... **xiv**
Dedication ..... **xvi**
Acknowledgement ..... **xvii**
Co-Authorship Statement ..... **xviii**
Chapter 1. Introduction **1**
1.1 Thesis Background & overview .; 1
1.1.1 Overview of UV radiation measurement techniques 2
1.1.2 Summary of indirect measurement techniques for UV radiation 2
1.1.3 Summary of direct measurement techniques for UV radiation 6
1.1.4 The originality of the concept & modification of the set-up configuration 8
1.2 Proposition 10
1.2.1 The innovation of the Experimental Set-up 10
1.3 Relevance of this thesis 11
1.3.1 The current scenario at Thunder bay wastewater treatment plant 11
1.3.2 The layout of the UV disinfection system at Thunder Bay WPCP 11
1.3.3 Technical difficulty & steps planned by Thunder Bay WPCP 12
1.3.4 Contribution of this research to resolve the problem at Thunder Bay WPCP 14
1.4 Objectives and goal 16
1.4.1 Specific objectives 16
1.4.2 Thesis goal 16
1.5 Significance of the thesis 18
1.6 Thesis Outline 19
1.7 References 20

Chapter 2. Literature review 28
2.1 History and development of UV disinfection technology 28
2.2 UV light description 29
2.3 Fundamentals of UV light generation based on UV lamp types 30
2.4 Lamp types based on mercury pressure and principle of UV light generation 31
2.4.1 Low pressure lamps and amalgams low pressure high output lamps 31
2.4.2 Medium pressure lamps 32
2.5 Components of mercury vapor pressure UV lamp 35
2.5.1 Lamp envelope 35
2.5.2 Lamp sleeve 35
2.5.3 Mercury fill 35
2.5.4 Electrodes 35
2.5.5 Inert gas fill 36
2.5.6 Lamp ballast 36
2.5.7 Mechanical wipers 36
2.6 Fundamentals of UV lamp operation 37
2.6.1 Lamp Start-up 37
2.6.1.1 General principle 38
2.6.2 Lamp power feed 42
2.6.2.1 Function of the lamp ballast 42
2.6.2.2 Function of the cathode and anode electrode 44
2.6.3 Radiation spectrum 45
2.6.3.1 UV output of the lamp 45
2.6.4 Parameters influencing UV emission output 46
2.6.4.1 Influence of the voltage 46
2.6.4.2 Influence of the surrounding temperature 46
2.7 Uncertainties in UV lamp operation and disinfection 48
2.7.1 UV lamp ageing 49
2.7.1.1 Overview of UV lamp ageing uncertainties 50
2.7.2 UV lamp sleeve fouling 52
2.7.3 Spectral shift 54

2.7.4 Precipitation of deposits and slime formation 55
2.7.5 UV Transmission and reflection 55
2.7.5.1 Effect of photo-chemical solarization 55
2.7.5.2 Effect of suspended solids and particle shading 56
2.7.6 UV lamp intensity & microbial reactivation 57
2.7.6.1 Type of microbial reactivation 57
2.7.6.1.1 Photoreactivation 57
2.7.6.1.2 Dark repair 57
2.7.6.2 Factors influencing microbial reactivation 58
2.7.6.2.1 Effect of improper UV dose 58
2.7.6.2.2 UV lamp intensity and exposure time 58
2.7.6.2.3 Type of the UV lamp and its correlation with microbial reactivation 58
2.7.6.2.4 Effect of the wavelength 59
2.7.6.2.5 Effect of water quality 59
2.8 Direct UV output measurement technique 60
2.8.1 Overview of direct measurement set-up assembly 60
2.8.2 Components of direct measurement set-up for UV radiation 61
2.8.2.1 Mechanical arrangement 61
2.8.2.2 Optical assembly module 62
2.8.2.2.1 Window 62
2.8.2.2.2 Diffuser 63
2.8.2.2.3 Focusing optics 64
2.8.2.2.4 Filter 64
2.8.2.3 Electrical signal processing 65
2.8.2.3.1 Signal processing by a radiometer 67
2.8.2.3.2 Data assembly 67
2.8.3 Calibration of the system component 68
2.8.4 Overview of the previously developed experimental set-up for direct measurements and research gaps 69
2.8.4.1 Direct measurement set-up for determination UV dose 69
2.8.4.2 Direct measurement set-up for monitoring for foulant

accumulation on lamp sleeve 70
2.8.4.3 Direct measurement setup for monitoring light penetration in the wastewater sample 71
2.8.4.4 Direct measurement setup for monitoring the ageing of MP lamps 72
2.8.4.5 Direct measurement of UV lamp performance with an on-line monitoring arrangement 73
2.8.4.6 Direct measurement setup for analyzing ageing of the ALPHO lamps 74
2.8.4.7 Direct measurement setup for quantifying UV transmittance of the quartz sleeve 76
2.9 Research gaps and modification in the setup 78
2.9.1 Research gaps related to the literature availability 78
2.9.2 Research gap related to the set-up 78
2.9.3 Research gap related to the imbalanced temperature profile across the lamp 79
2.9.4 Automation with Arduino microcontroller and LabVIEW interface 79
2.9.5 Thermal imaging camera to identify a non-uniform temperate profile of the UV lamp 80
2.10 Arduino overview 81
2.10.1 Arduino Hardware 81
2.10.2 Arduino software and programming 82
2.10.2.1 Command area 84
2.10.2.2 Coding area 84
2.10.2.3 Message window or Debugger 84
2.10.3 Working principle of Arduino board 85
2.11 Overview of Laboratory Virtual Instrumentation Engineering Workbench 86
2.11.1 Virtual Instruments (VI) programming 86
2.11.2 Previously followed LabVIEW based experimental applications 93
2.12 Overview of Arduino and LabVIEW interface 94
2.12.1 Previously developed Arduino and LabVIEW interfaces 95
2.13 References 96
Chapter 3. Material& methodology 107

3.1 Overview of experiment 107
3.2 Experimental arrangement and working mechanism 109
3.3 Setup components 111
3.3.1 UV lamp 112
3.3.2 Power feed, ballast and electric assembly 113
3.3.3 Aluminum rail profile 115
3.3.4 Stepper motor, lead screw and DC supply to compumotor 116
3.3.5 UV sensor and location encoder 119
3.3.6 Radiometer and measurement 123
3.3.7 Arduino circuit board and configuration with setup modules 126
3.3.8 Thermal imaging camera 130
3.3.9 Digital hygrometer and thermometer 132
3.4 Automated control of setup components 133
3.5 Data collection and logging 135
3.6 Method and procedure sequence 136
3.7 Result interpretation 137
3.8 References 138

Chapter 4. Results & discussions 140
4.1 Overview of the experimental results 140
4.2 Visual observations of UV lamp ageing 142
4.2.1 Darkening of the lamp end 142
4.2.2 Discoloration and sleeve fouling of the lamp sleeve 146
4.2.3 Solarization of the quartz sleeve material 151
4.2.4 Resonant darkening effect 152
4.3 UV lamp output stability test and results 153
4.4 UV lamp irradiance at 254 nm along the length of the lamp 160
4.4.1 UV output of new lamp 161
4.4.2 UV output variation during week 1 and 2 162
4.4.3 UV output variation during week 3 and 4 164
4.4.4 UV output variation during week 5 and 6 and consistent drop at position 12 166

4.4.5 UV output variation during week 7 and 8 169
4.4.6 UV output for variation during week 9 and 10 172
4.4.7 UV lamp output after 450th burn-in hour 175
4.5 Temperature profile of the lamp 177
4.6 References 181

Chapter 5. Conclusion & future recommendation 183
5.1 Conclusion 183
5.1.1 Conclusion related to lamp ageing and UV output 183
5.1.2 Conclusions related to the experimental setup 184
5.2 Recommendation for future work 185
5.2.1 Recommendation for future work 185
5.2.2 Recommendation for setup modification 185

List of Tables

Table 2. 1 Characteristics of mercury pressure UV lamp 34
Table 4. 1 Weekly peak and stable output at the beginning of the week for position 0.00 cm…156
Table 4. 2 Weekly peak and stable output at the end of the week for position 0.00 cm 159

List of Figures

Figure 2.1 Electromagnetic spectrum 29
Figure 2.2 Construction of mercury vapour lamps 33
Figure 2.3 Schematic of mercury lamp components 36
Figure 2.4 Lamp start up and mercury activation 37
Figure 2.5 UV radiation emitted after the lamp start up 38
Figure 2.6 Principle of UV light generation 40
Figure 2.7 Light distribution 41
Figure 2.8 Lamp power feed circuit 43
Figure 2.9 Temperature gradient at lamp electrode and central part 47
Figure 2.10 Schematic of the direct measurement setup 61
Figure 2.11 Configuration of the UV sensor 62
Figure 2.12 Schematic of two radiometers with different spatial response 63
Figure 2.13 Schematic of radiometry measurement 65
Figure 2.14 Components of Arduino circuit board 81
Figure 2.15 Labelled IDE 83
Figure 2.16 Front panel and block diagram 86
Figure 2.17 Controls in LabVIEW programming 87
Figure 2.18 Connector pane and patterns 88
Figure 2.19 Toolbar features in LabVIEW 89
Figure 2.20 Functions in LabVIEW programming 89
Figure 2. 21 LabVIEW expanded functions 91
Figure 2.22 VI properties and features 92
Figure 2.23 LabVIEW error resolve feature 92
Figure 3.1 Schematic diagram of the setup 110
Figure 3.2 Setup arrangement 111
Figure 3.3 Components of the LP UV lamp 112
Figure 3.4 Illumination of the UV lamp after preheating 112
Figure 3.5 Power supply to UV lamp 113
Figure 3.6 Electronic ballast and power feed to UV lamp 114
Figure 3.7 Aluminium profile and assembled setup components 115
Figure 3.8 Steeper motor components and power feed 116
Figure 3.9 Compumotor and Arduino circuit board 118

Figure 3.10 UV sensor configuration with the setup 119
Figure 3.11 Internal components of the UV sensor 120
Figure 3.9 Sensor arrangement and motion mechanism 121
Figure 3.13 Signal input to the radiometer 122
Figure 3.14 Front panel of the radiometer IL 1700 123
Figure 3.15 Back panel of the radiometer IL 1700 124
Figure 3.16 Arduino circuit board modules 127
Figure 3.17 Arduino circuit board and I/O pin assembly 129
Figure 3.18 Thermal imaging IR camera from FLIR Systems Inc 130
Figure 3.19 Sample thermal image and IR scale 131
Figure 3.20 Arrangement of the digital hygrometer and thermometer 132
Figure 3.21 Computer program to control setup components 133
Figure 3.22 Experimental commands 134
Figure 3.23 Sample textual data log format 135
Figure 4.1 Darkening of the lamp sleeve (occurred after 224 burn-in hours) 142
Figure 4.2 Darkening of the lamp end after 328 hours 143
Figure 4.3 Darkening of the lamp edge after 450 burn-in hours 144
Figure 4.4 Lamp electrode prior to begin experimentation 145
Figure 4.5 Lamp sleeve prior to begin experimentation 146
Figure 4.6 Quartz sleeve fouling after 289 burn-in hours 146
Figure 4.7 Quartz sleeve fouling on other end of the lamp after 298 burn-in hours 147
Figure 4.8 Quartz sleeve fouling after 419 burn-in hours 147
Figure 4.9 Quartz sleeve fouling on other side of the lamp after 419 hours 148
Figure 4.10 Temperature profile inside and at a surface of the quartz sleeve 149
Figure 4.11 Temperature profile at central part of the lamp 150
Figure 4.12 Formation of the spots on lamp sleeve 151
Figure 4.13 Preliminary resonant darkening after 419 burn-in hours 152
Figure 4.14 Lamp UV output stability test arrangement at position 0.00 153
Figure 4.15 UV output peak and stability at the beginning of every week 154
Figure 4.16 Lamp end darkening 155
Figure 4.17 UV output stability test during lamp warm up phase after lamp ignition 157
Figure 4.18 Darken area around the lamp electrode during week 9 158
Figure 4.19 UV output of the new lamp at 254 nm 161
Figure 4.20 UV output at 254nm along the length of the lamp during week 1 and 2 162

Figure 4.21 UV output at 254nm along the length of the lamp during week 3 and 4 164
Figure 4.22 UV output at 254nm along the length of the lamp during week 5 and 6 166
Figure 4.23 Thermal image showing cold spot formation position 12 168
Figure 4.24 UV output at 254 nm along the length of the lamp during week 7 and 8 169
Figure 4.25 Scaling of the lamp sleeve during week 7 170
Figure 4.26 Thermal image showing inconstant temperature profile at lamp area 171
Figure 4.26 UV output at 254 nm along the length of the lamp during week 9 and 10 172
Figure 4.27 Scaling spots at position 8 and 12 after 370 burn-in hours 173
Figure 4.28 Uneven discoloration and sleeve fouling after 419 burn-in hours 174
Figure 4.29 UV lamp output after 5 and 450 burn-in hours 175
Figure 4.30 Thermal image of the lamp during 370 to 381 operating hours 177
Figure 4.31 Temperature profile at the lamp electrodes (after 385 operating hours) 178
Figure 4.32 Temperature profile of the lamp after 450 operating hours between 8 to 14 cm.....179
Figure 4.33 Temperature profile of the lamp after 450 operating hours between 18 to 32 cm...180
Figure 5.1 Radial and axial sample points 185

List of Equations

Equation 2. 1 Ionization process 39
Equation 2. 2 Subsequent stage in the ionization process or Penning effect 39
Equation 2. 3 Electric discharges during penning effect 39
Equation 2. 4 Collision between mercury atom and electron 39
Equation 2. 5 Formation of the excited mercury atoms 39
Equation 2. 6 The emission of a photon by an excited mercury atom 40
Equation 2. 7 Ballast efficiency factor 40
Equation 2. 8 Lamp ageing factor 51
Equation 2. 9 Germicidal output 51
Equation 2. 10 Combined ageing and fouling factor 53
Equation 2. 11 Combined ageing and fouling factor formula 53
Equation 2. 12 Sleeve fouling factor 53
Equation 2. 13 Rearrangement 53
Equation 2. 14 Signal measurement 125

Nomenclature

Symbol/Aberration	Description
.OH	Hydroxyl radical
#	Model number
°	Angle in degrees
°C	Temperature in Celsius
0-13	Digital pins
A0 to A5	Analog pins
AOP	Advanced oxidation process
API	Application programming interface
BF	Ballast factor
BFF	Ballast efficiency factor
BMF	Battery monitoring systems
BOD	Biochemical oxygen demand
$CaCO_3$	Calcium carbonate
CAF	Combined ageing and fouling factor
DWI	Drinking Water Inspectorate
E	Irradiance distribution of the source
e^-	Electron
Fe	Iron
$Fe(OH)_3$,	Ferric hydroxide
$FePO_4$	Ferric phosphate
GUI	Graphical user interface
H_2O	Water molecule
i	Signal observed by detector
I	Current
I-v	Current- voltage
I/O	Signal input and output
IDE	Integrated Development Enviromment
IESNA	Illumination Engineering Society of North America
IL	International Light Inc.
ILCS	Intelligent Lighting Control System
In	Indium
IR	Infrared spectrum
kV	Kilo Volts
LabVIEW	Laboratory Virtual Instruments Engineering workbench
LAF	Lamp ageing factor
LP	Low Pressure
LP	Low pressure lamp
LPHP	Low Pressure High Output
mA	Milliampere
Min	minutes
msec	Milliseconds
mW/cm^2	Miliwatt per square centimeter
NIST	National Institute of Standards and Technology

O^3	Ozone
P	Spectral Power
Pa	Pascal
P-v	Power voltage
Pa	Mercury Pressure in pascals
Pb	Lead
PTB	Physikalisch-Technische Bundesanstalt
PV	Photovoltaic
SFF	Sleeve fouling factor
S	Instrument responsivity
SiC	Silicon carbide
Sn	Tin
UI	User interface
USEPA	United States Environmental Protection Agency.
UV	Ultra-violate
UV-A	Ultraviolet range from 315-400 nm
UV-B	Ultraviolet range from 280-315 nm
UV-C	Ultraviolet range from 200-280 nm
UVT	Ultraviolet transmittance from quartz sleeve
$\mu W/cm^2$	UV output in micro watts per square centimeters
V	Volts
VI	Virtual Instruments
W/cm^2	UV output in watts per square centimeter
WPCP	Water Pollution Control Plant

Dedication

This thesis is dedicated to my parents,
Prof. Ravindra Nikam my father, and Dr. Vasudha Nikam my mother,
for their endless source of support and encouragement during the challenges of postgraduate school life.
This work is also dedicated to my best friend Mr. Avinash Mhetre, who have been moral support during my research work, without his support and sacrifices, I would have been in the initial stage of my research.

Acknowledgements

The author acknowledges the Department of Chemical Engineering at Lakehead University Thunder Bay Canada and Thunder Bay WPCP for giving an opportunity to conduct this research. The author solely acknowledges thesis supervisor Dr. Siamak Elyasi, for his encouragement and moral support during all phases of this research.

The author also admits the support received from Patricia Johnson and Nancy Cahill through student accessibility services to provide accommodation for a disability.
The author would like to express gratitude to Environmental Engineering Coordinator Dr. Leila Pakzad for her unending support during the academic phase of a postgraduate degree.
The author profoundly acknowledges the support received from Dr. Baoqiang Liao during the academic phase of the postgraduate degree.
The author genuinely acknowledges the examiner Dr. Carlos Zerpa for his valuable time and consideration.

The author wishes to express her gratitude to her family for their understanding and consideration throughout her studies.

Co-authorship statement

This thesis is presented in five different manuscripts. The manuscript's authors are Mrunmayee Nikam and Dr. Siamak Elyasi. Dr. Siamak Elyasi is my thesis supervisor at Lakehead University.

The research activities were performed was performed at Lakehead University, Thunder Bay and experimental analysis, result findings and preparation of the report was performed by Mrunmayee Nikam, under the guidance of the Dr. Siamak Elyasi.

NOTES

CHAPTER 1
INTRODUCTION

1.1 Thesis Background and overview

Ultraviolet light (UV) has been proven to be effective disinfection technique which has gained importance over past few decades for disinfection of drinking water, secondary effluent and air purification systems (Blatchley et al.,1997; Kowalsski, 2009; Jacangelo et al., 1995; USEPA 2006). The UV disinfection has been proven alternative to chemical methods of disinfection because it is a physical treatment and it is environmentally safe with no toxic side effects and by-products (Jacangelo et al., 1995; Sommer et al., 2004). The implementation of UV disinfection is accomplished by the arrangement of UV reactor systems with a germicidal lamp which radiates monochromatic light at 253 nm at the peak of germicidal effectiveness (IESNA, 2000; Linden et al., 2001; Reed, 2010). The microbial inactivation mechanism implicates by the absorption of this germicidal UV light within DNA or RNA of pathogens which alters nucleic activities of pathogens, resulting in inhibition of formation of new DNA and cell replication (Dai et al., 2012; McLeod et al., 2017; Rutula et al., 2010; Weber, 2005).

The applications of UV disinfection systems have been increasingly implemented, despite the fact that a direct, cost-effective and precise method for determination of change in UV lamp intensity over the time is still under investigation, which is a challenging issue and has limited the practicality of UV disinfection technology (Ducoste et al., 2005; Sommer et al., 2004).
Further measurement of UV output and lamp efficiency varies from one testing facility to the other (Sasges and Robinson, 2005), which is a significant limitation.
An important issue with all germicidal lamps is non-uniform lamp aging, which impacts UV lamp life and UV output over time and this variation can affect UV dose delivery also it can trigger uneven dose distribution of germicidal intensity in the reactor. UV lamp exhibits technical difficulties due to aging and fouling of the lamp, electrode sputtering and darkening at the lamp edges due to amalgam deposits (Heath et al., 2013; Schmalwieser et al., 2014; Sheriff and Gher,2001).

1.1.1 Overview of UV radiation measurement techniques

Over the years numerous efforts were taken to investigate the UV lamp aging phenomenon and its correlation with the lamp performance as well as diverse approaches have been anticipated to evaluate the UV radiation measurement based on the electric energy of the lamp, UV-C output and fluence rate from the UV lamp (Keyser et. al., 2008; Muller et al., 2011). UV lamp performance has been studied by two distinct methods that are, an indirect method by testing the resultant outcome and direct radiometric set-up arrangement (Braunstein et al., 1996; Siegel, 1995).

1.1.2 Summary of indirect measurement techniques for UV radiation

The first measurement method is followed by indirect measurement of the absolute amount of UV light received by an object, dose response of various microorganisms, pathogens and indicators by observing the effect of heat and radiation on the object or on the microorganisms, which are exposed to the UV light during the experiment (Braunstein et al., 1996; Chevrefils et al., 2006; Government of Canada, 2015; Qualls and Johnson, 1983; Sommer et al., 1997). Three types of indirect UV measurement approaches have been established to estimate the UV intensity biological assay/ bio-dosimetry, chemical actinometry and mathematical models (Braunstein et al., 1996).

In practice, UV irradiance has been determined by indirect measurement technique such as bio-dosimetry by the various scientist (Quintern et al.,1992; Ronto et al., 1994); however, their research was mainly focused on measurement of solar UV radiation in the air. Furthermore, laboratory dose-response analysis followed by collimated beam arrangement is renowned and acceptable UV output measurement technique (Darby et al., 1995; Harold W., 2000; Scheible, 2000), though it is a time intense and variable dependent technique when involved with microbial dose-response analysis (Kuo et al., 2003). Bio-dosimetry has been considerable technology to evaluate the efficacy of the UV lamp by engineers and researchers as this method has gained significant recognition in a water and wastewater treatment practices to perform UV radiation measurement to verify bacterial inactivation spectral responsivity and efficacy of UV reactor systems (Cabaj and Sommer, 2000).

In bio-dosimetry measurement technique, a suspension of the test sample is injected upstream of the UV system, and samples are collected at the downstream (Bolton, 1999; Sommer et al., 1999). The ratio of counts of effluent to that of the influent sample is compared with the UV dose-response curve which is obtained by a collimated beam test (Blatchley, 1997; Bolton, 1999). This UV response curve is determined in a collimated beam apparatus to obtain data which is essential to develop the relationship between UV dose and the response curve. After irradiation of UV light the distribution of fluence among the sample, which results scattering of UV radiation inside the reactor, this scattering affects the overall range of UV fluence, which is often referred as, Reduction Equivalent Dose (RED) (Cabaj et al, 1996; Sommer et al, 1997; Sommer et al, 1999). Further, Wright et al. (2007), measured incident UV intensity by using a collimated beam arrangement, with the average reading of two radiometers and sensor assembly. However, the main focus of their study was to examine the dose-response of the suspension organisms. Further, the microorganism action spectrum was estimated, based on the UV dose-response data obtained by the collimated beam testing arranged by medium pressure (MP) UV lamp and optical bypass filter. Additionally, their analysis stated, this method is suitable for the comparison of wavelength response among two microbial samples.

Numerous researchers have attempted to anticipate another indirect UV radiation measurement technique a chemical actinometry (CA), (Jin et al., 2005; Rahn et al., 2006; Wols et al., 2012). Chemical actinometry technique works on the principle of photochemical conversion that is, chemical change occurred in a chemical sample due to an absorption of photon from the light radiation such as destruction or a buildup of the molecules and change occurred in the properties of the chemical sample with the application of a calibrated chemical actinometer or dosimeter (Kuhn et al., 2004). The chemical actinometry performs absolute measurement of the incident radiation by determining the amount of the reactant transformed during the photo-kinetic activity with analytical technics (Maafi, 2010). Further, the obtained amount of reactant transformation is then used to calculate the intensity of the irradiating light in units of Einstein's per unit time and area (Comerford, 1998). Chemical actinometry has been comparatively simple and applied method for radiation measurement. (Kuhn et al., 2004; Leighton et al., 1930).
In past chemical, actinometry was practiced with the implementation of iodide actinometer consisting of iodide-iodate solution. The fluence (UV dose) was calculated based on the amount

of triiodide yielded during the irradiation of the UV light between 200-300nm (Rahn et al., 2006). Furthermore, the study evaluated the fluence rate at each site to predict the mathematical model. However, the results were presented to confirm the implementation of actinometry to measure the spatial distribution of the UV fluence rate in the spherical reactor (Rahn et al., 2003; Rahn et al., 2006).

Uncertainties in the UV light measurement has encouraged researchers to find alternative techniques to estimate UV irradiance (Blatchley et al., 2008; Wols et al., 2012). Some mathematical models have been developed over the time for the hypothetical measurement of UV dose in a UV reactor such as Point Source Summation (PSS) model (Jacob and Dranoff 1970), Extense Source Volumetric Emission (ESVE) (Bolton, 2000; Irazoqui et al., 1973). Moreover, in the last decade Spherical actinometry method was validated by Rahn et al., (2000) and Stefan et al., (2001). More recently, multi-point source summation method was studied by Liu et al., 2004. Based on these mathematical and numerical methods commercialized software packages have been developed by engineering companies and consultancies to validate the fluence rate distribution and performance of the reactor system. However, these software packages are expensive and mainly focused on the improvement of fluence rate measurement and fluence distribution. Moreover, The application of these pre-developed models is limited due to operational parameters of the systems. Despite the fact that these models can evaluate fluence rate these models fail to validate UV lamp life and aging of the lamp and change in the lamp characteristics after the specific period. However, indirect measurement techniques do not give an exact measurement of the UV intensity. Also, it fails to provide real-time analysis of UV intensity variation occurred at different locations of UV lamp across the lamp's axial and radial directions.

Furthermore, indirect UV radiation measurement techniques are comprehensive and extensive techniques, which cannot be applicable to quantify the characterizable changes occurred in the UV lamp over time. Indirect measurement techniques are precise and accurate, but these techniques are focused on the estimation of the UV dose from the UV lamp and its implicit effect on the resultant sample. Also, even if the measurement is performed for the same microbial sample with same surrounding characteristics the dose-response relationships obtained from the analysis, significantly varies from one another study (Kuo et al., 2003; Linden, 2000).

This experimental limitation can lead to imprecise measurement because it does not directly quantify the amount of UV-C radiation emitted from the UV lamp (Cabaj et al., 1996; Nicholson and Galeano 2003), which makes indirect measurement techniques practically inadequate to perform onsite UV lamp analysis.

1.1.3 Summary of direct measurement techniques for UV radiation

The second method is the direct measurement of UV-C radiation, emitted by the germicidal UV lamp containing wavelength between 200-300nm. Direct measurement techniques are performed with the configured set-up comprising of collimated beam arrangement, a radiometric measurement unit, and a UV sensor, specially designed and calibrated to detect the precise wavelength of UV-C radiation. (Chevrefils et al., 2006; Kuhn et al., 2004; Sigel, 1995). The conventional UV sensor is consisting of sensitive photodiode or photodetector which produces a small photocurrent when exposed to the UV radiation and further, this photocurrent is transmuted into a voltage signal, and then intensified with the amplifier (Chen et al., 2015; Lee et al., 2012; Pounce et al., 2017). To collect radiometric data, the UV detector of spectrophotometer accumulates photons and transforms photons into an electric signal according to the quantified relationship, established at the time of radiometer-sensor calibration against the reference source from National Institute of Standards and Technology (NIST) or Physikalisch-Technische Bundesanstalt (PTB) or other standard body to ensure that, UV detectors response is associated with the absolute standard (Sasges and Robinson, 2005; Wright et al., 2007). This transformation due to the photon absorption by a light absorbing material gives enough energy to free an electron from the surface and cause change in the electric properties of the photon absorbing material is known as photoelectric effect due to a phenomenon recognized as a photoconductivity of a semiconductor (Pan and Zhu, 2015).

The measurement method has to be followed by calibrated radiometer and UV detector, which is ideal, more precise and more proficient because it and enables continuous data collection by an automated sensor-radiometric assembly (Chevrefils et al., 2006; Kuhn et al., 2004; Schmalwieser et al., 2014; Siegel, 1995). However, evaluation of lamp aging phenomenon and its correlation with decreased UV intensity typically involves long term analysis, highly expensive and specialized instruments. Many UV disinfection systems do not implement any strategy to monitor UV lamp performance due to a technical constraint. Moreover, lack of onsite direct measurement practices, consumers rely on the assumption centered monitoring such as, visual observation of the ageing signs appeared on the UV lamp i.e., sleeve fouling and darkening, which is highly inaccurate.

Usually, lamp performance statistics are provided by the manufacturer based on precise laboratory testing (Heath et al., 2013). However, these statistics cannot be applicable all the time because the performance of the UV lamp depends on operating conditions such as surrounding temperature, operating hours and voltage supplied to ballast (Adamse and Britz,1992; Lankhorst and Nilemann, 2000). Furthermore, even though lamps have manufactured for the same criteria with the same manufacturing condition and under the same batch, can experience the differentiable aging phenomenon (Heath et al., 2013; Sigel 1995). Additionally, there is no accurate and precise explanation available to confirm this non-uniform behavior of the UV lamp which affects UV lamp intensity over time (Holmes et al., 2002; Lankhorst and Niemann, 2000; Schmalwieser et al., 2014). Also, it has been identified that as UV lamp ages, the UV output also decreases (Braunstein *et al*., 1996; DWI, 2016).

In past Safari et al. (2015) presented the study to examine the correlation between UV emission and illuminance of compact fluorescent lamps (CFL), with the set-up arrangement consisting of optical bench technique, UV meter, and flux meter. The measurement was conducted for different lamp burn-in hours at fixed locations (i.e., 10, 25,50,100 cm). However, their study involved measurement of UV-A and UV-B radiation for the comparison among the different CFL lamps manufactured by different companies. Very recently, Schmalwieser et al. (2014) measured the spatial distribution of the spectral irradiance for 200 to 600nm wavelength with the use of UV reactor modeling software UVXPT to predict the UV dose delivery. Further, the experimental set-up involved radiometer-sensor assembly to measure the UV output along the axial length of the lamp with 15 mm increments. The study was conducted for amalgam low-pressure high output (ALPHP) lamps to examine the impact of lamp aging on the germicidal dose delivery with the computer simulation with the Computational Fluid dynamics (CFD) software known as FLUENT, to model flow of the fluid and trajectories of the microorganism within the UV reactor. The detail about previously followed direct measurement techniques and their outcomes are elaborated in next chapter, Literature Revie

1.1.4 The originality of the concept and modification of the set-up configuration

Previously, it has been identified that UV intensity will decrease with time (DWI, 2006); therefore, lamp manufacturing companies equip UV reactors with the UV sensors at the quartz sleeve of the UV lamp (Bolton 2002; Infilco Degremount Inc. 1996). These on-line sensors perform a measurement to identify the decrease in the UV intensity with respect to the initial UV intensity for the same UV lamp. If the UV system is not outfitted with a real-time UV-sensor-radiometer assembly, the lamp manufacturer provides lamp statistic for lamp intensity vs. lamp burn-in hours.

The purpose of this research was to build an experimental setup and establish a method to test UV lamp followed by direct UV radiation measurement technique which can be a substitute to record the change in the UV intensity as lamp ages. If the statistics provided by the lamp manufacturing companies are not sufficient, on-site lamp testing can be facilitated with the use of established set-up. In this research, an instrument was developed to evaluate UV lamp performance over time. Furthermore, an automated experimental setup was established with the use of the Arduino Uno microcontroller and LabVIEW (Laboratory Virtual Instrumentation Engineering Workbench) programming language to perform interface between the setup components.

In recent years LabVIEW base data acquisition systems has been used to study and develop an advanced measurement and control techniques in the field of light measurement, especially for the applications involving the ultraviolet spectrum (Abbasi et al., 2016; Kita et al., 2015; Samah et al., 2017; Walsh, 2001). Furthermore, the use of Arduino Uno microcontroller to regulate the functioning of the devices and module has been prospered. There have been numerous designs, and device control mechanisms have been implemented to study UV-C radiation and its effect, to control germicidal lamps remotely with the mobile app (application), to develop a portable smartphone spectrophotometer (Das et al., 2016; Denzina and Punkaja et al., 2018; Gomes and Ventura, 2018).

Nevertheless, in referred literature related to the UV intensity monitoring for burn-in lamp hours with optical bench arrangement using radiometer and sensor configuration, there is no declaration for the set-up that has implemented Arduino UNO microcontroller to operate the linear movement of the photovoltaic detector fixed on the 3-D printed adapter casing to perform the linear motion in the axial direction of the UV lamp. Further, the linear movement of the photodetector attached 3-D printed adapter is encoded to perform the linear measurement in micrometer (μm) to minimize the error and improve the precision of the measurement. The set-up components were interfaced together with LabVIEW algorithm for the signal processing and the hardware control followed by the PC assembly (Personal Computer). The data obtained after each measurement contained information about the date, time, exact location (μm) of the sensor across the length of the lamp and UV intensity (a. u.) for that location.

1.2 Proposition

This thesis will demonstrate an instrument and its functionality, to study the performance of the UV lamp, UV lamp aging and variations in lamp performance over time.
The research was mainly focused on the developing a reliable automated setup, which can be used to verify the lamp statistics provided by the manufacturer, i.e., UV lamp life, lamp performance, the effect on lamp sleeve and lamp aging pattern caused by uneven heating of the electrode.

1.2.1 The innovation of the experimental set-up

The set-up has designed in such a way that, the measurements will be taken by the provision of the automatic operational controller (Arduino UNO Microcontroller), which will record lamp intensity detected by photovoltaic detection sensor for the selected position across the length of the lamp in a linear motion across the length of the lamp. The measurements logged by the photovoltaic sensor will be computed into the supervisory computer program by LabVIEW programming language which was designed explicitly for this experimental analysis (as previously mentioned in section 1.1.4). The developed set-up will enable Thunder Bay Waste Pollution Control Plant (WPCP) to test, analyze, and compare the results, obtained by on-site lamp testing at Thunder Bay WPCP with the statistical results provided by the lamp manufacturing company for the corresponding lamp. Also, the developed set-up will enable Thunder Bay WPCP to perform UV lamp testing independently to evaluate and analyze the UV lamp performance for the comparison among the different UV lamps, which are produced by diverse manufacturing companies.

1.3 Relevance of this thesis

The Thunder bay WPCP wishes to reduce the operating cost of their UV lamp replacement cycle by finding appropriate low-cost UV lamp which will last longer and perform adequately during the expected lifetime of 10000-12000 hours, which is an approximate lifespan of the UV lamp (First et al., 2013). Also, the intensity of the lamp life is affected by surrounding temperature and burn-in time, and after first 100 burn-in hours, the UV lamp intensity will start to drop with respect to the time (Darby et al., 1993; Thampi 1990). However, finding an appropriate UV lamp involves testing and analyzing the lamp performance as well as a scientific provision to perform a comprehensive study to compare lamp characteristics with other distinctive lamp manufacturing companies. Hence, they are seeking technical support, to find reasonable solutions to their questions. Moreover, this research will help them to resolve and find answers to their questions.

1.3.1 The current scenario at Thunder bay waste pollution control plant (WPCP)

The Thunder Bay Water Pollution Control Plant (WPCP) provides primary and secondary treatment for phosphorus and ammonia removal, which is followed by seasonal UV disinfection, and at the end of disinfection, water is discharged to the Lake Superior (WPCP City of Thunder Bay, 2017). Earlier Thunder Bay WPCP followed chlorination, however recently they have replaced chlorination with UV disinfection by eliminating annual chlorine use of 20000 kg (Net News-Ledger, Thunder Bay, 2010).

1.3.2 The layout of the UV disinfection system at Thunder Bay WPCP

The currently installed UV disinfection systems at Thunder Bay WPCP (Trojan Model UV 3000 plus) has designed to disinfect a flow up to 169 ML/day. The system is consisting of two (2) channels (11.50m long and 2.1365 m wide), each channel has two (2) banks of twenty four (24) modules of eight (8) low pressure high intensity UV lamps (total lamps are 768), designed to produce UVC radiation to achieve UV dose of 26 mJ/cm^2, which is equipped with soft brushing with chemicals to clean quartz sleeve after a period of time of operation . In the end, final effluent

is discharged to the sewer to the 2700 mm final effluent outfall (Government of Ontario, Ministry of the Environment, 2008).

1.3.3 Technical difficulty and steps planned by Thunder Bay WPCP

At the present moment, Thunder Bay WPCP is experiencing a problem related to the lamp replacing cycle due to an uncertain lamp aging phenomenon also an unreliable lamp life expectancy and economic statistic of currently installed lamps. The disinfection unit of Thunder Bay WPCP consisting of LPHO UV lamps with an expected life span of 12000 hours and 98% stable germicidal output throughout their anticipated usage. However, these lamps are experiencing non-uniform aging and inconstant output as well as less life expectancy than the predicted life even though installed lamps have the same manufacturing specification and operational conditions. This is a genuinely critical issue experienced by all lamp consumers for UV lamps because non-uniform aging affects the overall quality of the germicidal disinfection. As lamp undergoes continuous use, the lamp intensity reduces over time (Braunstein *et al*., 1996; DWI, 2007). The drop in UV lamp intensity is interdepended to the change occurred in the internal components of a UV lamp such as a change in the mercury pressure, decaying of the electrode, and the deposition of the tungsten on interior quartz and lamp's overall output degrades (Siegel S. B. 1995). Moreover, fouling of the quartz sleeve is often observed, when UV lamps are used to disinfect the wastewater (Blatchley et al., 1996; Peng et al., 2005; Wait and Blatchley III, 2010). This alteration in the lamp characteristic can be problematic because as lamp performance changes the efficiency of the germicidal output of a lamp might change as well (Sheriff and Gehr, 2001).

To overcome this difficulty Thunder Bay WPCP has decided to find an alternative UV lamp as a replacement for currently installed UV lamps. However, replacement of installed 768 lamps should be taken with care because of technical and economic challenges. The primary concern of Thunder Bay WPCP is that, if they replace currently installed lamps with the alternative lamps, will the alternative lamps have similar or more performance with profound life expectancy and whether it will be economically beneficial or not? Henceforth, Thunder Bay WPCP is pursuing the assurance of the functionality of the alternative lamps. At present situation, Thunder Bay WPCP is dependent on the lamp statistics provided by the lamp manufacturing companies. Usually, these lamp

statistics are precise but, based on the standard lamp testing procedure, operational or validation conditions (i.e., UV fluence rate, UV lamp status) and parameters (i.e., lamp aging and sleeve fouling) for which lamps are being validated. These circumstances might not be similar to the operational conditions followed by the lamp consumer. Therefore, the lamp characteristics obtained by the manufacturer during the standard lab testing can be dissimilar than the lamp characteristics noticed by the consumer after the lamp installment. The dissimilar characteristics include variable UV lamp intensity, time taken by the lamp to stabilize the output after each operating cycle, subsequent power interruptions, hours spent in operation, ambient temperature and humidity and outer lamp sleeve fouling due to a fluctuating characteristic of water and wastewater, etc. (DWI, 2016; He et al., 2017; Qiang et al., 2013; Wait et al., 2008; Wait and Blatchley III, 2010).

Likewise, every UV lamp manufacturing company has distinctive features to their corresponding lamp, if low pressure (LP) and medium pressure (MP) UV lamps are compared, the LP lamps produce narrow band UV-C (200-300nm) radiation only and can be used across the whole range of water and air disinfection (Heering et al., 2004; Kowlski, 2009), however, MP lamps produce polychromatic spectrum, i.e. UV-C/UV-B radiations. Furthermore, lamps are field with mercury and argon (Ar) a starting gas LP and MP lamps, works at 1 mbar (1 Pa) and 1 bar (100kPa) respectively. Moreover, recently Mercury free lamps have developed which are also known as Excimer Technology, containing Xenon (Xe_2) molecule, which forms dielectric barrier discharge after the provision of the modulated electric field to the quartz lamp body. These lamps are mercury free, instant on lamps with no warm-up time; however low in UV-C efficiency compared to amalgam LP lamps also expensive in the cost (Schalk et al., 2005; Voronov et al., 2004).

The life expectancy of these lamps is different; LP lamps can last up to 10000 hours and MP lamps last up to 6000 hours; however, their UV output can be affected by ambient temperature and humidity (Schalk et al.,2004). Further, The Low-Pressure High Output (LPHO) amalgam lamps, which are also known as Germicidal High Output (GHO) Lamps with a lifespan up to 12000 hours. Further Voronov et al. (2003) developed long life technology which stabilizes optical properties of lamp tube extending their life up to 16000 hours. In contrast, MP lamps have low electric efficiency but require much higher operating temperature than the LP and LPHO amalgam lamps

(Bolton and Cotton, 2008). Therefore, lamp characteristics intensely depend upon the lamp's type, inert gas pressure, operating temperature, and electric supply. Consequently, due to these distinctive features among the variety of UV lamps, it is challenging to choose an appropriate lamp without an accurate understanding of the lamp behavior and its characteristics and verify their competency over one another.

1.3.4 Contribution of this research to resolve the problem at Thunder Bay WPCP

To overcome this problem, we can test the UV lamp and compare the performance characteristics obtained by on-site lamp testing with the lamp statistics provided by the manufacturer. To obtain these comparative statistics, we need to perform long term analysis, which involves study of the UV intensity variation occurred after each operating cycle of the UV lamp, time difference to reach a stable output after every turn on cycle, also we need to observe the variation occurred in the UV intensity after particular burn-in time such as UV intensity after 50hr, 100hr,150hr and, 200hr. Further, we can graphically elaborate the results by plotting UV intensity vs. time to observe how UV intensity has dropped for corresponding lamp operating hours. Furthermore, the results can be generated based on the UV lamp output change in percentage for the lamp burn-in hours based on the onsite lamp testing. The results obtained by the onsite lamp testing can be compared with the statistics for different lamp manufacturing companies to find appropriate lamp after the verification of the test outcomes.

However, to perform this comparative study, we need a highly specialized and expensive lamp testing instrument similar to the instrument used by the lamp manufacturing company to understand and study lamp characteristics. Nevertheless, Thunder Bay WPCP does not have that instrument, which can be used to test the UV lamps for comparative analysis based on the UV lamp performance throughout the life span of the lamp. Therefore, this research has demonstrated the innovative idea for the set-up development and comparatively advanced approach to operate and control the experimental set-up by using Arduino UNO microcontroller, interfaced with the LabVIEW algorithm.

The data obtained during the experimental analysis can be plotted for UV lamp intensity at a specific location across the axial length of the lamp with respect to the burn-in lamp hours. Furthermore, this research has performed thermal analysis of the lamp to study the non-uniform temperature profile of the lamp with Thermal imaging Infrared (IR)camera. The research specific objectives and the final goal of the thesis is described in the next section (1.4).

1.4 Objectives and goal

The primary objective of this research was to develop a set-up which can be functioned with the provision automatic recording of the measurement taken by the photovoltaic sensor and further computed with a software platform.

1.4.1 Specific objectives

a) Build an instrument to test the UV lamps specifications claimed by the manufacturing company
b) Develop a set-up that can be functioned and controlled automatically
c) Develop a supervisory computer program to record and analyze data
d) Develop a sequential method for the user to be followed to justify the manufactures
e) claim with data obtained with the developed experimental setup
f) Develop an operating manual and procedure
g) Interpret the data and provide a guideline for decision making
h) Perform in-house tests to be sure that everything is working correctly and to be ensured that WCPC can use the setup and obtain the information that they are seeking for.

1.4.2 Thesis goal

The goal of this thesis is to provide, a fully developed and optimized experimental set-up to the Thunder Bay WPCP, which will enable them to test and evaluate the UV lamp characteristics, correlation between UV lamp performance and burn-in time, accurate life expectancy of the UV lamp for the operational conditions that, Thunder Bay WPCP wishes to monitor, and at the end Thunder Bay WPCP can justify these statistics with the statistics provided by the corresponding lamp manufacturer. By using the developed experimental setup; Thunder Bay WPCP can perform realistic analysis, and indeed, they can trust the performance results that are obtained for the replacement lamp to verify the suitability of the replacement lamp.

This thesis involves an experimental analysis to understand UV intensity variation with respect to the lamp burn-in hours, during the initial 5% life span of the UV lamp. This study was intended to observe the change that occurred in a UV lamp for each 45 burn-in hours span. Further, this research observed temperature variation at various location across the axial direction of the lamp with the help of Thermal imagining Infrared (IR) camera. The thermal analysis with the IR camera validated temperature variations across the length of the lamp; also it enabled observation of cold and hot spots/ temperature zones formed on the quartz sleeve of the UV lamp.

1.5 Significance of the thesis

This thesis was focused on developing and building an instrumental set-up which will have the following implications:

1) The set-up can be operated remotely and with automatic recording of the experimental data which, saves time and the labor cost.

2) The set-up performs safe implementation due to remote controlling operation feature; hence zero risk of human exposure to UV radiation as the set-up can be turned on and turned off by distant command before entering or leaving the lamp testing area.

3) The set-up can be functioned in consecutive cycles by the setting the timer to turn on and turn off data collection because of its automatic operation feature. This provision simplifies the daily routine of experimental practice as the set-up can be turned on and turned off and by programmed operating schedule.

4) The set-up will be helpful to evaluate the lamp performance statistics claimed by the manufacturer. (i.e., lamp life, aging of lamp sleeve and change in the UV intensity over time). By comparing the experimental results obtained from this set-up with the statistical data provided by the manufacturer of the corresponding lamp and based on the analysis the best suitable lamp can be selected as per the requirement.

5) This set-up contributes to saving on economic attributes because the purpose of this set-up is to test numerous UV lamps and compare the results with manufacturer's statistics for the corresponding lamp. Hence it strengthens the decision-making while performing a mass selection of UV lamp from a wide range of competitor companies and it limits the chances of selecting inappropriate lamp replacement.

1.6 Thesis outline

This thesis consists of five chapters:

Chapter 1 provides a summarizing introduction about UV disinfection, thesis proposition, the relevance of the thesis, objective and final goal of the research and significance of the research.

Chapter 2 discusses a comprehensive review of the topic-specific theory, previously performed scientific practices, techniques followed, experimental findings, and research outcomes published by scientific expertise and research gaps to improve the configuration of direct measurement setup.

Chapter 3 introduces the setup functioning and the configuration of the setup components, working mechanism of the setup and the procedure followed.

Chapter 4 focuses on study outcomes after the experimental analysis and the discussion of results.

Chapter 5 concludes the study and offers a recommendation for future work.

1.7 References

Abbasi, H., Nazeri, M., & Mireei, S. A. (2016). Design and development of a LabVIEW-based LED-induced fluorescence spectroscopy system with applications in non-destructive quality assessment of agricultural products. *Journal of Physics: Conference Series*, *672*, 012010. doi:10.1088/1742-6596/672/1/012010

Adamse, P., & Britz, S. J. (1992). Spectral quality of two fluorescent UV sources during long-term use. *Photochemistry and Photobiology*, *56*(5), 641-644. doi:10.1111/j.1751-1097. 1992.tb02215.x

Blatchley, E. R., Bastian, K. C., Duggirala, R. K., Alleman, J. E., Moore, M., & Schuerch, P. (1996). Ultraviolet irradiation and chlorination/dechlorination for municipal wastewater disinfection: Assessment of performance limitations. *Water Environment Research*, *68*(2), 194-204. doi:10.2175/106143096x127389

Blatchley, E. R., Hunt, B. A., Duggirala, R., Thompson, J. E., Zhao, J., Halaby, T., Alleman, J. E. (1997). Effects of disinfectants on wastewater effluent toxicity. *Water Research*, *31*(7), 1581-1588. doi:10.1016/s0043-1354(96)00396-x

Blatchley, E., Shen, C., Scheible, O., Robinson, J., Ragheb, K., Bergstrom, D., & Rokjer, D. (2008). Validation of large-scale, monochromatic UV disinfection systems for drinking water using dyed microspheres. *Water Research*, *42*(3), 677-688. doi: 10.1016/j.waters.2007.08.019

Bolton, J. (2000). Calculation of ultraviolet fluence rate distributions in an annular reactor: Significance of refraction and reflection. *Water Research*, *34*(13), 3315-3324. doi:10.1016/s0043-1354(00)00087-7

Bolton, J.R. 2002. New Developments in UV Photolysis and Advanced Oxidation, Proc. First Asia Regional Conference of Ultraviolet Technologies for Water, Wastewater & Environmental Applications, CDROM, International Ultraviolet Association, PO Box 1110, Ayr, ON, Canada N0B 1E0.

Braunstein, J. L., Loge, F. J., Tchobanoglous, G., & Darby, J. L. (1996). Ultraviolet disinfection of filtered activated sludge effluent for reuse applications. *Water Environment Research*, *68*(2), 152-161. doi:10.2175/106143096x127334

C. Lee, F. Matsuno, Y. Hashimoto, H. Okada, K. Sawada, and A. Wakahara, "Intelligent ultraviolet sensor composed of GaN-based photodiode and N-channel metal oxide semiconductor Si-charge transfer type signal processor," Japanese Journal of Applied Physics, vol. 51, no. 4, Article ID 044101, 2012.

Cabaj, A., & Sommer, R. (2000). Measurement of Ultraviolet Radiation with Biological Dosimeters. *Radiation Protection Dosimetry*, *91*(1), 139-142. doi:10.1093/oxfordjournals.rpd.a033183

Chevrefils, Gabriel & Caron, É & Wright, Harold & Sakamoto, G & Payment, P & Barbeau, Benoit & Cairns, B. (2006). UV dose required to achieve incremental Log inactivation of bacteria, protozoa and viruses. IUVA News. 8. 38-45.

Chen, H., Liu, K., Hu, L., Al- Ghamadi, A. A., & Fang, X. (2015). New concept ultraviolet photodetectors. *Materials Today Volume 18, Issue 9, November 2015, Pages 493-502*, *18*(9), 493-502. Retrieved from https://doi.org/10.1016/j.mattod.2015.06.001

Comerford, J. (1998). *UV Instruments at work - Investigation of photochemical reactions using UV-Vis spectroscopy* (UV-76). Retrieved from Varian Australia Pvt. Ltd. website: https://www.ncnr.nist.gov/userlab/pdf/E136uvpaper.pdf

Das, A. J., Wahi, A., Kothari, I., & Raskar, R. (2016). Ultra-portable, wireless smartphone spectrometer for rapid, non-destructive testing of fruit ripeness. *Scientific Reports*, *6*(1). doi:10.1038/srep32504

Dai, T., Vrahas, M. S., Murray, C. K., & Hamblin, M. R. (2012). Ultraviolet C irradiation: an alternative antimicrobial approach to localized infections? *Expert Review of Anti-infective Therapy*, *10*(2), 185-195. doi:10.1586/eri.11.166

Darby, Jeannie L., Snider, Kile E., Tchobanoglous, George. (1993). "Ultraviolet disinfection for wastewater reclamation and reuse subject to restrictive standards." *Water Environment Research*, 65, 169-180. Environment Canada. 1990a. Biological test method: reference method for determining acute lethality of effluents to rainbow trout. Environmental Protection, Conservation and Protection, Environment Canada. Ottawa, Ontario, Reference Method EPS 1/RM/13.

Darby, J., Heath, M., Jacangelo, J., Loge, F., Swaim, P., and Tchbano- glous, G. (1995). ''Comparison of UV irradiation to chlorination: Guidance for achieving optimal UV performance.'' *Project 91- WWD-1*, Water Environment Research Foundation, Alexandria, Va.

Denzina, N., & Pankaja, K. (2018). Ultraviolet Radiation Measurement via Smart Devices. *International Journal of Engineering Development and Research*, *6*(2).

Ducoste, J., Linden, K., Rokjer, D., & Liu, D. (2005). Assessment of Reduction Equivalent Fluence Bias Using Computational Fluid Dynamics. *Environmental Engineering Science*, *22*(5), 615-628. doi:10.1089/ees.2005.22.615

Drinking Water Inspectorate, DWI guidance on the use of ultraviolet (UV) irradiation for the disinfection of public water supplies. (2016). Retrieved from Drinking Water Inspectorate website: http://www.dwi.gov.uk/stakeholders/guidance-and-codes-of-practice/uv-irradiation.pdf

Mariano Gomes, L. M., & Ventura, L. (2018). Development of a low cost UV index datalogger and comparison between UV index sensors. *Ophthalmic Technologies XXVIII*. doi:10.1117/12.2289153

Government of Canada, Conservation and Preservations, Canadian Conservation Institute (CCI). (2015). *Measurement of Ultraviolet Radiation – Canadian Conservation Institute (CCI) Notes 2/2* (ISSN 1928-1455). Retrieved from Government of Canada website: https://www.canada.ca/en/conservation-institute/services/conservation-preservation-publications/canadian-conservation-institute-notes/measurement-ultraviolet-radiation.html

Heath, M., Wright, H., & Schmalwieser, A. W. (2013). UV lamp aging is predicted by direct measurement of UV transmittance. *International Ozone Association, International Ultraviolet Association Proceedings of the World Congress and Exposition, September 22-26, 2013, Las Vegas, Nevada*.

Hijnen, W.A.M., Beerendonk, E.F. and Medema, G.J. 2006. Inactivation credit of UV radiation for viruses, bacteria and protozoan (oo)cysts in water; a review, Wat. Res., 40(1): 3-22.

IESNA. 2000. Lighting Handbook: Reference & Application IESNA HB-9-2000. New York: Illumination Engineering Society of North America.

Jacangelo, J., Darby, J. L., Loge, F., Tchobanoglous, G., Heath, M., and Swaim, P. 1995. Comparison of UV irradiation to chlorination: Guidance for achieving optimal UV performance. Final Report Water Environment Research Foundation, Project 91-WWD-1.

Jin, S., Linden, K.G., Ducoste, J., Liu, D., 2005. Impact of lamp shadowing and reflection on the fluence rate distribution in a multiple low-pressure UV lamp array. *Water Research*, 39 (12), 2711-2721

Keyser, M., Műller, I. A., Cilliers, F. P., Nel, W., & Gouws, P. A. (2008). Ultraviolet radiation as a non-thermal treatment for the inactivation of microorganisms in fruit juice. *Innovative Food Science & Emerging Technologies*, *9*(3), 348-354. doi:10.1016/j.ifset.2007.09.002

Kita, N. T., Sobol, P. E., Kern, J. R., Lord, N. E., & Valley, J. W. (2015). UV-light microscope: improvements in optical imaging for a secondary ion mass spectrometer. *Journal of Analytical Atomic Spectrometry*, *30*(5), 1207-1213. doi:10.1039/c4ja00349g

Kowalski, W. (2010). *Ultraviolet Germicidal Irradiation Handbook: UVGI for Air and Surface Disinfection*. doi:10.1007/978-3-642-01999-9

Kuhn, H. J., Braslavsky, S. E., & Schmidt, R. (2004). Chemical actinometry (IUPAC Technical Report). *Pure and Applied Chemistry*, *76*(12), 2105-2146. doi:10.1351/pac200476122105

Kuo, J., Chen, C., & Nellor, M. (2003). Standardized Collimated Beam Testing Protocol for Water/Wastewater Ultraviolet Disinfection. *Journal of Environmental Engineering*, *129*(8), 774-779. doi:10.1061/(asce)0733-9372(2003)129:8(774)

Lankhorst, M. H., & Niemann, U. (2000). ChemInform Abstract: Amalgams for Fluorescent Lamps. Part 1. Thermodynamic Design Rules and Limitations. *ChemInform*, *31*(48), no-no. doi:10.1002/chin.200048008

Lee, C., Matsuno, F., Hashimoto, Y., Okada, H., Sawada, K., & Wakahara, A. (2012). Intelligent Ultraviolet Sensor Composed of GaN-Based Photodiode and N-Channel Metal Oxide Semiconductor Si-Charge Transfer Type Signal Processor. *Japanese Journal of Applied Physics*, *51*(4R), Article ID 044101. doi:10.7567/jjap.51.044101

Leighton, W. G., & Forbes, G. S. (1930). Precision Actinometry with Uranyl Oxalate. *Journal of the American Chemical Society*, *52*(8), 3139-3152. doi:10.1021/ja01371a015

Li, M.K., Qiang, Z.M., Li, T.G., Bolton, J.R., Liu, C.L., 2011. In situ measurement of UV fluence rate distribution by use of a micro fluorescent silica detector. *Environmental Science and Technology,* 45 (7), 3034e3039

Linden, K. G., Shin, G. A., and Sobsey, M. D. Relative efficacy of UV wavelengths for the inactivation of Cryptosporidium paryum. *Water Science Technology*, 2001; 43(12),171-174

Maafi, M. (2010). The potential of AB(1Φ) systems for direct actinometry. Diarylethenes as successful actinometers for the visible range. *Physical Chemistry Chemical Physics*, *12*(40). doi:10.1039/c0cp00469c

McLeod, A., Hovde Liland, K., Haugen, J., Sørheim, O., Myhrer, K. S., & Holck, A. L. (2017). Chicken fillets subjected to UV-C and pulsed UV light: Reduction of pathogenic and spoilage bacteria, and changes in sensory quality. *Journal of Food Safety*, *38*(1), e12421. doi:10.1111/jfs.12421

Müller, A., Stahl, M. R., Graef, V., Franz, C. M., & Huch, M. (2011). UV-C treatment of juices to inactivate microorganisms using Dean vortex technology. *Journal of Food Engineering*, *107*(2), 268-275. doi:10.1016/j.jfoodeng.2011.05.026

Net News Ledger, Thunder Bay. (2010, October 28). Waste Water Treatment Generates Award for Thunder Bay. Retrieved from http://www.netnewsledger.com/2010/10/28/waste-water-treatment-generates-award-for-thunder-bay/

Pan, A., & Zhu, X. (2015). Optoelectronic properties of semiconductor nanowires. In J. Arbiol & Q. Xiong (Eds.), *Semiconductor Nanowires Materials, Synthesis, Characterization and*

Applications [Woodhead Publishing Series in Electronic and Optical Materials] (pp. 327-363). Retrieved from doi.org/10.1016/B978-1-78242-253-2.00012-8

Peng, J., Qiu, Y., & Gehr, R. (2005). Characterization of Permanent Fouling on the Surfaces of UV Lamps Used for Wastewater Disinfection. *Water Environment Research*, *77*(4), 309-322. doi:10.2175/106143005x51897

Ponce, E. (2017). Ultraviolet radiation detector to obtain the energy and rate of particles at different heights. *Proceedings of 35th International Cosmic Ray Conference — PoS(ICRC2017)*. doi:10.22323/1.301.0236

Qiang, Z., Li, M., & Bolton, J. R. (2013). Development of a tri-parameter online monitoring system for UV disinfection reactors. *Chemical Engineering Journal*, *222*, 101-107. doi:10.1016/j.cej.2013.02.046

Quintern, L. E., Horneck, G., Eschweiler, U., & Bücker, H. (1992). A biofilm used as ultraviolet-dosimeter. *Photochemistry and Photobiology*, *55*(3), 389-395. doi:10.1111/j.1751-1097.1992.tb04252.x

Rahn, R. O., Stefan, M. I., Bolton, J. R., Goren, E., Shaw, P., & Lykke, K. R. (2007). Quantum Yield of the Iodide-Iodate Chemical Actinometer: Dependence on Wavelength and Concentration. *Photochemistry and Photobiology*, *78*(2), 146-152. doi:10.1562/0031-8655(2003)0780146qyotic2.0.co2

Reed, N. G. (2010). The history of ultraviolet germicidal irradiation for air disinfection. *Public Health Reports*, *125*(1), 15-27. doi:10.1177/003335491012500105

Rontó, G., Gaspar, S., & Gugolya, Z. (1994). Ultraviolet dosimetry in outdoor measurements based on bacteriophage T7 as a biosensor. *Photochemistry and Photobiology*, *59*(2), 209-214. doi:10.1111/j.1751-1097.1994.tb05024.x

Rutala, W. A., Gergen, M. F., & Weber, D. J. (2010). Room Decontamination with UV Radiation. *Infection Control & Hospital Epidemiology*, *31*(10), 1025-1029. doi:10.1086/656244

Safari, S., Dehkordy, S. E., Kazemi, M., Dehghan, H., & Mahaki3, B. (2015). Ultraviolet Radiation Emissions and Illuminance in Different Brands of Compact Fluorescent Lamps. *International Journal of Photoenergy, Hindawi Publishing Corporation*, *2015 Article ID 504574*. Retrieved from http://dx.doi.org/10.1155/2015/504674

Samah, A. H., Rahman, M. F., Omar, A. F., Ahmad, K. A., & Yahaya, S. Z. (2017). Sensing mechanism of water turbidity using LED for in situ monitoring system. *2017 IEEE 7th International Conference on Underwater System Technology: Theory and Applications (USYS)*. doi:10.1109/usys.2017.8309443

Sasges, M., & Robinson, J. (2005). Accurate Measurement of UV Lamp Output. Retrieved from Trojan Technologies Inc. website: http:/https://iuvanews.com/stories/pdf/archives/070303SasgesAndRobinsonArticle_2005.pdf

Scheible, O. K. (2000). ‘‘Generic verification protocol for high-rate, wet- weather flow disinfection applications Draft 4.1, Report., prepared for NSF International and U.S. Environmental Protection Agency by HydroQual, Inc., Mahwah, N.J.

Schmalwieser, A. W., Wright, H., Cabaj, A., Heath, M., Mackay, E., & Schauberger, G. (2014). Aging of low-pressure amalgam lamps and UV dose delivery. *Journal of Environmental Engineering and Science*, *9*(2), 113-124. doi:10.1680/jees.13.00009.

Sheriff, M., & Gehr, M. (2001). Laboratory investigation of inorganic fouling of low pressure UV disinfection lamps. *Water Quality Research Journal*, *36*(1), 71-92. doi:10.2166/wqrj.2001.00

Sommer, R., Cabaj, A., Haider, T., & Hirschmann, G. (2004). UV Drinking Water Disinfection-Requirements, Testing and Surveillance: Exemplified by the Austrian National Standards M 5873-1 and M 5873-2. *International Ultraviolet Association (IUVA News)*, *6*(4), 27-35.

Sommer, R., Cabaj, A., Pribil, W., & Haider, T. (1997). Influence of lamp intensity and water transmittance on the UV disinfection of water. *Water Science and Technology*, *35*(11-12), 113-118. doi:10.1016/s0273-1223(97)00244-8

Stefan, M. I. (2005). UV-Lamps for Disinfection and Advanced Oxidation - Lamp Types, Technologies and Applications. In *UV Congress in Whistler, BC, Canada in May 2005* (pp. 32-37) Retrieved from https://iuvanews.com/stories/pdf/archives/080103Schalk_Article_2006.pdf

Thampi, Mohan V. (1990). “Basic Guidelines for Specifying the Design of Ultraviolet Disinfection Systems.” *Pollution Engineering*, XXII, 65-69.

The Corporation of the City of Thunder Bay. (2008, May 13). *Amended Certificate of Approval Municipal and Private Sewage Works* (1224-7DYK7H). Retrieved from Government of Ontario, Ministry of the Environment website: https://www.accessenvironment.ene.gov.on.ca/instruments/9438-7AUL3A-14.pdf

United States Environmental Protection Agency. Ultraviolet Disinfection Guidance Manual for the Final Long Term 2 Enhanced Surface Water Treatment Rule. 2006.

UV dose required to achieve incremental log inactivation of bacteria, protozoa and viruses, G. Chevrefils, E. Caron, H. Wright, G. Sakamoto, P. Payment, B. Barbeau and B. Cairns, 2006. IUVA News, 8(1), 38–45.

Voronov, A. M., Reber, S., Schilling, F. J., & Arnold, E. (n.d.). Mercury-free UV-Light Sources: Technology and Perspectives of Excimer Lamps, Proceedings of the XV. In *International Conference on Gas Discharges and their Applications, Toulouse, France* (pp. 32-37).

Wait, I. W. (2008). Multiple-Barrier Disinfection by Chlorination and UV Irradiation for Desalinated Drinking Waters: Chlorine Photolysis and Accelerated Lamp-Sleeve Fouling Effects. *Water Environment Research*, *80*(11), 2183-2188. doi:10.2175/106143008x304668

Walsh, J. E. (2001). Quantification of the ultraviolet radiation (UVR) field in the human eye in vivo using novel instrumentation and the potential benefits of UVR blocking hydrogel contact lens. *British Journal of Ophthalmology*, *85*(9), 1080-1085. doi:10.1136/bjo.85.9.1080

Water Pollution Control Plant, City of Thunder Bay, Environment Division. (2017). *Wastewater Treatment Annual Report 2017.* Retrieved from https://www.thunderbay.ca/en/city-services/resources/Documents/Water-and-Sewer-Services/2017-Wastewater-Treatment-Annual-Report.pdf

Weber, S. (2005). Light-driven enzymatic catalysis of DNA repair: a review of recent biophysical studies on photolyase. *Biochimica et Biophysica Acta (BBA) - Bioenergetics*, *1707*(1), 1-23. doi:10.1016/j.bbabio.2004.02.010

Wright, H. B. (2000). Comparison and Validation of UV Dose Calculations for Low- and Medium-Pressure Mercury Arc Lamps. *Water Environment Research*, *72*(4), 439-443. doi:10.2175/106143000x137978

Wright, H., Mackey, E. D., Gaithuma, D., Fonseca, C., Baumberger, L., & Dzurny, T. (2007). *Optimization of UV Disinfection*. Retrieved from AWWA Research Foundation and New York State Energy Research and Development Authority website: https://www.nyserda.ny.gov/-/media/Files/EERP/Commercial/UV/Optimization-of-UV.pdf

NOTES

CHAPTER 2
LITERATURE REVIEW

This chapter elaborates comprehensive review of previously performed practices in UV disinfection, direct measurement techniques followed for evaluating the UV lamp performance, experimental finding about lamp life and ageing phenomenon. Furthermore, this chapter covers description of UV lamp components, to create contextual understanding about the UV lamp's structural configuration. The material covered in this chapter was necessary to develop suitable methodology and upgrade the instrument design based on the previously reported studies.

2.1 History and development of UV disinfection technology

The Ultraviolet disinfection technology was first discovered by Dowens and Blunt (1877), which revealed germicidal property of sunlight. The first use of mercury lamp as an artificial UV light was reported in 1901. The first UV lamp was developed in 1906 by Kuch (Loach, 1987) which lead to the fundamental application of UV lamp as a water disinfection technology at Marseilles, France, in 1910 (Henri et al., 1910). In 20^{th} century considerable research was conducted on UV disinfection mechanism (Brandt and Giese, 1956; Dulbecco,1952; Gates, 1929). The first practical implementation of UV disinfection was conducted in 1955 at Switzerland and Austria with low pressure mercury lamp.

The application of UV disinfection technology increased over years across the world for disinfection of water, wastewater and air. In 1970's amalgam low pressure high throughput UV lamps were introduced to provide efficient germicidal effect as an alternative to regular low and medium pressure lamps (Bloem et al., 1977). In late 1978, a fully developed UV disinfection system was established at Northwest Bergen wastewater treatment plant, Waldwick, New Jersey (Scheible and Bassell 1981). In 1982 a modular UV system with gravity feed and parallel arrangement of UV lamp system was introduced (Whitby et al., 1984).

A survey in 2003 by the Water Environment Federation showed that there are approximately 18000 wastewater treatment plants in North America and there are at least 4000 UV systems among them (Water Environment Federation, 2004). Throughout the years UV disinfection technology has become popular due to its safe simple, effective and chemical free application (Dai et al., 2012; McLeod et al., 2017)

2.2 UV light description

UV light is a form of electromagnetic radiation which lies between the X-ray and infrared light region as shown in following figure 2.1 of electromagnetic spectrum in a range of 10nm-400nm band width which are subdivided into UV-A, UV-B and UV-C radiation.
However, UV-B and UV-C spectrum has germicidal properties (USAPHC,2004). The bandwidth containing 200nm wavelength has maximum germicidal properties (Reed,2010). UV-C radiations are created artificially to perform disinfection with the use of mercury vapor lamps, quartz lamps, florescent lights and high intensity discharge lamps (Chadysiene and Girgzdys, 2004).

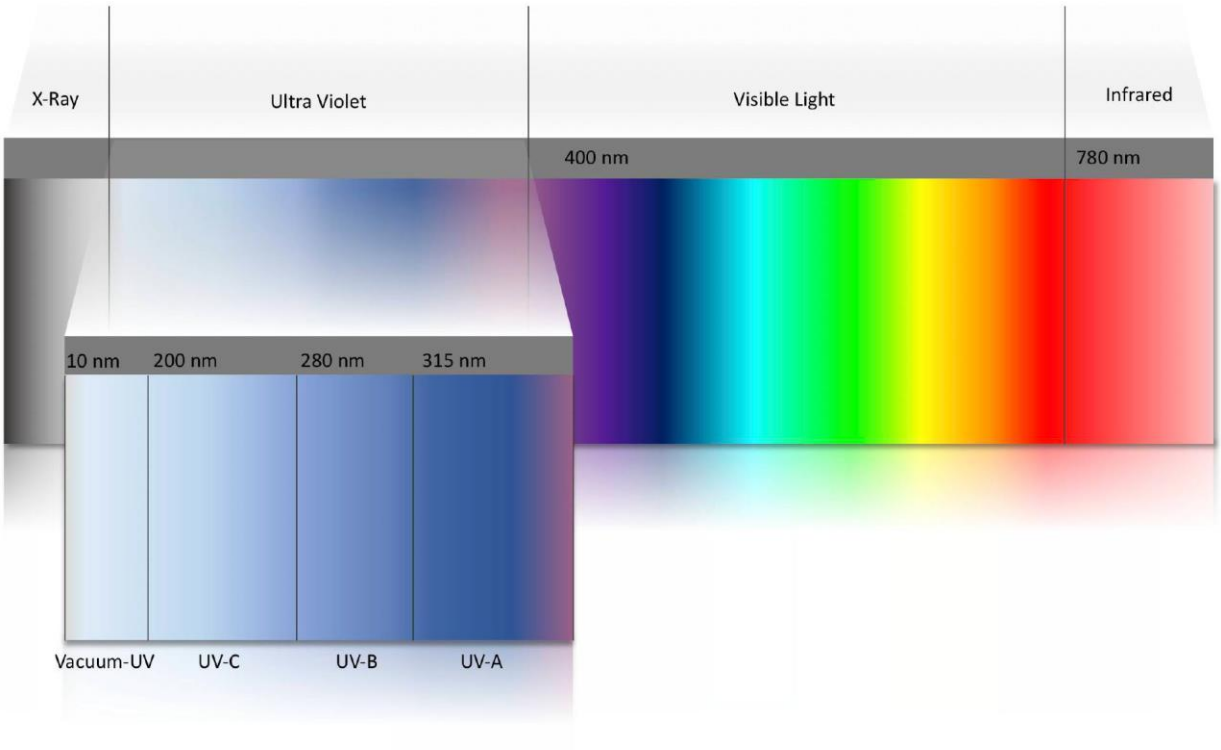

Figure 2. 1 Electromagnetic spectrum

2.3 Fundamentals of UV light generation based on UV lamp types

UV light is generated by variety of lamps such as gas discharge lamps, UV-light emitting diode (UV-LED), excimer lamps (mercury free lamps), metal halide lamps, Xenon lamps (USEPA UV light, 2006). In gas discharge lamps, electrons are accelerated by an electric field. Further due to the collision with atoms, molecules, ions and electrons they transfer kinetic energy, which results into excitation of heavy gas ions and molecules making them to release energy into a form of radiation. In UVLED, when voltage is applied to a nitrite semi-conductors *pn* junction, electrons are injected from the *n*-type semi-conductor (*n*-GaN) and holes from the *p*-type semiconductors (*p*-GaN) into the active layer of (InGaN). The electrons, which were injected, combines with the finite well energy levels (for electron 0.64 eV) resulting into the emission of blue light or UV radiation. Usually UV light emerges from wider band gap material such as Silicon carbide (Sic) or Sapphire.

Excimer lamps are also known as high pressure gas discharge lamps, which emits quasi-monochromatic radiation (single wavelength). In Excimer lamps electrodes are detached from the filler gas by a dielectric barrier. Excimers are the molecules which are stable only in the excited stage. The excited gas atoms produce an excimer after infusing with the rare gas, metal or halogen atoms which are filled inside. The most efficient excimer lamp contains Xe^2 gas atoms inside. These lamps are also known as mercury free lamps as it contains rare gas halogen instead of the mercury. However their efficiency is significantly less i.e., by ~8% when compared with ALPHO lamps i.e., by ~35% (Schalk, 2005). The metal halide lamps work on the same principle as gas pressure lamps. The gas discharge works through the excitation of the metal halide salts and mercury atoms.

2.4 Lamp types based on mercury pressure and principle of UV light generation

The UV lamps and florescent lamps work on the same principle (USAPHC, 2004) that is, when voltage is applied to a UV lamp containing an inert gas argon or liquid mercury, some amount of an inert gas vaporizes. The primary role of inert gas is to facilitate the starting of the discharge and promote ionization of the mercury. Free electrons and ions then collide with mercury atoms, which generate higher energy state into mercury atoms and these exited mercury atoms discharge energy while approaching back to their normal state. The energy discharged from mercury atoms is in the for of electromagnetic radiation, which has bandwidth 200-300nm of ultraviolet region in the electromagnetic spectrum. The UV light intensity depends on the amount of inert gas pressure present in the lamp casing (USEPA, 2003;).

Depending on the mercury vapor pressure UV lamps are categorized into three types (USEPA,2003)

a) Low pressure mercury lamp (LP)
b) Amalgam Low pressure high throughput lamp (ALPHO)
c) Medium pressure mercury lamps (MP)

2.4.1 Low pressure lamps and amalgams low pressure high output lamps

The LP and LPHO lamps possess greater germicidal output with monochromatic wavelength at 254 nm, which is also known as UV-C radiation. The spectral irradiance from LP mercury lamp is dominated by the two bandwidths 253 nm and 185 nm (Heering, 2004). The radiation in a range of 200-300nm is responsible for deactivation of DNA of the microorganisms, however 254 nm wavelength is more lethal (Heering, 2004; Linden, 2001; USAPHC,2004). Hence, to avoid photoreactivation and dark repair of microorganism's DNA; sufficient germicidal dose has to be provided to the water and air during the disinfection. The phenomenon of reactivations and its relationship with UV lamp intensity is explained in the section 2.7.6. UV-C radiation at 185 nm is primarily suitable for Advanced Oxidation Processes (AOP) such as, UV/O_3 or UV/H_2O_2 (Gonzalez and Braun, 1995; Stefan and Williamson, 2004). These applications are targeted on direct photolysis of ozone(O_3) or water molecule (H_2O) resulting in to the formation of highly reactive hydroxyl radicals (·OH).

The lamp envelope is made up of fused quartz, soft glass or fused quartz amalgam, however quartz is most preferred material for disinfection purposes due to its physical property of allowing higher UV-C transmittance at 254 nm (Schalk, 2005). Likewise, soft glass is suitable for general lighting purpose. The mercury pressure in UV LP lamp is 0.8 Pa and LP lamps are operated at 42°C with current of 430mA resulting into the germicidal outcome of 0.2 W/cm (USEPA UV light, 2006). To enhance UV disinfection with cost effective approach ALPHO lamps were introduced (Bloem et al., 1977; Heering, 2004). ALPHO lamps consisting of amalgam of mercury infused with other elements indium (In), lead (Pb), bismuth (Bi) and, tin (Sn) (Schmalwieser, 2014). Usually mercury/indium infusion is used, to regulate the optimum mercury vapor pressure 0.01 mbar or 1000Pa with temperature inside quartz envelope reaching close to the 100°C. Further, ALPHO lamps are less affected by ambient temperature (Heering, 2004; Schalk, 2005) and ALPHO lamps maintain 90% UV-C output, above the 60°C temperature inside the envelope (Schalk, 2005).

2.4.2 Medium pressure lamps

MP lamps have considerably greater power or UV-flux per unit 30 to 35 W/cm, when compared with LP lamps ~ 1W/cm (Schalk, 2005; USEPA UV light, 2006). MP lamps have extremely high quartz envelope temperature ranging from 500°C to 950°C (USEPA UV light, 2006). However, the efficiency of MP lamps for UV-C radiation is in range of 5 to 15 % which is relatively less than LP lamps. The figure 2.2 describes components of LP, LPHO and MP lamps

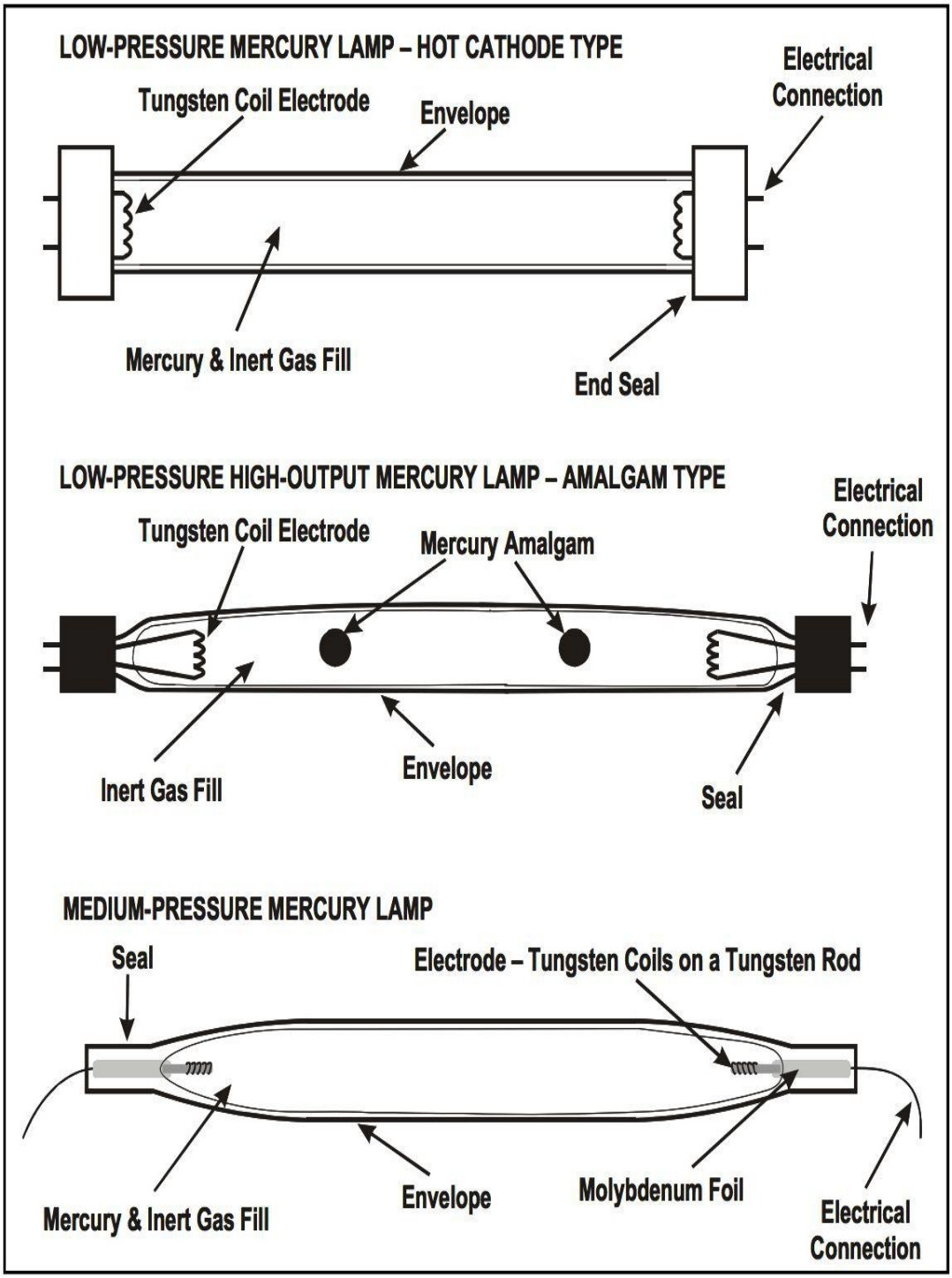

Figure 2. 2 Construction of mercury vapour lamps (Retrieved from USEPA UV light, 2006)

The table 2.1 elaborates characteristics of mercury vapor pressure lamps

Table 2. 1 Characteristics of mercury pressure UV lamp

Parameter	Low pressure lamp	Amalgam low pressure high output	Medium pressure lamp	Reference source
UV light spectrum	254 nm	254 nm	200-300nm	USEPA, 2006
Wavelength type	Monochromatic	Monochromatic	Polychromatic	USEPA, 2006
Sleeve temperature °c	30-50	60-100	600-900	Heering, 2004
Sleeve diameter (cm)	2.5-5.0	2.5-5.0	3.5-10.0	USEPA, 2006
Mercury pressure (pa)	0.93	0.18-1.6	>1000	USEPA, 2006
Power (w/cm)	0.5	1.5-10	50-250	USEPA, 2006
UV output (w/cm)	0.2	0.5-3.5	5-30	USEPA, 2006
Lamp life (hours)	8000-10000	8000-12000	4000-8000	Schalk et al., 2005; USEPA, 2006
UV-C efficiency (%)	35-38	35	10-20	USEPA, 2006; Schalk et al., 2005
Lamp start up time	>15 seconds	4-7 minutes (Cold Start) 2-7 minutes (Warm Start)	1-5 minutes (Cold Start) 2-5 minutes (Warm Start)	USEPA, 2006; Cotton et al., 2006
Heat development	Low	Low	High	Sommer, 2004

2.5 Components of mercury vapor pressure UV lamp

LP, ALPHO and MP lamps are consisting of the following components as shown in figure 2.3.

2.5.1 Lamp envelope

The lamp envelope of the UV lamp acts as an electric insulator made up of fused quartz and transparent silica due to its ability of allowing UV transmittance. The lamp envelope is 1-2 mm in thickness. The lamp envelope is often called as arc tube.

2.5.2 Lamp sleeve

UV lamps are housed within the lamp sleeves which protects lamp from overheating and physical damage. Lamp sleeves are usually made up of quartz. The size of the sleeve diameter depends upon the lamp type, for LP and LPHO lamps sleeve diameter is 2.5-5.0 cm. Likewise for MP lamps sleeve diameter id 3.5-10.0 cm. However, solarization and sleeve foiling reduces UV transmittance of the lamp (Polymicro Tecnologies, 2004).

2.5.3 Mercury fill

The mercury filled inside the lamp envelope can be solid, liquid or vapor phase in LP lamps.
ALPHO lamps are typically filled with mercury alloys such as gallium and indium.
In MP lamps vapor phase mercury is filled.

2.5.4 Electrodes

The electrodes promote heat transfer to provide optimum temperature inside the lamp envelope. The electrodes are made up of tungsten coil embedded with barium (Ba), strontium (St) or calcium (Ca).

2.5.5 Inert gas fill

MP lamps are filled with an inert gas. The rare/inert gas filled inside the lamp together with the mercury is commonly among the argon, krypton and xenon (Morimoto et al., 2004); however, the most preferred inert gas is argon (Ar). The purpose of adding inert gas is to accelerate gas discharge and reduce the disintegration of the tungsten electrode.

2.5.6 Lamp ballast

The lamp ballast is used for regulating the power supply to the UV lamp. Ballast can be magnetic or electronic based on the requirement. Magnetic ballast powered UV lamp can have more darkening at the edge, also magnetic ballasts have short life. Electronic ballast can cause power quality problems. However, ballast's performance depends upon electric design.

2.5.7 Mechanical wipers

Mechanical wipers maintain optimum UV radiations transmission by performing scheduled cleaning and maintenance work (not shown in figure 2.3).

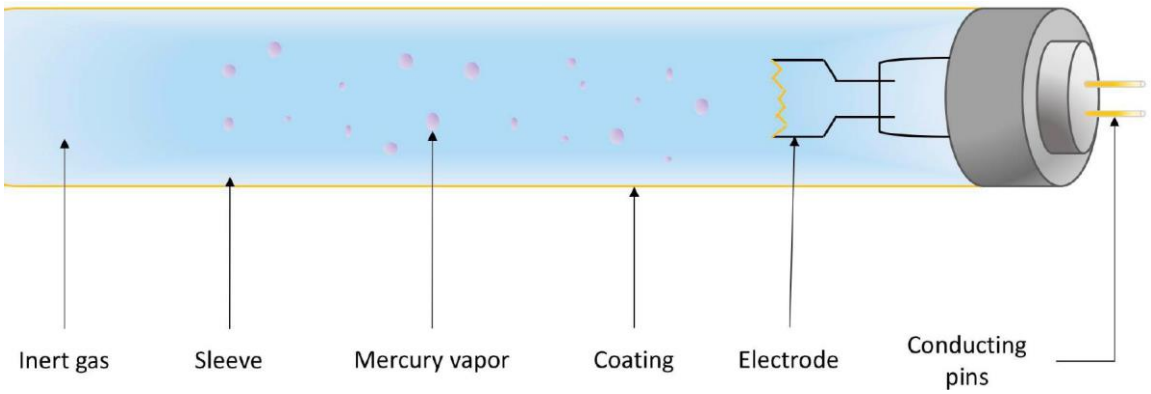

Figure 2. 3 Schematic of mercury lamp components

2.6 Fundamentals of UV lamp operation

This section elaborates UV lamp operation for mercury pressure UV lamps. The UV lamp is constructed using the fused quartz tube, which is transparent and allows UV radiation to pass through the lamp sleeve. The lamp is enclosed by protective quartz sleeve which protects lamp components from the external damage. Further electric or electromagnetic ballasts are used to control power supplied to the UV lamp (Harley et al., 2008).

2.6.1 Lamp start-up

When voltage is supplied to the lamp ballast, tungsten electrode emits electrons which undergoes into collision with the inert gas atoms, resulting into the ionization of the inert gas atoms. This effect creates plasma which allows movement of the electrons and results into heating of the inert gas. The temperature increase causes mercury atoms to reach to the highly excited state and further collide with the free electron present in the plasma. The energy generated during the collision is then emitted in the form of UV light (USEPA, 2006). LP lamps can reach to operating state within 15 seconds after voltage has supplied to the ballast. However, for LPHO lamps it can take several minutes to reach to the stable UV output. Likewise, MP lamps can require start-up time to emit stable UV output. The lamp start-up depends upon the cold start up and warm start up conditions and the lamp configuration designed by the manufacturer (Cotton et al., 2005).

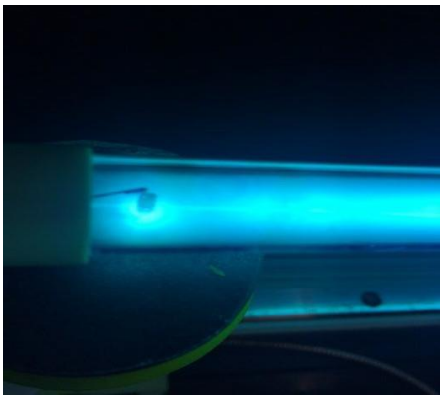

Figure 2. 4 Lamp start up and mercury activation

2.6.1.1 General principle

As mentioned in section 2.4.1, LP UV lamps are filled with mercury, which has ~1 Pa pressure. The activation of the mercury atoms by an electrical discharge at an optimal temperature (Heering, 2004). This activation process is called as ionization of atomic mercury by the transfer of kinetic energy upon the inelastic collision between electrons and the mercury atoms. As a result of the collision, the UV light is produced with the wavelength of 254 nm, which is blue in colour. The UV radiation is invisible however, it has more energy than the visible light.

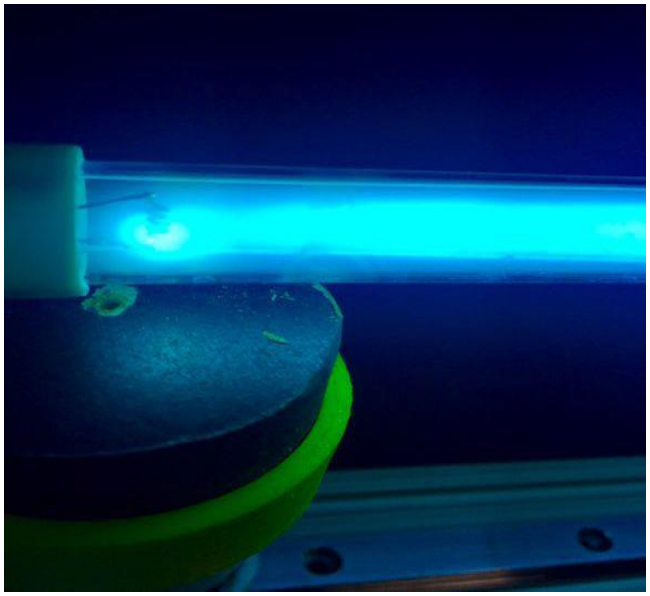

Figure 2. 5 UV radiation emitted after the lamp start up

When, voltage is applied to the electrodes of the mercury pressure lamps, an electric field is created inside the lamp envelope. In this electric field, a free electron tries to move away from a negative electrode towards the positive electrode; during this accelerated movement of the free electron, electron collides with mercury atom, which causes mercury atom to reach to its excited state (Masschelein and Rice, 2017, 2002; Sahin et al., 2010).

The following equation represents the ionization process.

$$Hg + e = 2e + Hg^{\bullet} \qquad \text{Equation 2. 1}$$

The exited mercury in an electrical field, does not remain at high-energy state for a long period, and returns to its lowest energy state by transmitting the UV light.
Further, electron-ion recombination occurs, resulting into the re-formation of the mercury atoms.

The entire process of ionization is carried out in subsequent stages. One of the stages involves Penning effect of the filler gas (argon) during the electrode ignition step (Druyvesteyn and Pennings, 1941; Sahin et al., 2010). The penning effect named after Frans Penning, who discovered mechanism of electrical discharges in low pressure gases.

$$) = *+ = \ *+^{*} (+)) \qquad \text{Equation 2. 2}$$

$$*+^{*}(+)) + /0 = \ /0^{\bullet} +) + *+ \qquad \text{Equation 2. 3}$$

The electrons in low pressure mercury lamps do not possess enough active energy to perform mercury atoms ionization in a single stage and requires multiple collisions in accelerated electric field, for the formation of excited mercury atoms.

$$) \ + /0 = /0^{*}()) \qquad \text{Equation 2. 4}$$

$$/0^{*}()) +) = 2) + /0^{\bullet} \qquad \text{Equation 2. 5}$$

The atoms can exist only in a specific energy state, hence the energy emitted by the high state mercury atoms, is the difference between the two stages, and only certain energies in the form of

the light at specific wavelength is emitted as shown in following equation.

$$/0^{*}()1234)5\ 64789) \rightarrow /0\ (0{+}7;{<}5\ 9464)) + h{>} \qquad \text{Equation 2. 6}$$

The emission of a photon by an excited mercury atom is reversible, hence after emitting the UV radiation, photons are reabsorbed by another mercury atom. This phenomenon is known as self-absorption of mercury atoms.

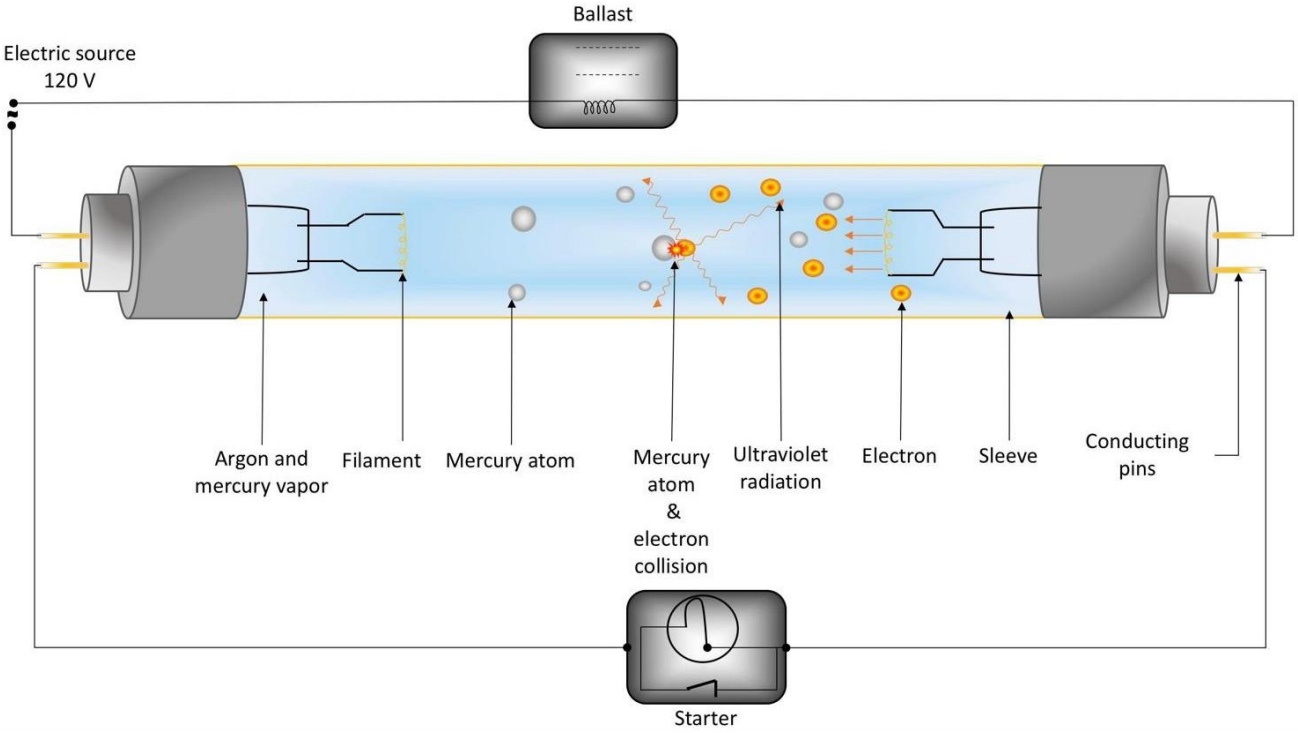

Figure 2. 6 Principle of UV light generation

LP UV lamps are usually tubular, which contributes to the non-uniform electric field, and several zones can be form across the length of the lamp contributing the variation in the UV dose and temperature variation (Masschelein and Rice, 2017, 2002). The figure 2.7 displays the distribution of the UV light after the lamp was properly warmed up.

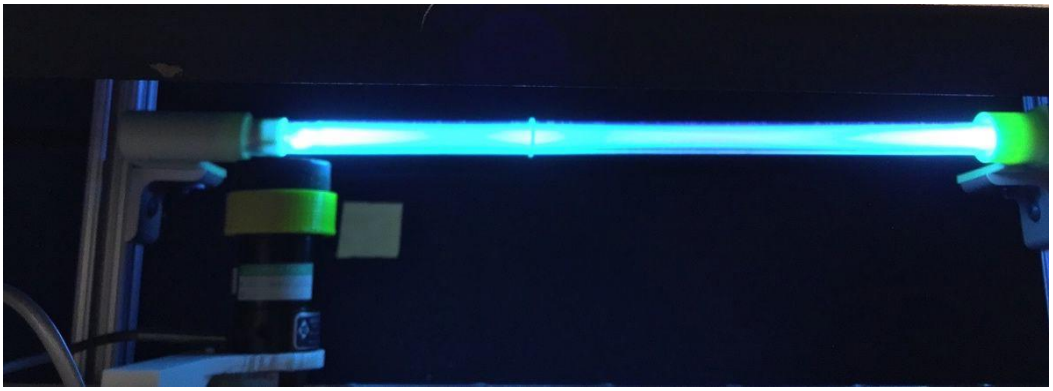

Figure 2. 7 Light distribution

2.6.2 Lamp power feed

LP lamps are supplied alternate electric current to the electrodes known as cathode and anode, which contributes to mercury ionization inside the silica glass tube of the UV lamp. As mentioned in the previous section 2.6.1.1, the excited state of the atoms can exist up to certain time interval, hence electron-ion pair generated during the ionization lasts about 1msec. However, this process continues until lamp has provided stable voltage. The electric feed, that is provided to lamp can be cold or hot cathode type.

2.6.2.1 Function of the lamp ballast

The UV lamps cannot be operated with direct AC supply due to their negative resistance. Hence without the provision of the ballast to limit an electric current, UV lamp would be damaged quickly. The ballast's crucial purpose is to limit an electric current to the rated value by the lamp manufacturer (Lindsay, 1997; Newsome, 2006) and provide the starting voltage pulse to ionize the gas mixture in the UV lamp tube (Kowalski, 2009). An electric circuit of the ballast has effect on the UV lamp especially on the arc striking. To obtain appropriate dose and stable output UV lamps are often preheated before initiating the disinfection practice. To preheat the lamp, the lamp is connected with the starter, which is the component of the ballast. The starter heats up the lamp electrode for 1- 2 seconds before the lamp gets ignited completely. In recent years there have been technical advancement in starter-ballast operations depending upon its function e.g. triggered start with no starter, rapid start ballast and instant start ballast (Newsome, 2006).

The ballast factors (BF) specifies the lamp output (Lindsay, 1997). The efficiency of the ballast is measured in terms of ballast efficiency factor (BEF), which is the ratio of ballast factor in percent, to the power provided in watts (Kowalski,2009).

$$?@A = \frac{BC}{D}$$ Equation 2. 7

BF = Ballast factor in percent

P = Power in watts (W)

There are two types of ballast used for UV lamps electric and magnetic as mention in previous section (section 2.5).

The figure below illustrates typical electric feed system of the UV lamp.

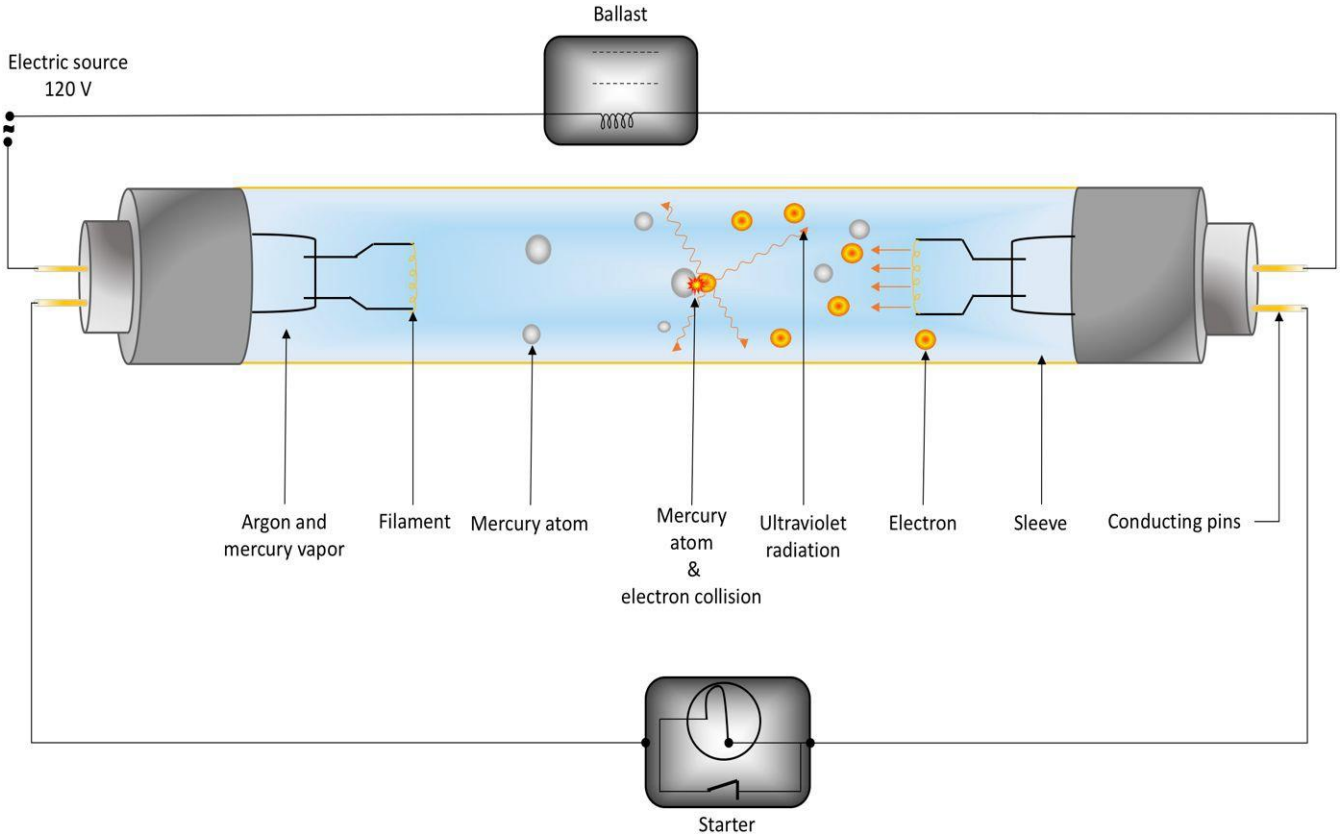

Figure 2. 8 Lamp power feed circuit

2.6.2.2 Function of the cathode and anode electrode

As mentioned previously the electric feed to the lamp can be cold cathode or hot cathode. The cold cathode type requires structure with iron (Fe) or nickel (Ni) electrode to release the electron after the bombardment with the positively charged ions in to the gas mixture or a plasma (Masschelein and Rice, 2017, 2002). This type is less preferred because it requires high voltage up to 2kV. The hot cathode type works on the thermionic emission of the electron from the electrode. The structure of this type of the electrode is consisting of coiled tungsten wire glazed with the alkaline oxides of calcium, barium, aluminum and strontium, sometimes thorium is used as well (MA electrodes, 2003). Hence another term for hot cathode is oxide-coated cathode. When current is supplied to the electrodes, after the heating of the electrodes enough electrons are discharged which then collide with the ionized mercury atoms, resulting in the emission of the light spectra. In past various studies reported the cathode and anode effect (Heberlein et al., 2010; Redwitz et al., 2006). The mercury lamps work by the alternate electric feed to maintain temperature equilibrium of inside the tube.

2.6.3 Radiation spectrum

LP lamp emits UV-C radiation between the bandwidth of 200-300 nm, with the resonance lines at 253.7 (peak germicidal wavelength) and 185 nm (responsible for oxidation). The brief about this has explained in previous section (section 2.4.1). The resonance line 253.7 nm is responsible for 85% of the total UV intensity emitted, which is essential for the disinfection of the water, air and the surface (IESNA, 200; Masschelein and Rice, 2017, 2002; Reed, 2010). The most effective wavelength among the emission spectrum is 254 nm emitted by LP mercury lamp, allowing 100% germicidal effectiveness (Calvert and Pitts, 1966).

2.6.3.1 UV output of the lamp

The UV output or photochemical yield of the lamp is a function of the mercury pressure, which is reliant upon the lamp surface temperature . Also, the UV output is variable depending upon the surrounding air or water temperature, type of the lamp, lamp orientation and flow pattern of the disinfecting entity (Lau et al., 2008; Kowalski, 2009). As previously motioned in section 1.3.3, the UV output can be variable depending upon the lamp manufacturing standard, burn-in hours, turn on and turn off cycles, subsequent power interruption and voltage variation and type of the lamp utilization i.e. air disinfection or water disinfection (DWI, 2016; Lau et al., 2009; Qiang et al., 2013; Wait et al., 2008). The UV lamps emit maximum efficient intensity in lamp surrounding temperature range of 21°C to 25°C at 100% UV output efficiency and 110% UV output efficiency at 32°C- 40°C under steady surrounding temperature.

2.6.4 Parameters influencing UV emission output

In this section influence of the lamp operating parameters and surrounding conditions i.e. voltage provided to the lamp and, surrounding temperate to the lamp has described.

2.6.4.1 Influence of the voltage

Mercury pressure lamp needs a certain amount of voltage to start up the lamp. The voltage supplied to the lamp through a tungsten electrode assembly, further results into the ionization of the mercury-argon gas atoms. During this stage an arc gets produced between the two electrodes resembling a bridge. The heat produced during this event also contributes to the ionization of the mercury atoms (Soo, 2005). As current continues to increase to its full potential, a ballast limits the supply of the voltage keeping the mercury lamp at stable operating condition. However, a faulty ballast can cause overheating of the electrical components, resulting into over voltage or under voltage, which causes fluctuation of the electric supply to lamp electrode. Furthermore, fluctuating electric feed can cause intensity variation and due the formation of the gas discharge zones as a result of non-uniform electric field.

2.6.4.2 Influence of the surrounding temperature

The surrounding temperature to the lamp has direct influence on the UV output because it affects the surface temperature of the lamp tube, and as result it affects the stability of the mercury pressure inside the tube. If surrounding temperature is too cool, the mercury will cool down and condense, causing the drop of UV output. Likewise, if surrounding temperature is too hot, the mercury will transform into liquid state resulting into the rise in vapor pressure. The reabsorption of the plasma radiation inside the tube wall affects the temperature depending upon the constituents used during the fabrication of the quartz tube (Franke et al., 2006; Schöpp and Steffen, 2016). The optimum pressure for mercury in LP lamps is ~ 0.9 to 1pa with temperature range from 21°C to 40°C (Kowalski, 2009; Masschelein and Rice, 2017, 2002). The figure 2.5 shows temperature profile at electrode and central part of the lamp.

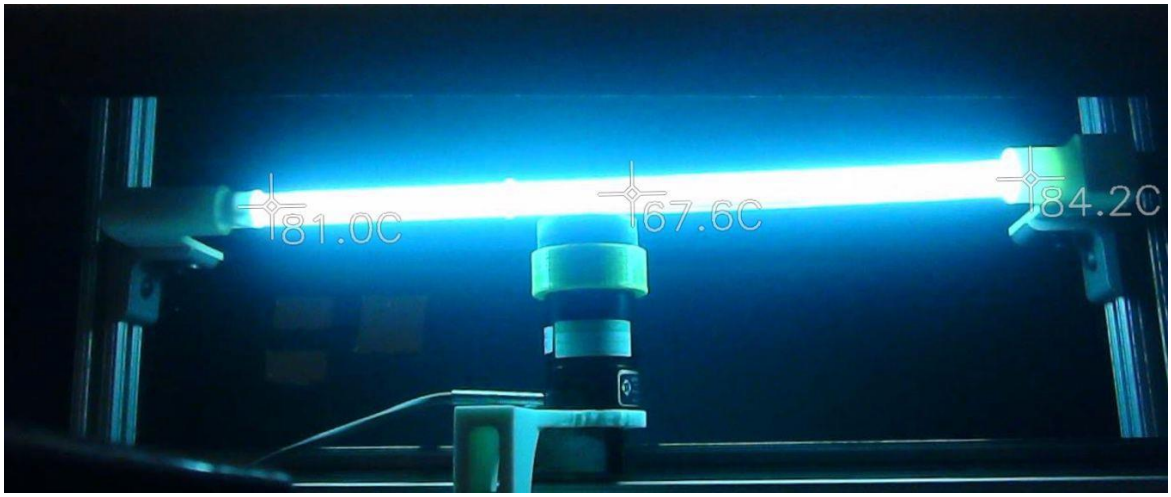

Figure 2. 9 Temperature gradient at lamp electrode and central part

(image has taken thought thermal imaging camera with visible plate mode)

2.7 Uncertainties in UV lamp operation and disinfection

The performance of the UV lamp decreases as lamp ages and fouls, which contributes to the reduced photochemical yield. During the first 100 hours of UV lamp operation initial drop in UV, outpour appears after that UV lamp emission is stable for several months (Masschelein, 2002).
As mentioned in previous sections 1.3.3 and 2.6.4, the lamp output deprivation occurs with both LP and MP lamps, which can be accounted for lamp hours in operation, operating cycle or turn on and turn off cycles, electrical feed, ambient conditions and the type of lamp and the purpose of the application. There are number of other a contributing constraint which affects the UV lamp output such as, solarization of the lamp sleeve material (i.e. quartz), accumulation of the sputtered oxides of the electrodes inside the lamp sleeve and the fouling of the lamp sleeve due to the characteristic of ambient air (for air disinfection application) or effluent characteristics of the waste-water (for wastewater disinfection application). The impure lamp sleeve structure can contain metal impurities, which can absorb UV light and can cause reduction in the UV output due to premature lamp ageing.

In mercury pressure lamps, mercury can combine with mineral constituents present in a quartz glass, which results in the formation of the UV absorbing layer inside the lamp sleeve.
As mentioned earlier in section 2.6.2.2, the tungsten electrodes are glazed with an alkali oxide which, contributes the formation of the non-uniform UV absorbing layer inside the lamp sleeve as a result of overheating of the electrode and deficient cooling during the continuous lamp operation (USEPA UV Light, 2006). Furthermore, these uncertainties in UV lamp operation varies from one lamp to another though the lamps were manufactured for the same specification among the same batch (Heath et al., 2013; Siegel, 1995).

2.7.1 UV lamp ageing

The UV output of the mercury pressure lamps progressively declines throughout the lifetime of the UV lamp, which is potentially unfavorable for the disinfection of the water and air. The non-uniform ageing of the UV lamp contributes to the less effective UV dose as a result of the formation of low irradiance regions in a UV reactor (Schmalwieser, 2014). The lamp ageing can be noticeable by structural changes occurred in the lamp envelope such as darkening of the lamp envelope near the electrode. As previously mentioned in section 1.1.3, numerous studies were performed to understand the non-uniform ageing phenomenon of the lamp with direct UV output measurement technique (Heath et al., 2013; Schmalwieser, 2014; Siegel, 1995).

The UV output from the lamp significantly changes over time, when compared with the UV output at the time of installation and after several hundred hours (Darby, 1993). The expected lifetime of the UV lamp is approximately 10000 to 12000 hours for LP lamps and ~8000 hours for MP lamps (Masschelein, 2002). Usually, the lamp performance statistics are provided by the lamp manufacturing companies based on standard laboratory testing (Heath et al., 2013). However, UV lamp performance significantly contrasts, when compared with the statistical data provided by the manufacturer due to a non-uniform and unpredictable ageing pattern of the UV lamps as a result of the distinctive operational condition followed during the lamp operation (Holmes et al., 2002; Lankhorst and Niemann, 2000).

2.7.1.1 Overview of UV lamp ageing uncertainties

In past various studies have been performed to understand the non-uniform ageing of the UV lamp, and its consequence with the reduced output over time (Braunstein et al., 1996; Hanzon and Vigilia,1999; Heath et al., 2013; Siegel, 1995; Schmalwieser, 2014). Siegel (1995) performed the test to evaluate the UV lamp performance during the life of the UV lamp for consecutive 18 days until the lamp failure. During the UV lamp monitoring the experimental data collected showed uncertain peaks, plateaus and slopes in the intensity for a specific wavelength. Further, their study found, altered performance in the UV lamp intensity as a consequence of inconsistency in the supplied electrical feed, operating temperature of the lamp and ventilation method around the lamp testing area that had a profound effect on the UV intensity. Their study observed several changes in the UV lamp intensity profile during the testing period of the lamp performance, which is explained in the next section 2.8.

Another study was conducted by Heath et al. (2013), to compare the UV output statistics provided by the lamp manufacturer with the UV transmittance measurements obtained by the experimental analysis. Their study confirmed that the lamp ageing graph that was obtained after the direct measurement of UV transmittance has significantly higher ageing profile than the reported by the lamp manufacturer. Based on the graphical illustration of their study for the lamp ageing comparison between data reported by the lamp manufacturer vs data obtained after the lamp testing, had ~20-25% dissimilarity in the results of the UV transmittance; during the 8000-12000 hours of the lamp operation. This substantial dissimilarity in the obtained lamp ageing curve by direct monitoring of the lamp vs assumed lamp ageing curve based on the provided statistical estimation can have an extensive impact on the UV systems due to reduced UV output, resulting into insufficient UV dose to inactivate the harmful microorganism present in air or in water (Heath et al., 2013; Sheriff and Gehr, 2001). The detail about the direct measurement technique followed for the research mentioned above and setup arrangements are elaborated in the next section 2.8 (section 2.8.5).

Previously, lamp ageing factor (LAF) was calculated based on the ratio of the germicidal output of the old lamp to the new lamp (AwwaRF and NYSERDA, 2007). The formula was used to estimate LAF for MP lamps, and it is quoted below.

$$E^*A = \frac{\text{FGH I JKJLMN OPQRPQ OS ONL NM I RT}}{\text{FGH I JKJLMN OPQRPQ OS QUG VGW NM I R}} \qquad \text{Equation 2. 8}$$

LAF = Lamp Ageing Factor

Germicidal output was described in Output W/Cm

To obtain germicidal output (IG) following formula was quoted

$$X_F = \sum_{a}^{} Z(\lambda) \times X(\lambda) \qquad \text{Equation 2. 9}$$

I_G = Germicidal output W/cm

$G\lambda$ = UV sensitivity of the microorganisms

$I\lambda$ = Spectral output of the lamp measured in W/cm

2.7.2 UV lamp sleeve fouling

As mentioned earlier in section 2.5.2, the UV lamp is enclosed into the quartz sleeve to provide the lamp defense against the external damage and enable plug-in module configuration to the lamp structure. The common problem with the UV lamps is fouling of the outer quartz sleeve when lamps have used for the disinfection of drinking water and waste effluent. The inorganic particles present in the water accumulates on the outer wall of the sleeve, as a result of the formation of the thin layer on the outer wall of the quartz sleeve. This accumulation of the particles can obstruct the UV transmission of the UV system by absorbing part of the UV radiation that was emitted from the lamp. As a consequence, reduced UV dose efficiency (Sommer et al., 2001; Wait and Blatchley III, 2010).

The sleeve fouling can be a result of the accumulation of the chemical compounds present in the water as a combination of thermal effect and photochemical reaction (USEPA, 2006). These chemical compounds can be oxides, carbonates, phosphates and sulphates of calcium, magnesium and aluminum (Nessim and Gher, 2006; Sehnaoui, 2002; USEPA, 2006). Furthermore, Lin et al. (1999) mentioned that particles could accumulate on the sleeve surface as a result of gravity settling and instability stimulated interaction (Sehnaoui, 2002). One of the main reasons for lamp sleeve fouling can be an improper lamp cleaning cycle and maintenance.

Heath et al. (2013) performed study over the quartz sleeve fouling with simple optic bench setup to estimate the sleeve fouling factor (SSF) by comparing new lamp and aged lamp. This study was conducted to understand the effect of the internal, external fouling and degradation of the quartz sleeve material. Further, their experimental analysis estimated lamp ageing factor (LAF) based on the reference value obtained from the new lamp.

The formulae used during Heath et al. (2013) have cited below.

$$b^*A = \frac{c}{c_d} \qquad \text{Equation 2. 10}$$

$$b^*A = eAA \times E^*A \qquad \text{Equation 2. 11}$$

$$eAA = \sqrt{\frac{g(ONL\ NM\ I\ R)}{g(VGW\ NM\ I\ R)}} \qquad \text{Equation 2. 12}$$

After rearranging the previous equation

$$E^*A = \frac{hiC}{cCC} \qquad \text{Equation 2. 13}$$

CAF = Combined ageing and fouling factor

S = Measurement reading by sensor

S_P = Predicated reading value of the new lamp

SFF = Sleeve Fouling Factor

LAF = Lamp Ageing Factor

I = Radiometric Measurement for an old and new lamp

2.7.3 Spectral shift

The UV spectral range varies from one lamp to the other lamp depending upon lamp's characteristics. The composition of the UV gives unique ability to lamp to emit a specified range of the UV light, identifies as UV-A, UV-B and UV-C. The details about UV radiation types are explained in section 2.1, and UV light generation principle is described in section 2.6. The spectral output range is of a UV lamp ranges from 100 to 460 nm depending upon the requirement of wavelength bandwidth and the lamp configuration. The spectral irradiance is studied by the spectrometer (Schmalwieser, 2014). As stated earlier in section 2.6, mercury fill is the main constituent, which enables the generation of the UV lamp in LP and MP lamps.

The mercury lamp emits distinctive UV spectrum of a shorter wavelength continuum and series of a spectral line, which has sharp peaks at specific wavelengths, i.e. 260, 290, 310, 365, 400 nm wavelengths. However, presentence of other material in a lamp quartz sleeve in excess amount can initiate spectral shift due to inference with the plasma, which can shift UV output wavelength from specific range to the element induced range. To provide stability to the lamp and extend the lamp's life, generally protective coating is applied to the lamp. Without the stability of the lamp, the UV spectral range can shift towards longer wavelengths. The reason behind the spectral shift is the excess concentration of the additives and the impurities in the lamp casing. During the ionization stage of UV light generation, the present impurity combines with the plasma, which affects stimulation process of mercury atoms resulting in the spectral enhancement. Further, an extended presence of the impure element in the lamp's quartz enclosure becomes immobilized either by reaction or by the migration into the quartz as a result of consistent heating of the quartz wall during the lamp operation.

One of the primary additives, which can trigger the spectral shift, is iron. Iron iodide it boils at 849 °C and at 1 atm pressure, which is relatively higher temperature range than the normal UV lamp and reactor operating temperature, which can result into the condensation of the Iron iodide on the quartz wall when the lamp is cooled and revision back into the plasma during the lamp operation. (Borsuk and Armitage;2010)

2.7.4 Precipitation of deposits and slime formation

The mineral salts (calcium, magnesium and iron) present in water and air has solubility which, reduces with increase in the temperature, and as a consequence of photochemical reaction, mineral deposition occurs on the quartz sleeve of the UV lamp. Due to the higher operating temperature of the UV lamp compared to the surrounding water and air these mineral salts precipitate on the lamp sleeve (Bolton and Cotton; 2008; Harley et al., 2008). The predominant minerals salts deposits are calcium and magnesium between 30% to 80%; however, iron, manganese and aluminum salts can be accountable for 10 %to 40% for the groundwater disinfection for drinking water purposes (Masschelein, 2002).

2.7.5 UV Transmission and reflection

The UV transmittance (UVT) is the amount of UV light that reaches the micro-organisms present in the water. The UVT depends upon the quality and characteristics of the water (suspended particles, hardness, organic materials) and spacing between the lamps in the UV reactor. The UV lamp transmissivity also depends upon the lamp envelope material.

2.7.5.1 Effect of photo-chemical solarization

As mentioned earlier in section 2.5, the preferred material for LP lamps is fused quartz, due to its higher efficacy of UV-C transmittance compared to other materials, i.e. soft glass (Sodium-barium glass), optical glass and Vycor 791 (Masschelein, 2002; Schalk et al., 2005). The solarization is one of the reasons for the reduced UV transmittance by the lamp sleeve, which is caused by photo-thermal damaged to the quartz sleeve due to the persistent effect of the high energy radiations such as UV light (USEPA, 2006) The solarization is a consequence of the UV lamp ageing. Previously, it has been reported that LP UV lamp can drop UV transmittance up to 50% due to photo-chemical solarization of the lamp material.

2.7.5.2 Effect of suspended solids and particle shading

The reduction in UVT due to the presence of the suspended particles and the formation of the aggregates is a challenging issue in the application of the UV disinfection for wastewater (Mamane, 2011). Usually suspended solids are removed prior to the disinfection stage. However, some particles and flocs can reach to the disinfection stage (Templeton et al., 2008). Furthermore, some microorganisms have ability to self-aggregate to the floc upon the exposure to the UV light, allowing them to survive throughout the UV disinfection process (Blatchley et al., 2001; Emerick et al., 1999, 2000; Jolis et al., 2001; Madge and Jense, 2006).

The presence of suspended particles and the flocs in the water absorbs, blocks or scatters UV light emitted in the water, which reduces chances of the UV light reaching to the microorganisms present in the water (Mamane, 2011). The Iron has been identified as a substantial foulant accountable for UV lamp fouling from the outer side of the lamp sleeve (Sun et al., 2008). The suspended particles not only block but scatters UV light as well, which affects UVT as well it allows microorganisms to embed within the particles. (Darby et al., 1993; Sun et al., 2008; Wait et al., 2007; Wait and Blatchley III, 2010). These phenomena are also known as particle shading and enmeshment or embedding. These phenomena and effect of low UVT have described in section 2.7.6 and 2.7.5.6 in detail.

2.7.6 UV lamp intensity and microbial reactivation

The inactivation of microbial nuclei is carried out by exposing water and air entity to UV-C radiation. When micro-organisms are sufficiently exposed to the UV light, thymine and cytosine dimerization takes place, which either inhibits the replication or sudden death by nuclei rupture (Lindene et al., 2002). However, it does not instantly result in the inactivation because inactivated micro-organism can evoke DNA restoration capability through repair mechanism (Malley et al., 2004). This event takes place when there is insufficient UV dose to inactivate the microorganisms. The UV-C radiation at the peck of 253 nm possesses highest germicidal efficiency, compared to other wavelengths in the UV spectrum, also elaborated in section 2.1. The microbial reactivation takes place by photoreactivation and dark repair, which are explained in the next section, 2.7.6.1.

2.7.6.1 Type of microbial reactivation

There are two types of microbial reactivation as described below:

2.7.6.1.1 Photoreactivation

The photoreaction involves the release of the specific enzyme photolyase, which is capable of restoration of DNA segments in the presence of UV light. This event occurs, when there is insufficient UV light of required germinal wavelength, allowing the microorganism to release photolyase enzyme by two-step reaction, first by binding with dimer pair and second breaking of dimer by utilizing wavelength from 310 -490 nm (Friedberg et al., 1995; Friedberg et al., 2006).

2.7.6.1.2 Dark repair

The dark repair of the DNA is carried out in the absence or presence of UV light (Hanawalt et al., 1979). The dark repair can occur either by excision repair by removing the damaged DNA segment and with regenerating new segment by recombination repair using complementary DNA strand (Hanawalt et al., 1979). As mentioned in section 2.6, UVT is affected by the presence of the suspended particles in air and dust particles in the air, responsible for shadowing effect, allowing UV shielding to the microorganisms against the germicidal light rays emitted from the UV lamp.

2.7.6.2 Factors influencing microbial reactivation

The photoreactivation depends on the UV dose, UV lamp type and UV exposure conditions. These factors are discussed below.

2.7.6.2.1 Effect of improper UV dose

Higher the UV dose, more time will be required by the microorganisms to repair the DNA (Martin and Gehr, 2007). It was reported that UV dose is essential to minimize the microbial reactivation rate (Gehr and Nicell, 1996; Lindenauer and Darbyreported, 1994). Their study observed the effect of lower UV dose and higher UV dose on the microbial inactivation.

2.7.6.2.2 UV lamp intensity and exposure time

Bohrerova and Linden (2007) observed photo repair at higher and lower UV intensities and found that the rate of photo repair is correlated to the UV intensities. Higher intensities had higher repair rate (Bohrerova and Linden, 2007; Zimmer and Slawson et al., 2002). Further, Bohrerova and Linden (2007), stated that photo repair depends on UV lamp intensity and exposure time together, and not independently under the term UV fluence.

2.7.6.2.3 Type of the UV lamp and its correlation with microbial reactivation

Oguma et al., (2002) and Zimmer and Slawson (2002) found decreased levels of photoreactivation when MP lamp is used instead of LP lamp when tested for *E. coil*. In monochromatic LP lamp microorganisms were able to repair DNA; however, in polychromatic MP lamps microorganism were unable to repair DNA.

2.7.6.2.4 Effect of the wavelength

Zimmer and Slawson (2002), assumed that the wide variety of wavelength emitted by MP lamp, UV-A (320-400nm) and UV-B (290-320) along with the germicidal wavelength range UV-C (290-185nm), was responsible for lowering photoreactivation level. Oguma et al. (2002) reported that the wavelength between the range of 220-300 nm reduced photo repair due to the dysfunction of photolyase.

2.7.6.2.5 Effect of water quality

As mentioned previously in section 2.7.5.2, the water entity, containing suspended solids has low UVT due to reflation and scattering of the light (Chan and Kilick, 1995; Darby et al., 1993; Martin and Gehr, 2007). Lindenauer and Darby (1994) reported that improved water quality resulted in improved initial inactivation and less photoreactivation in the microbial sample.

2.8 Direct UV output measurement technique

In this section, previously developed sensor-radiometer or sensor-photometer assembled set-up arrangements for UV radiation measurement has elaborated.

2.8.1 Overview of direct measurement set-up assembly

The direct measurement of the UV lamp output is performed by optical bench arrangement with the provision of the photovoltaic sensor and radiometer, which precisely calibrated for the detection of a specific wavelength of UV-C radiation (Chevrefils et al., 2006; Kuhn et al., 2004). Previously, it has been recognized that, the direct measurement technique followed by radiometer and sensor assembly is more ideal for the measurement of the UV output, which provides accurate measurement of UV intensity (Chevrefils et al., 2006; Kuhn et al., 2004; Schmalwieser et al., 2014; Siegel, 1995); recapped from section 1.1.3. Hence, lamp output can be monitored by the on-line or regular radiometer, which can evaluate irradiance produced by the UV lamp from one or multiple fixed points (Bolton, 2002).

If a manufacturer has not provided on-line radiometer monitoring systems to the corresponding lamp; usually lamp statistics are provided for the corresponding lab based on the laboratory testing for lamp burn-in time and its subsequent UV output for the expected life span of the lamp; recapped from section 1.1.4. The components of a typical radiometer-sensor based set-up are described in the next section.

2.8.2 Components of direct measurement set-up for UV radiation

The direct measurement set-up is consisting of the three essential components: The mechanical arrangement, optical assembly module and electrical signal processing unit, as shown in the following figure.

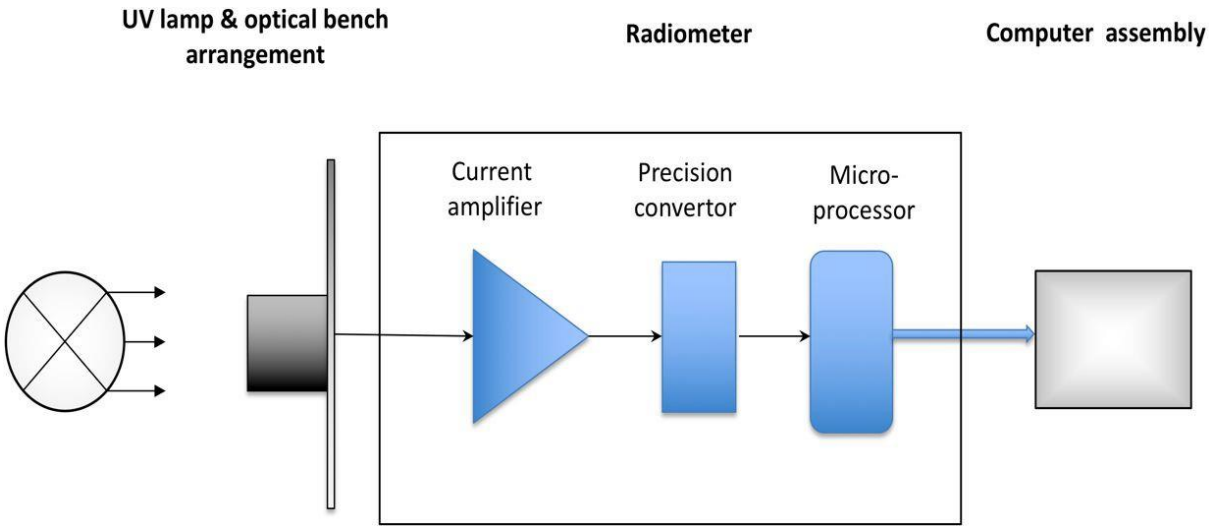

Figure 2. 10 Schematic of the direct measurement setup

2.8.2.1 Mechanical arrangement

The mechanical arrangement is comprised of an optical beam set-up consisting of a UV lamp, mounting assembly to arrange a UV sensor, radiometer-computer configured segments to record and store the collected data. In the past, Siegel (1995) monitored UV lamp performance with the help of on-line UV measurement system, which comprised of PC- based data acquisition system in conjunction through an optical probe, fiber optic cable and optical bench set-up.

2.8.2.2 Optical assembly module

The optical assembly module usually called a UV sensor, which is comprised of quartz window, diffuser, focusing optics and filter. The figure below illustrates the photodetector and its components.

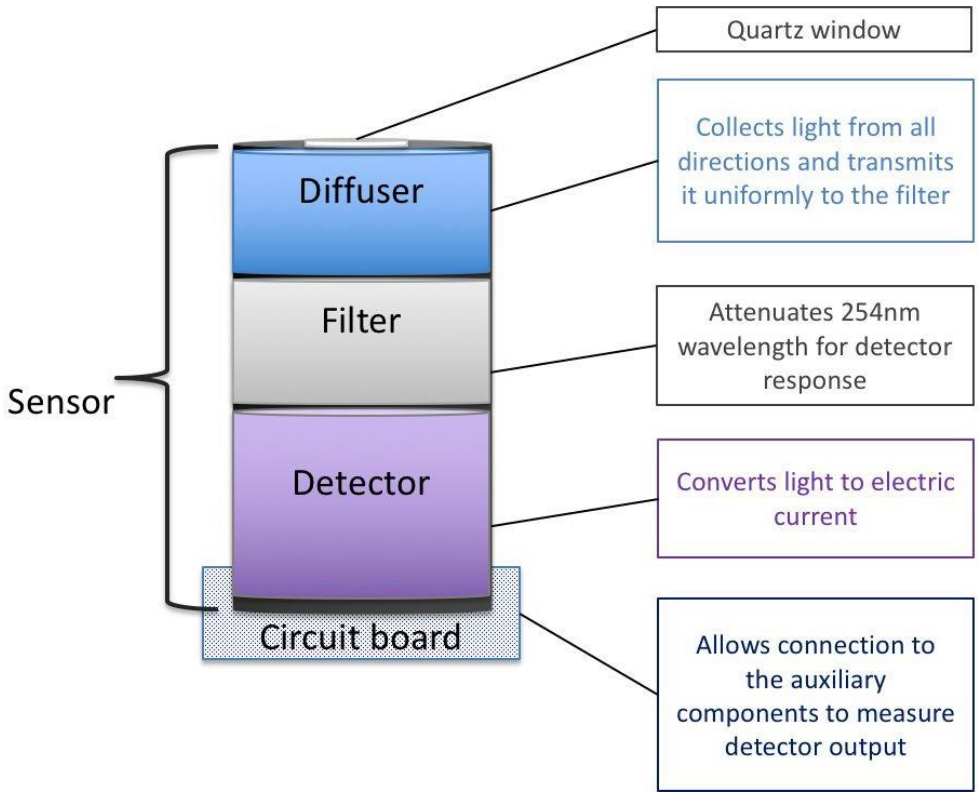

Figure 2. 11 Configuration of the UV sensor

2.8.2.2.1 Window

The window is usually made of the quartz or synthetic sapphire, allowing protection to the internal components of the sensor protection against the pressure and flow inside the disinfection chamber (Goin et al., 2004).

2.8.2.2 Diffuser

The diffuser is commonly used to obtain cosine response for the wide acceptance angle of the input UV radiation. The primary function of the diffuser is to provide an appropriate spatial response and regulate the irradiance level to avoid excessive radiant power to the photodetector. The diffuser is also known as an attenuator, which acts as supplementary sift to prevent damage to the filter unit due to saturation during the high-power settings (Xu and Huang, 2000). The diffuser with attenuation properties prevents premature photodetector degradation (Goin et al., 2004).

The spatial response is a measurement of UV radiation at different incident angles, and it is essential to recognize the spatial response of a radiometer to determine how effectively it detects incident radiation. Further, the spatial response depends on angular response and axial symmetry of the UV sensor (Goin et al., 2004). For radiometer monitoring single lamp, a unit with narrow spatial response will have more precise sensitivity than the wide spatial response as shown in the figure below.

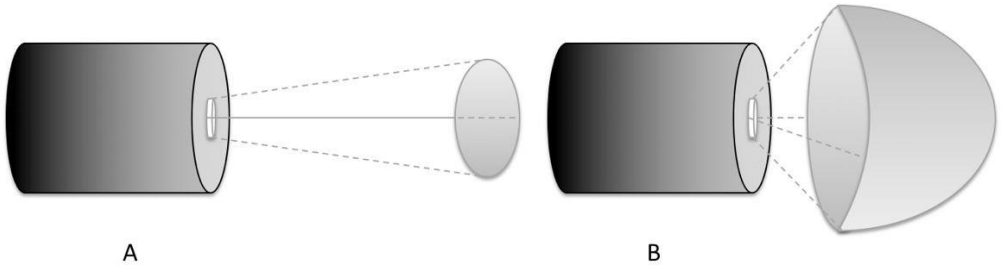

Figure 2. 12 Schematic of two radiometers with different spatial response
A- Narrow and focused response
B- Wide response (Adopted from Goin, 2004)

2.8.2.2.3 Focusing optics

The focusing optics is an aperture that converges the incoming UV radiation into the detector. The focusing optics or aperture is used to mask the edges of the photodetector to allow uniform spatial responsivity to the radiometer detection (Xu and Huang, 2000).

2.8.2.2.4 Filter

Filters are used to attenuate the specific radiation wavelength by eliminating wavelength other than the required bandwidth. Usually, a filter has a thin metal film which is coated with dye, which allows passage to the specific wavelength by absorbing wavelength containing colour other than the specified range, allowing absolute measurement of the specific bandwidth from UV spectrum.

2.8.2.3 Electrical signal processing

The electrical signal processing unit is comprised of UV photodetector, radiometer or PLC units for online radiometer measurements. Figure 2.13 illustrates the signal processing sequence of the detector and radiometer.

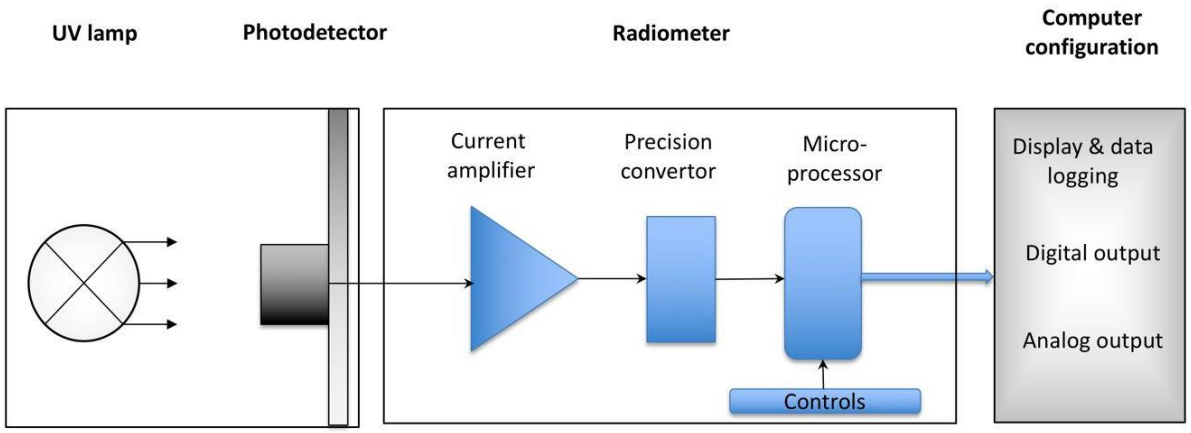

Figure 2. 13 Schematic of Radiometry measurement

2.8.2.3.1 UV photodetector

Most of the radiometry measurement involves UV sensitive cathode that converts the incident UV radiation into the electric current; this phenomenon is also called as photoelectric effect photodetector converts photons into an electric signal (Garipov et al., 2010; Pan and Zhu, 2015; Pounce, 2017). The photodetectors are often identified as photodiodes or photocells, which are semiconductors, fabricated to detect a specific part of the electromagnetic spectrum (Photoelectric effect, 2018). The photodetector or photodiode, formerly called as an electron tube or vacuum tube, consisting of the sealed-glass or metal-ceramic enclosure containing a cathode made up of metal which allows electron transmission. The release electrons released by the cathode then gather around the anode seized at a positive voltage similar to the cathode.

However, these tubes were replaced by semiconductor materials, that can detect UV light, measure UV intensity, control illumination of the source and convert photon energy into the electric energy, that can be processed to obtain value into electron volts (Photoelectric effect, 2018).

Every UV radiation spectral range has a different wavelength and corresponding photon energy output (Omnès, 2007).

UV-A, for wavelengths between 400 and 320 nm (from 3.1 to 3.87eV)

UV-B, for wavelengths between 320 and 280 nm (from 3.87 to 4.43 eV)

UV-C, for wavelength between 280 and 200 nm (from 4.43 to 6.20 eV)

Far UV, for wavelengths between 200 and 10 nm (From 6.2 to 124 eV)

Previously, narrowband semiconductor-based photodetectors were used for UV radiation detection such as silicon and III-V compounds. However, lately new generation semiconductor-based photodetectors have been introduced such as silicon carbide, diamond and gallium nitride alloys, allowing precise measurements (Erturk et al., 2019; Lin et al., 2014; Omnès, 2007; Wright and Horsfall, 2007; Zou et al., 2018). Photodetector further can be the photoconductive or photovoltaic detector. The Photoconductors works on the principle of photoconductive effect when photon energy is greater than the band-gap energy, it absorbs photons and produces electron-hole pair, consequently changing the electrical conductivity of the semiconductor, which is detected by the external circuit (Takahashi et al., 2014; Zou et al., 2018).

The second type is the photovoltaic detector that detects UV light of specific frequency infiltrated on the metallurgical junction. When UV light of specific wavelength irradiated on the active region of the detector, a photon-generated transferor releases a photocurrent in the circuit, which is detected and recorded by the radiometer. During this event, bias is applied in *p-n* junction photodiodes. Usually, *p-i-n* photodiodes work at the zero bias and at the reverse bias (Photoelectric diode mode) to provide improved sensitivity. Both *p-n* and *p-i-n* work at faster response speed with an increase in the light transmission rate (Razeghi and Rogalski,1996; Zou et al., 2018).

2.8.2.3.2 Signal processing by a radiometer

The primary function of the radiometer is a provision of electric signal that is proportional to the absorption of the wavelength by the photodiode. The radiometer further processes the small voltage formed due to the photovoltaic effect. The radiometer amplifies the received signal by the photodetector and converts the voltage into the current with the prebuilt amplifying unit.
After accurate conversion and processing of the current irradiance level of the incident UV radiation are expressed as $\mu W/cm^2$, mW/cm^2, pW/cm^2 or intensity a.u. Radiometer can provide absolute or relative measurement depending upon the requirement (i.e., 0 to 1Volt, 4 to 20 mA, digital RS232 etc.), for on-line remote-radiometer monitoring system, SCADA systems or assembly to PLC's for an advanced facility to measure UV lamp output based on irradiance reduction over time. The digital readouts are favored for the clarity of the readings, which can be linked to the microprocessor. The recorders can be added to the system which can store the data obtained for the incident spectrum by the photodiode. Further, the controller enables monitoring systems can trigger an audible alarm to an automatic system shutdown until damaged or aged UV lamp has been replaced.

An on-line radiometer cannot determine UV dose because the sensor unit is fixed and does not travel through the reactor (Goin et al., 2004) ; making it challenging to identify the burned out lamp in a reactor, which adds up to cross-checking of the algorithm confirmation and testified values during the reactor validation (Goin et al., 2004).

2.8.2.3.3 Data assembly

If radiometer and measurement set-up has been configured with predominantly developed software for automated data logging and analysis; the measurements will be recorded for the prefixed time intervals and will be stored in a sequential statistics logbook for the preceded date, distance or position and specific time intervals between the measurements.

2.8.3 Calibration of the system component

The NIST tracible metrology laboratories purchase calibrated transfer standard detector directly from the National Institute of Standards and Technology.

From 400 nm to 1100 nm, this transfer standard is S1337-1010BQ photodiode, a 10 x 10 mm planner silicon sell with synthetic quartz coating. The photodiode is fixed behind an accurately measured 7.98 mm circular aperture, yielding active area of 0.5 cm^2. Calibration labs then use this transfer standard to calibrate their working standards using a monochromatic light source.

These working standards are identical to the equipment that will be calibrated (e.g. photocell, radiometer etc.) Detectors are calibrated to the peak wavelength range of the detector/diffuser/filter arrangement using equivalent optics for the proposed application. Fundamental to the precise calibration is a consistent kinematic base (mounting arrangement) that allows movement of detectors in the optical path. Though the working standards of the unknown detector are fixed in the precise kinematic base in front of the precisely controlled light source, a small error can be generated due to transfer error. Hence, properly calibrated sensor/detector and radiometer has to be obtained or purchased from certified metrology laboratories for precise measurements.

2.8.4 Overview of the previously developed experimental set-up for direct measurements and research gaps

The direct measurement technique is followed by the optical bench arrangement with a calibrated detector and radiometer assembly. The background of direct measurement set-up, setup components and their working principles are described in previous sections (section 2.8.1 and 2.8.2). Over the years the direct measurement techniques are used to study and analyze the performance of the UV lamp, efficiency of the UV dose based on the incident intensity and the consequences of the non-uniform ageing pattern during the expected lifetime of the UV lamp (Harrington and Valigosky, 2007; Loge et al., 1999; Nessim and Gher,2006; Siegel,1995; Schmalwieser et al., 2014; Vasilśev et al., 2006).

2.8.4.1 Direct measurement set-up for determination UV dose

Harrington and Valigosky (2007) performed experimental analysis for decontamination of surfaces in a biological safety cabinet for UV-C radiation to optimize the UV dose to kill the microorganism. Their study involved evaluation of the correlation between UV lamp output and its effect on the microorganism to find the appropriate dosage amount. The experimental setup that was used for the measurement of the UV intensity was consisting of the photometer IL1400 (from International Lighting Inc.) and photodetector # SEL240/TD. Their analysis was performed by exposing the microbial sample to UV-C radiation of intensity 510µW/cm^2 to 20 µW/cm^2, by the UV lamp G30T8 MP lamp within less than 500 hours of use. The UV exposure studies were confirmed by the Labconco purifier Class II Model #36204 BSC (Labconco Co. Kansas City MO). However, their main focus was to estimate the appropriate UV intensity to inactivate the microorganism. Their study reported that the measured UV intensity of the UV lamp at the center was 510µW/cm^2 (51 mW/cm^2). Further, it was stated that UV lamp after 8000 hours of operation produced 125µW/cm^2 (12.5 mW/cm^2) and killing time for microorganism was ~20 to 40 seconds, even at the end of the useful life of the MP lamp. Furthermore, their study quoted that time taken more than 120 seconds would suggest dosage level below ~40 µW/cm^2(~4 mW/cm^2), which is below the minimum desirable dosage stated by New York health department (Clinical Laboratory Evaluation Program, 2006).

2.8.4.2 Direct measurement set-up for monitoring for foulant accumulation on lamp sleeve

In another study by Nassim and Gher (2006), the fouling mechanism in Laboratory-scale UV disinfection system (reactor) was studied by monitoring of foulant accumulation. The basics of lamp sleeve fouling are described in the previous section (section 2.7.2). This analysis was performed by the direct periodical measurements of UV intensity at 253.7 nm, 2mm above the fouling surface, on the top of the quartz sleeve of the lamp. The radiometer IL1400(from International Lighting Company) fitted with the water submersible optic detector #SEL 240 with the wavelength filter P2 # 954, performed the monitoring of foulant accumulation.

The experimental study for every measurement involved intensity reading was recorded as a reference value, and succeeding readings were normalized with respect to it. Their study reported intensity values ranging from 100 to 2400 $\mu W/cm^2$ (~ 10 mW/cm^2 to 240 mW/cm^2) depending upon the water temperature and quality. Their analysis reported fouling of the quartz sleeve and predominately because of the iron and volatile solids. Further calcium and ferric iron recombined and precipitated as calcium carbonate and ferrous hydroxide and attributed to sedimentation.
Further, their remark for one the experiment stated calcium, iron, phosphorus and BOD resulted into the highest accumulation of foulant in the form of foulant film predominantly on the top region of the UV lamp, reducing UVT by 50%. Furthermore, it was mentioned that UV radiation-induced precipitation of $Fe(OH)_3$, $FePO_4$ and $CaCO_3$ among the length of the lamp, consequently blocking UV transmittance in the water.

The main focus of their research was to understand the fouling mechanism of the wastewater constituent and the amount of the UV transmittance that was able to penetrate after the foulants accumulation the UV lamp surface. However, their study did not involve sensor arrangement which can enable scanning of each position along the length of the lamp to understand the change of the lamp output along the axial length of the lamp after each experimental run with respect to the burn-in lamp hours.

2.8.4.3 Direct measurement set-up for monitoring light penetration in the wastewater sample

In another study by Loge et al. (2000), fiber optic microelectrode set-up was used. However, their study was focused on the analysis of light-attenuation within the wastewater. The set-up was consisting of two main components, a fiber-optic microelectrode to detect the light and radiometer systems that measure radiant light. The fiber optic microelectrode was constructed by inserting 60µm silica fiber optic cable inside 60 mm long stainless-steel tube. The set-up had a compartment to hold the wastewater sample with solids. The set-up was constructed with the installment of MP lamp equipped with radiometer IL1700 (from International Light Inc.) with was connected to a photomultiplier (Model # 400a with tube IL101). The set-up had motor-driven micromanipulator to control the movement of the fiber-optic with 1µm increments.

Their study involved analysis of UV light that can be passed through the sample and overall intensity reaching a particular point within the wastewater containing solids as a function if the light that is reaching towards the receptor plus the amount of light coming from all directions, i.e., scalar irradiance. This study justified the effect of the solids in UV disinfection. However, this experimental set-up did not involve the analysis of the UV lamp output, and the change occurred in the UV intensity over time at specific length intervals along the length of the lamp.

2.8.4.4 Direct measurement set-up for monitoring the ageing of MP lamps

Jin et al. (2007), studied the ageing of the MP lamps using a closed vessel UV reactor system for drinking water disinfection purposes. Their analysis involved the evaluation of the UV lamp output during the expected lifetime MP lamp with four different lamps which were able to last for 6006, 13600 and, two lamps for 16500 hours (from 2002 to 2007-year span). Their study stated that the lamps output dropped below 70% efficiency until the end of the lamp's life for the burn-in hours, as mentioned earlier.

The test equipment was consisting of, calibrated radiometer IL1700 (from International Light Inc.) and detector SED 240 equipped with the W- diffuser and a QNDSI filter, to test the irradiance.
The lamp spectrum was analyzed by the handheld spectrometer (S200, Ocean Optics, Inc. Dunedin, FL), based on the direct record and conversion into the spectral irradiance
This study involved detailed analysis of fluence rate change, occurred during the life span, of the MP UV lamps. Additionally, the analysis also involved the measurement positions at 25%, 37% and 50% distance from the ends of the arc, mentioned by USEPA UV Disinfection Guidance Manual (USEPA, 2003) for conservative measurements.

However, this study did not involve a consistent motor driven sensor movement to study the change occurred in UV lamp output across the axial length of the lamp at multiple measurement locations with specific increments during each measurement (i.e. in centimeters, millimeters or micrometers).

2.8.4.5 Direct measurement of UV lamp performance with an on-line monitoring arrangement

Siegel (1995), experimented with direct measurement technique to study UV lamp performance over time. The direct measurement set-up was consisting of on-line monitoring tool LM-9000 UV Lamp Monitor connected by PC-based assembly and software-based data acquisition system combined with an optical probe, optical bench and sensor unit. The optical probe was mounted on the lamp, which was connected with fiber optic to an optical bench, which converts incoming light into an electric signal voltage. The software was developed for on-line monitoring, to displays wavelength distribution based on the real-time sampling at 5 seconds interval.
During this analysis, the life of the lamp test was performed on a single lamp for 408 operating hours until the lamp failure. The study found that, as lamp undergoes continuous use, the lamp intensity degrades over time due to changes in the mercury pressure, electrode degradation and deposition of material on the inside of the quartz sleeve. The study also observed an unexpected decline in output with multiple peaks, drops and pluteus. The main discovery of this study was the nonuniformity of the lamp output.

Furthermore, another test was performed, to compare lamp characteristics among 14 UV lamps of the same specification and few lamps were new, and few had up to 1000 hours of operation (lamp life specifically has not been mentioned)
The comparison test was performed for similar lamps from the same manufacturer; however, the experimental analysis did not show any exact pattern in lamp ageing and variable output.
This non-uniform behavior of the new lamp, on which life of lamp test was performed in this study by Siegel (1995), helped to realize lamp of the similar specification can show variable performance through the lamps have been manufactured under same conditions by the same manufacturer.

2.8.4.6 Direct measurement set-up for analyzing ageing of ALPHO lamps

Recently Schmalwieser et al. (2014) studied the spatial distribution of ALPHO lamps for irradiance measurement at 254 nm wavelength. The part of this study was to examine the UV dose monitoring to predict UV dose delivery based on reactor modelling. The analysis was performed on five different lamps obtained from Pitkäkoski Water Treatment Plant, Finland. The lamps had different burn-in hours 100, 432, 940, 1472 and, 6696 hours.

The experimental arrangement involved horizontal arranged lamps inside the black box. The set-up involved radiometric measurement by IL1700 research radiometer (International Light Inc.) equipped with SED240 and 245 interference filter and diffuser. The sensor was mounted on the rail system which was able to move across the axial length of the lamp with 15mm increments. After the lamp was scanned along the length of the lamp. After, the lamp was turned off and rotated to the 90°, and measurements were performed again. During this analysis, researchers have noticed darkening of the electrode, which was first visible at the lamp, ends than the middle part. Further, their analysis stated that as lamp ages darkening becomes severe and expands towards the middle part of the lamp. Their examination for a new lamp reported a formation of the two wavelength maxima near the lamp ends and between the two maxima output decreases at the middle part of the lamp. Also, it was confirmed that as lamp ages, it not only reduces the UV output but also changes the profile of the output measurements obtained for the maxima between the two electrodes. Additionally, their analysis reported total irradiance from 500 to 1500 hours was 75%, and from 1500 to 6700 hours it was 50% for pre-used lamps with prior burn-in hours.

Further, their study stated that the non-uniform output along the length of the lamp could be related to the temperature gradients, because lamp possesses a cooler temperature profile in the middle part. However, their study did not provide justifiable temperature profile analysis across the length of the lamp to show temperature variation at the electrode and the middle part of the lamp.
As mentioned earlier, the irradiance of one new and 4 old lamps was observed and monitored by Schmalwieser et al. (2014). The study reported non-homogeneous UV radiation firm the ALPHO lamps. Their analysis noticed emittance increased from the lamp end reached to its maximum and then dropped towards the middle part of the lamp. The primary difference between the maximum

and minimum irradiance range was 7% for 500 hours, 16% after 1500 hours and, 20% after 7000 hours. Also, there was a discontinuity in rising and drops in the intensity across the length of the lamp as well reduction in the output between the two maxima formed across the length the lamp as explained earlier (section 2.8.4.6) Further, their study reported visual ageing signs of brownish discoloration of the quartz sleeve near the electrode.

2.8.4.7 Direct measurement set-up for quantifying UV transmittance of the quartz sleeve

In 2013 Heath et al. (2013) presented UV lamp ageing by direct measurement of the UVT. Health et al. (2013) demonstrated a detailed measurement technique to calculate the quartz sleeve fouling with simple optic bench arrangement to measure UVT of the quartz sleeve. Further, the field testing of the experiment was performed by Carollo Engineers, USA. To perform this experiment, a custom optic bench set-up was developed to measure quartz sleeve transmittance, consisting of research radiometer IL1700 (from International Light Inc) and UV sensor (model # not provided). The one part of the analysis by Health et al. (2013), involved quantification of the lamp output by combined ageing and fouling index (CAF). It is also described in the previous section (section 2.7.2). The quartz SFF was measured directly with the optic bench for LP lamp for the 254nm wavelength. Following equations have recapped form section 2.7.2

$$\mathrm{CAF} = \frac{\mathrm{S}}{\mathrm{S_n}}$$

$$\mathrm{CAF} = \mathrm{SFF} \times \mathrm{LAF}$$

$$\mathrm{SFF} = \mathrm{p}\,\overline{\frac{\mathrm{I(old\ lamp)}}{\mathrm{I(new\ lamp)}}}$$

After rearranging previous equation

$$\mathrm{LAF} = \frac{\mathrm{CAF}}{\mathrm{SFF}}$$

CAF	=	Combined ageing and fouling factor
S	=	Measurement reading by sensor
S_P	=	Predicated reading value of the new lamp
SFF	=	Sleeve Fouling Factor
LAF	=	Lamp Ageing Factor
I	=	Radiometric Measurement for an old and new lamp

During this analysis, Heath et al. (2013) noticed SFF of 0.95, or ~5% reduction in the output for the aged sleeves. Further, when new lamps were arranged for the measurement readings obtained for 254 nm wavelength was 100%. Moreover, the old UV lamp had darkening across the length of the lamp. To obtain LAF, UVT was measured among the one old lamp with the darken quartz sleeve. However, the fouled sleeve cannot be cleaned; hence, the new lamp was used as a reference to calculate the LAF. Their result indicated LAF of 0.53 relatively to the new lamp, representing 47% output reduction (for the old lamp) when compared to the new lamp without out darkening of the sleeve.

Further, the ratio of UVT transmittance of the old lamp to the new lamp was estimated by dividing UVT of old lamp divided by UVT of the new lamp. The spectral transmittance was measured with the spectrometer (model # and set-up arrangement information not provided). The UVT analysis for old and new lamp reported, UVT of the old lamp was 53%, while new lamp had UVT above 70% (based on the graphical illustration provided by the Heath et al. 2013).
The second part of their study involved comparative analysis of MP UV output for old lamps (7500 to 9500 burn-in hours) and new lamp, using the optic bench set-up. The measured UVT for 254 nm for old lamps with darken quartz sleeve ranged ~55 to 66% after 8828 to 9500 burn-in hours. To validate the lamp output effect fecal coliform inactivation was performed with the aged lamps, and the aged lamp had a significant impact on the dose delivery (inactivation details not provided) Further, UVT for old lamps at the darken ends near electrodes had a significant decrease in UVT and 20 to 40% decrease in the UVT compared to the new lamp.

The spectral UVT transmittance of the old and new lamp was measured by using Ocean Optics JAZ spectroradiometer assembled with an optical sensor. The UVT measured performed during this experiment concluded LAF of 0.56 after 12000 burn-in hours while manufacture's claim was LAF 0.85. The LAF obtained by the direct measurement was significantly higher than the LAF claimed by the lamp manufacturer, when data was plotted as UVT transmittance as a function of lamp burn-in hours. Further, the experimental analysis confirmed the significant decrease in the UV output over time than the lamp ageing curve provided by the lamp manufacturer.

2.9 Research gaps and modification in the setup

During the literature review, previously followed measurement techniques and previously developed experimental arrangements were studied. During this review, few research gaps were notified, which aided to modify the set-up configuration.
In this section research gaps and set-up, modification has described.

2.9.1 Research gaps related to the literature availability associated with the UV lamp ageing

There are very few published findings available on the non-uniform lamp ageing and its effect on the UV output over time (Health et al., 2013; Schmalwieser et al., 2014; Siegel 1995). Furthermore, there are few published studies available, but these are limited to an impact of the UV lamp ageing and does not address the non-uniform ageing profile of the lamp. Additionally, analysis of UV lamp output involves intensive research and comprehensive understanding of UV lamp's behavior, which often takes a more extended period to perform an analysis depending upon the lamp life. Hence contribution in the field of UV lamp performance monitoring is inconsistent depending upon the time taken to perform an experiment during the expected life span of the lamp (~10000 to 12000 hours). Moreover, most of the literature available is related to the analysis related to fluence rate distribution to evaluate the UV dose, and the degradation occurred in the UV intensity over time based on the single sampling location.

2.9.2 Research gap related to the setup

Previously there have been very few studies published, which has involved the sensor movement to monitor UV lamp performance across the axial and radial direction of the ALPHO lamp (Schmalwieser et al., 2014). Jin et al. (2007) studied lamp ageing phenomenon for MP lamps measurement positions at 25%, 37% and 50% distance from the ends of the arc.
However, the experimental set-up developed for this analysis involves stepper motor driven axial motion of the sensor along the length of the lamp with specified distance increments. The detail about setup arrangements is explained in Chapter 3.

2.9.3 Research gap related to the imbalanced temperature profile across the lamp

As mentioned earlier in the section 2.8.4.6, Schmalwieser et al. 2014, mentioned non-uniform output might be related to the uneven temperature gradient along the length of the lamp, the cooler temperature at the central part and compared to the electrodes. Nonetheless, there was not any justifiable evidence displaying the uneven temperature profile. Furthermore, in previously referred studies, there was no reporting of the thermal imaging camera, which could be signified the uneven temperature distribution across the length of the lamp. However, this study has observed a differential temperature profile at the electrode and the central part of the lamp by modifying the set-up configuration with a thermal imaging camera (recapped from section 1.1.4 and 1.4.2). The details about the set-up components are explained in Chapter 3.

2.9.4 Automation with Arduino microcontroller and LabVIEW interface

As mentioned earlier in section 1.1.4 the setup that has developed for the experimental analysis of the change occurred in the UV lamp intensity performance over time, has prospered with the Arduino microcontroller to perform control over the set-up components with the specially developed program coding with LabVIEW interface with the Arduino. Furthermore, the movement of the photodetector has synchronized with the 3-D printed adapter housing, fixed on the stepper motor to allow linear motion of the adapter housing implemented with the clockwise and anticlockwise movement of the lead screw allowing forward and backward motion of the photodetector to scan the UV lamp.

The functioning (signal receiving) of the radiometer was controlled with the LabVIEW coded algorithm to stipulate digital input from the photodetector and corresponding output result with the user interface (.text file on a computer). The command over radiometer functioning was performed on the front panel of the LabVIEW generated virtual instrument program. The details about the virtual instrument program have described in the following section (2.11.1). Previously, Arduino and LabVIEW interfaced programs have been developed to control automation of instrument. However; the application of this interfaced was not performed to study UV lamp intensity, and change occurred in the lamp performance over time.

Moreover, the literature that was referred to study previously developed direct measurement techniques for UV lamp output has not mentioned which software or program interface that was used to perform measurement of the UV lamp and control over the set-up components.

2.9.5 Thermal imaging camera to identify a non-uniform temperate profile of the UV lamp

The study of UV lamp performance and variation in UV output also includes the observation of the uneven temperature gradients at the electrodes and the central part of the UV lamp. The uneven temperature profile was observed with the help of a thermal imaging camera. In previously reported UV lamp performance studies, the implementation of the thermal imaging camera was not included. There has been one reported image (partial image of the lamp), that we encountered during the literature review. The study was performed by Lau et al. (2008) for in-duct air disinfection to observe the influence of the air velocity and lamp temperature of the lamp output for the cold spot at the UV lamp for the prediction of the cold spot at the surface of the lamp. However, the study was performed to develop a model to predict the output based on the temperature and the UV output analysis was based on the stationary detector with only one sampling point and not multiple observation points, which could observe the change in the UV intensity along the axial length of the lamp.

The direct measurement setup that has developed in this research for the analysis of the UV lamp intensity has a UV detector housing attached, to lead screw and coordinated by a stepper motor motion to allow the movement of the detector along the axial direction of the lamp. This modification not only allows multiple sampling points but allows to select a specific observation location by inputting the distance in the numeric measure in the program through computer input. Moreover, this study includes multiple complete thermal images of the UV lamp showing temperature gradients at the lamp electrode and the central part of the lamp.

2.10 Arduino overview

Arduino is an open-source electronics platform used for performing control over devices and device movements. Arduino consists of physically programmable circuit board; the programmable circuit board is also known as microcontroller, and a software (C++) or Integrated Development Environment (IDE), that can be operated on the computer with different operating systems, i.e. macOS, Windows, Linux etc. (Arduino-Getting Started, 2017; Mins, 2013). The Arduino platform is more preferable because it does not need a sperate piece of hardware to load new program code onto a circuit board; it can be configured using a USB cable. The Arduino hardware and software (C++) can interact with buttons, motor, speakers, internet and motion control as well it can help to read information from input devices such as sensors, potentiometer etc. (Margolis, 2011). The Arduino board is classified into two components, hardware and software as explained in the next section (section 2.10.1 and 2.10.2).

2.10.1 Arduino hardware

The hardware of Arduino consists of the many parts to make it work and perform control over the experimental set-up. Figure 2.14 elaborates components of the Arduino board.

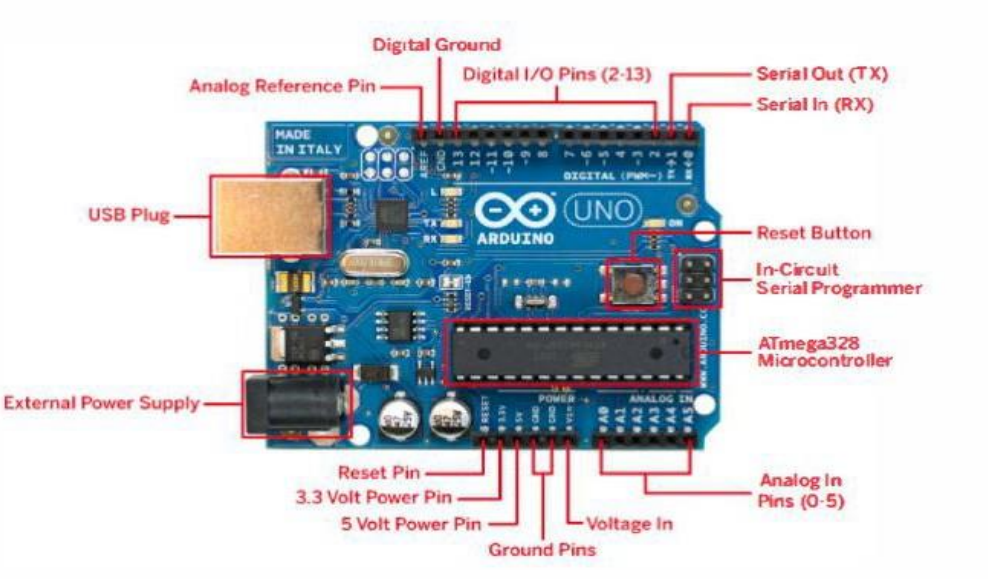

Figure 2. 14 Components of Arduino circuit board

The USB plug allows program upload by external devices (i.e. data drive, data disk) to the microcontroller (Gibbs, 2010) to regulate the power supply of 5 volts, by the same assembly connection (mostly direct connection from the computer USB port). However, the external power supply can be provided in case the USB plug does not provide sufficient power (9 to 12 volts) to the board. The reset button allows the upload of another command to retune the newly added feature to the code. The microcontroller receives and sends information as a command to the corresponding circuit units. The analog pins, A0 through A5 These pins, read and convert received signal from analog unit into a digital value. The Digital pins 0 through 13 are used for digital input to signal the command to the board and digital output to represent the output of the command (e.g. digital input= button on, digital output= powered light).

2.10.2 Arduino software and programming

The microcontroller of the Arduino board requires to be programmed with the software to perform specific tasks of the experiment or project. The main difference between the microcontroller programming and conventional computer programming (scientific or engineering computation) is that the microcontroller is specially programmed to control the hardware, or the motion of the hardware configured external components.

The Arduino uses C, C++, and Java-based programming language and its syntax and structures are similar to the JavaScript and PHP. The Arduino language refers to the object, which means code construction and, that define attributes containing properties of the object and methods, which defines procedure associated with the object. In Arduino programming, there is a serial object which contains methods for displaying the output after reading the signal from the serial port.
The Arduino programmed software is a set of instructions that informs a hardware component to perform the task, which is specified in the programming language.
The Arduino software components are divided into three constituents, command area, text area and message window area, as shown in figure 2.15.

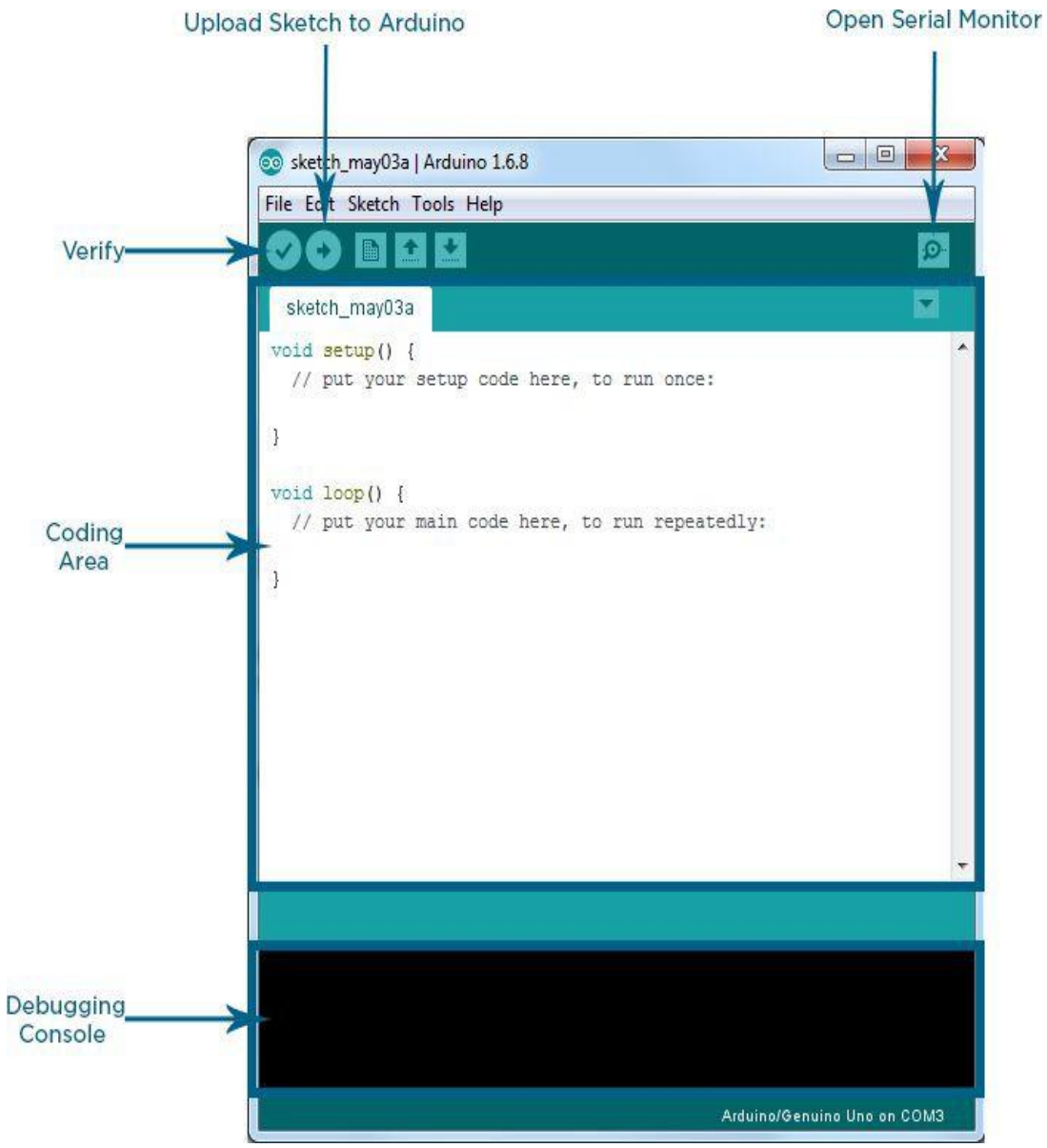

Figure 2. 15 Labelled IDE (adapted from Arduino-Getting Started, 2017)

2.10.2.1 Command area

The command area is also called as a programming text editor which allows the input code along with the other options such as File, Edit, Sketch and Tools to upload the program.

2.10.2.2 Coding area

The coding area is where we add written program and compiler compiles the uploaded program when Upload to I/O button has pressed. The code uses a simplified version of C++, which enhances the easiness of the program writing; it is also called as the sketch. The program follows two main functions set-up function and loop routine. Once the variables are initialized for the intended use for the assigned task, the setup routine launches to a set initial condition of the variables and to run the pilot code.
The second function is the Loop routine that allows program run and execution of the main code in a continuous cycle (Arduino- Getting Started, 2017; Badamasi, 2014).

2.10.2.3 Message window or Debugger

The serial monitor is used for the debugging and monitoring the data from the computer. It provides feedback and allows verification of the code (Badamasi, 2014; Gibbs, 2010)

2.10.3 Working principle of Arduino board

The Arduino board can be programmed with the Arduino software which works on C and C++ programming languages, which allows to generate a program to perform the application and control of the device components (Sudhan et al., 2015). As mentioned earlier in section 2.10.2, the program can be uploaded through microcontroller by using the jack cable. The Atmega-328 microcontroller saves created or uploaded program, and these internal circuits (IC) can act as a processor to process interaction without any error. Furthermore, Atmega-328 comes with the bootloader, that allows uploading feature to add new program code without the use of an external hardware programmer. After giving analog or digital input to the system, through a program in the developed software, we can perform control over the application process of the device.

If revision of the program code is needed, Arduino software allows an editing feature to modify as well as it provides a feature to upload a completely new program through jack cable or a USB port assembly, to the microcontroller of the Arduino board. After the provision of the new program, we need to reset the program to delete the previous program and to use the newly added program. Moreover, the Arduino Atmega-328 microcontroller can be used for numerous applications, especially in automation movement and control (Sudhan et al., 2015).

2.11 Overview of Laboratory Virtual Instrumentation Engineering Workbench (LabVIEW)

LabVIEW is a graphical programming approach and system design platform that helps to stimulate real-world application with the provision of visualization of the program from National Instruments. LabVIEW is commonly used for data acquisition, instrument control and automation on various operating systems (Travis and Kring, 2007). LabVIEW is written in C, C++ and .NET; however, it requires only logic to programming, and it is syntax intended. LabVIEW is a high-level design tool which provides interpreter programming; hence, it compiles the programming itself.

2.11.1 Virtual Instruments (VI) programming

LabVIEW programs are named as virtual instruments (VI), and each VI has three components a, a front panel, a block diagram and a connector pane as shown in the figure below.

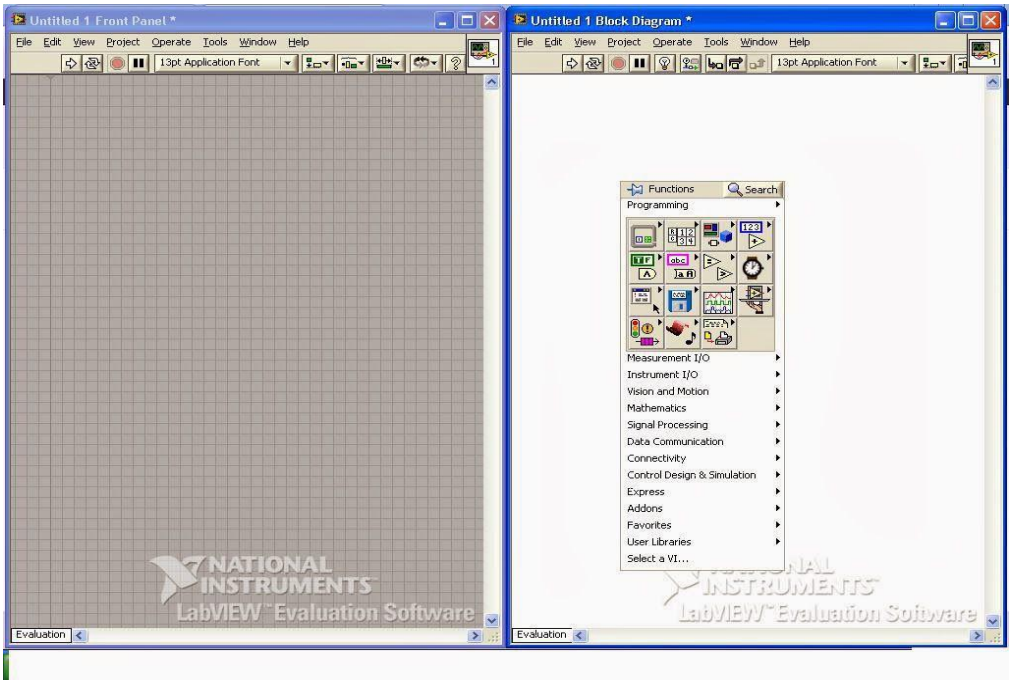

Figure 2. 16 Front panel and block diagram

The front panel is built using controls and indicators. Controls are inputs allowing the user to provide information to the VI. Indicators are outputs, displaying the results based on the inputs given to the VI. The back panel or block diagram contains the graphical source code of functions and structures, which performs an operation on controls and supply data to the indicators. All objects placed on the front panel appears as terminals on the back panel. The connector pane is used to represent the VI in the block diagram. The controls, structures and functions are referred as a node in the programming language, as shown in the following figure.

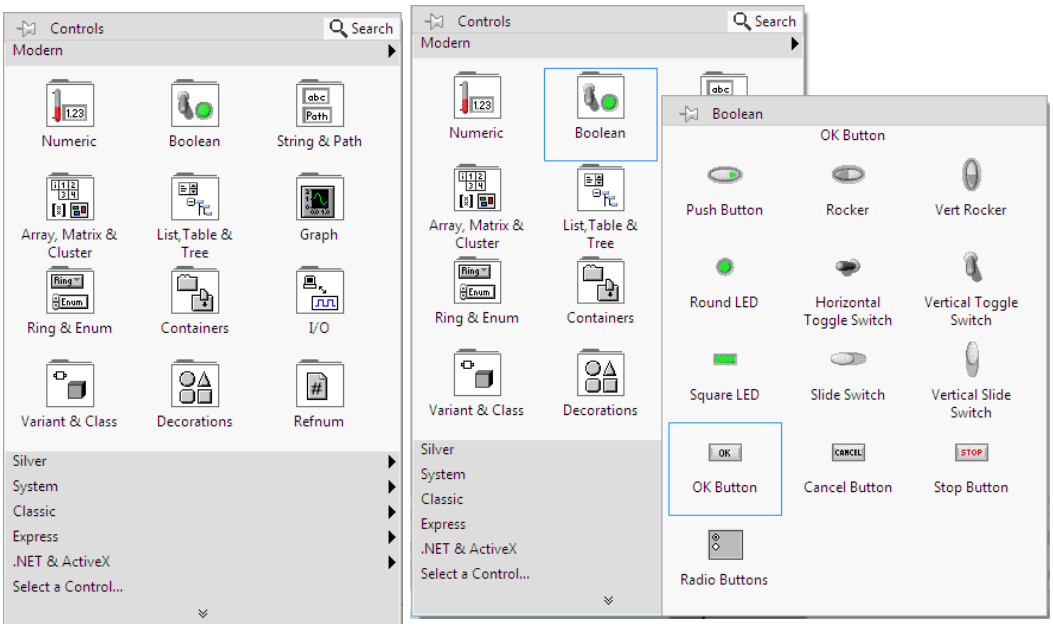

Figure 2. 17 Controls in LabVIEW programming

The VI can be run as a whole program, in which the front panel serves as a user interface when nodes are created on the block diagram. The front panel outlines inputs and outputs for the nodes through the connector panes (Christiano, 2015; Tamilvarshini, 2018). Connector pane has shown in the following figure.

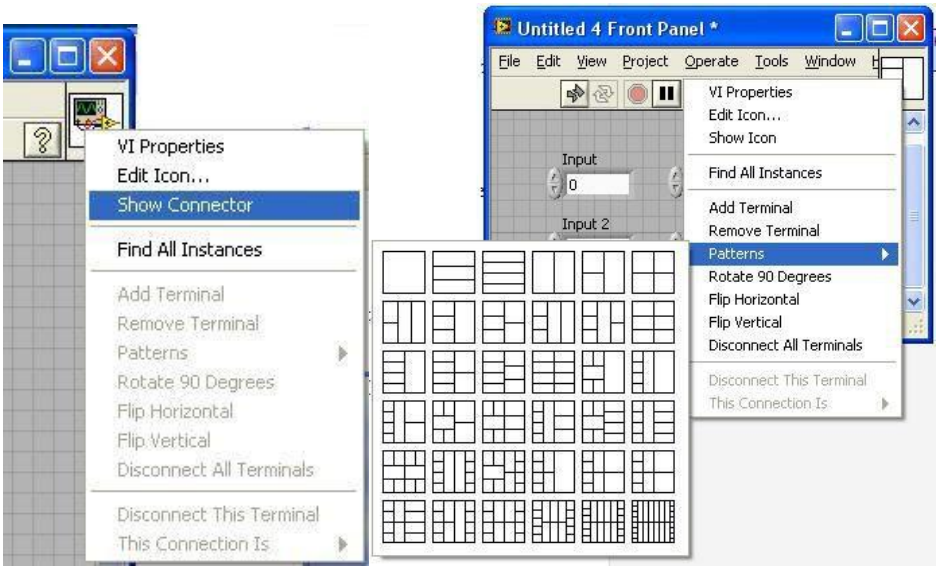

Figure 2. 18 Connector pane and patterns

As mentioned earlier, the front panel window offers tools menus and controls over all the controls required for the application. In LabVIEW programming, the command that we are expecting to be performed by the interfaced components is termed as coding. The coding is done by the selecting functional controls in the front panel window and if it is appropriate block can be added to the block diagram. Furthermore, signal generators, buttons (to turn on and off the experiment, sensor, meters, etc.), displays and graphs suitable based on the experiment can be added (Christiano, 2015).

In the block diagram inputs and outputs of the desired control over the experiment or device can be wired and configured. The generated program can run, aborted or paused from either front panel or from block diagram. The block diagram also supplements troubleshooting feature to figure out and resolve the errors in the programming.

Figure 2. 19 Toolbar features in LabVIEW

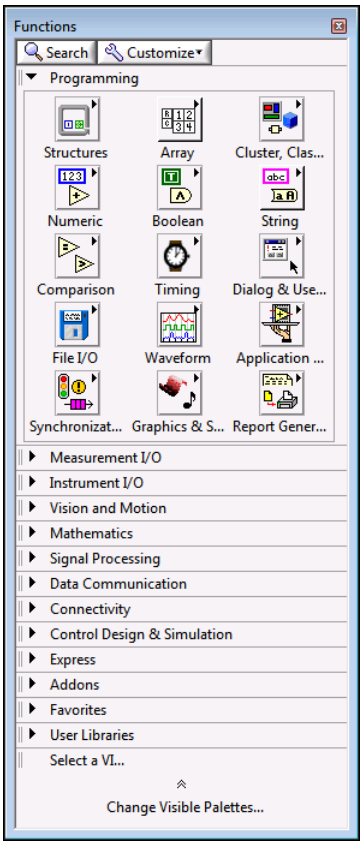

Figure 2. 20 Functions in LabVIEW programming

Wires (wires feature) are used to transfer the data among the block diagram. Wires connect the control and indicator terminals to the function. Each wire signals the data source, and it can be wired to numerous functions and VI that can read data. Different wire patterns can be used based on the data source. It also provides a feature that shows broken wire line for the incompatibility between two objects and data types if incompatible wire pattern is used, i.e. two indicators together, array output to the numeric input (National Instruments, 2019). Furthermore, if selected

object has to be moved in the block diagram close towards the other objects, LabVIEW temporary connects it with the wire, and once we release the mouse cursor holding the object, it automatically connects object and the wire. It connects two terminals that are suitable for one another automatically, as well we can perform manual wiring based on the required arrangement of the interfaced objects (National Instruments, 2019).

The LabVIEW provides built-in VI and functions that can be used to manipulate strings, format strings and edit the strings, which appears as a table, text entry box and labels. LabVIEW also represents numeric data as a fixed number, integer and complex number, complex numeric data with an orange colour and integer data in blue. Further, it also stores Boolean data as 8-bit values to represent binary code as a 0 or 1; TRUE or FALSE. The common application includes representation of the digital data and on the front panel control, which acts as a switch with the mechanical action that can be used to control execution. Usually, green coloured controls represent Boolean data.

Another essential function is Array, that combines data points of the same data type into a one data structure and cluster combines data points of the multiple types into a single data structure. It can be built from numeric, Boolean, path, string and cluster data types. Usually, arrays are preferred to the collection of similar data points, and repetitive computation has to be performed. Additionally, it stores collected data from the generated data loops during the program coding, where each iteration of a program loop produces one element of the array. LabVIEW provides auto indexing by default for every array wired for Loop input terminal (National Instruments, 2019). After auto-indexing, output array receives a new element from every iteration of the Loop.

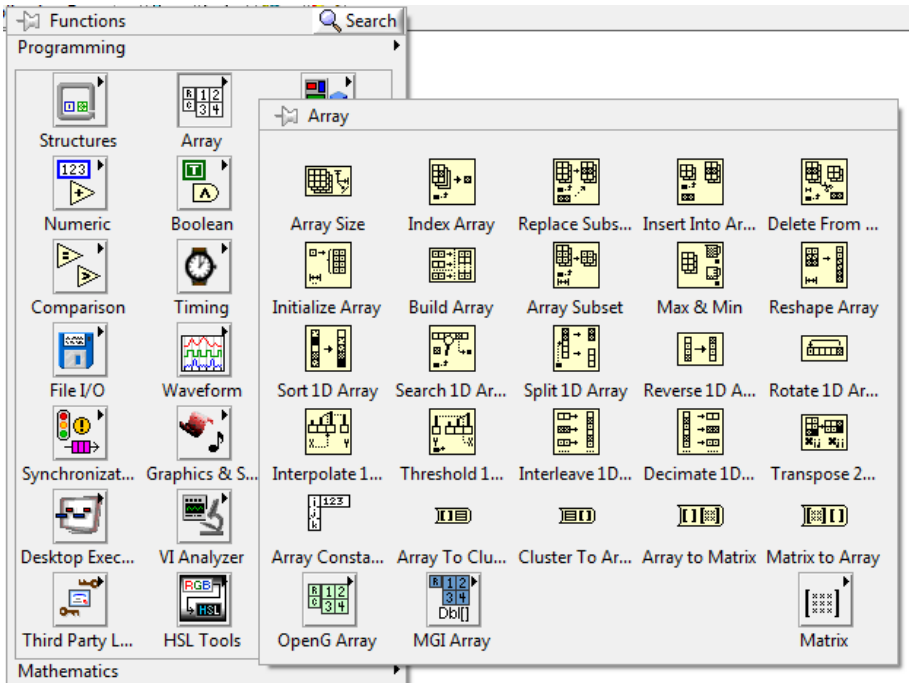

Figure 2. 21 LabVIEW expanded functions

Execution structures contain sections of the graphical code that provides control over the code functioning to run and stop the code. As mentioned earlier, most preferred execution structures are loops. When coding with the loops, data from previous structures have to be forwarded from previous iterations. Hence shift registers are used. Shift registers allow to pass values from the previous iteration through the loop to the next iteration. The terminal on the right side of the loop contains an up arrow and stores a data on the completion of an iteration of the front panel. The LabVIEW transfers the data associated with the right side of the register to the next iteration. After the loop executes, the terminal on the right side of the loop returns the last value stored in the shift register. Likewise, with the stacked shift register, we can access data from the previous loop iteration. Stacked shift register stores value from multiple iterations and carry these values to the next iteration.

Another feature of the LabVIEW is error handling. Usually, LabVIEW handles and resolves error automatically by default settings when VI runs the program by suspending execution, as shown in the following figure. It also highlights the subVI or function where an error has error occurred, with the displaying the error, in the dialogue box.

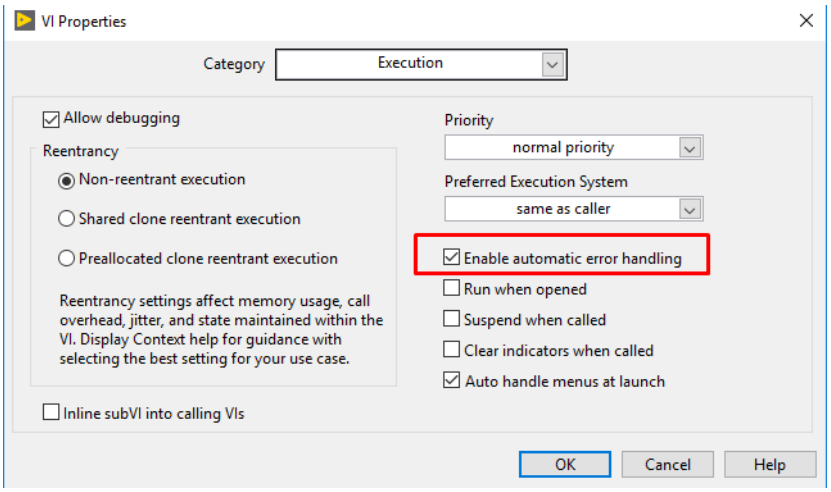

Figure 2. 22 VI properties and features

If right clicked on the error, it explains the error. Figure 2.23 shows the sample example of the Explain error feature.

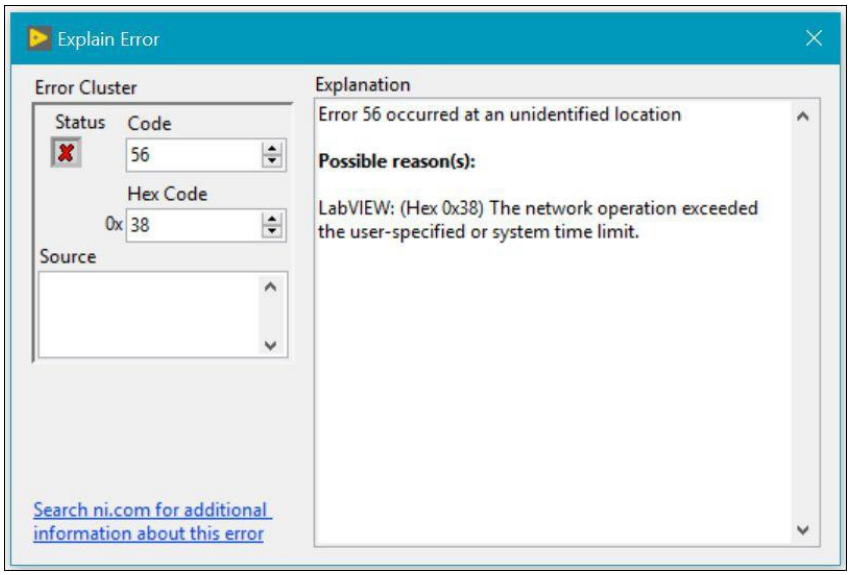

Figure 2. 23 LabVIEW error resolve feature

Virtually all the controls and functions in the LabVIEW can be configured, allowing each project to be custom-made to specialized requirements. To generate the block diagram and configured system components based on the coding.

2.11.2 Previously followed LabVIEW based experimental applications

Previously, there have been numerous applications developed by using LabVIEW graphical interface to develop control systems, monitoring systems and experimental analysis (Lin et al., 2011; Mohamed et al., 2018; Samah et al., 2017). Lin et al. (2011) developed a measurement method based on the LabVIEW and mathematical interpolation, for the domain wavelength (for visible light spectrum) of the LED based on the microcomputer interface and photoelectric interface, to control stepping motor movement along with the monochromator to obtain magnitude of the voltage received with the help of the spectrometer. Mohamed et al. (2018) developed an Intelligent Lighting Control System (ILCS), for ergonomic setting and energy efficiency with NI LabVIEW to design Graphical User Interface (GUI) to perform control over light dimming and adjustment feature.

Samah et al. (2017) performed analysis over efficiency and the suitability of an optical sensing mechanism for monitoring the water turbidity, with the LabVIEW based monitoring systems to evaluate the sample turbidity with the calibrated turbidimeter and photodetector configuration for different light wavelengths. The system was programmed to display the turbidity in NTU unit by using linear conversion between 0 to 9 volts and 0 to 1000 NTU. The program enables real-time measurement of water turbidity, which was displayed in the graphical user interface to indicate a continuous changing turbidity parameter.

2.12 Overview of Arduino and LabVIEW interface

The NI LabVIEW toolkit allows interface LabVIEW with the Arduino microcontroller, to control or acquire data from the Arduino microcontroller. (National Instruments, 2019; Navvenkumar and Krishna, 2013). Once the data is obtained, LabVIEW analyzes it by using built-in libraries and developed algorithms to perform control over the Arduino hardware assembly and delivers results on a User Interface (UI). A sketch for the Arduino microcontroller acts as an I/O platform that interfaces with LabVIEW VI's through a sequential linkage, allowing quick transfer of the information from Arduino pins (refer section 2.10.1) to LabVIEW program without the need of altering the communication, synchronization of the code. By using simple commands Open, Read, Write and, Close in the LabVIEW, to approach the digital and analog signals of the Arduino microcontroller.

The Arduino and LabVIEW provide a creative interface, which interacts with the system through a graphical interface, allows experiment design process with perceptive graphical programming with improved debugging. Furthermore, open Application Programming Interface (API) provides customization of the experiment and automation based on the specific needs of the user.

2.12.1 Previously developed Arduino and LabVIEW interfaces.

Hammoumi et al. (2019) developed a virtual instrument to monitor and trace the power-voltage (P-V) and current-voltage (I-V) characteristics of the photovoltaic (PV) panel based on the Arduino acquisition board and LabVIEW using LIFA interface. The current and voltage sensor detects the output current from the PV panel and measured data of the current, voltage and power was directly plotted on the monitoring platform developed by the LabVIEW. Jamaluddin et al. (2013) designed a real-time battery monitoring system (BMF) using the LabVIEW interface for the Arduino. The device was used for the sensing of battery voltage based on the current detection of the by the current sensor. The purpose of this experiment was to study moment and the kinetic energy by the inelastic and elastic collision between the two objects.

Furthermore, Jena et al. (2015) developed computerized greenhouse data acquisition system using Arduino with the LabVIEW to measure soil moisture, light and carbon dioxide (CO_2) for the simulation to obtain improved growth of the plants in the greenhouse. The monitoring system was established using calibrated sensors for detecting ambient temperature, humidity, CO_2, soil moisture and light intensity inside the greenhouse. The sensors were configured to Arduino board for the acquisition of the data through analog and digital I/O (input and output) which was processed by GUI through the LabVIEW coding. The developed system allowed continuous monitoring of the greenhouse environ characteristics to facilitate maximum plant growth. The working principle of the Arduino and LabVIEW based set-up automation and control of the stepper motor for the mounted UV light sensor is explained in Chapter 3.

2.13 References

Alfano, O. M., Romero, R. L., & Cassano, A. E. (1986). Radiation field modelling in photoreactors—I. homogeneous media. *Chemical Engineering Science*, *41*(3), 421-444. doi:10.1016/0009-2509(86)87025-7

A. M. Gibb, New media art, design, and the Arduino microcontroller: A malleable tool. PhD thesis, Pratt Institute, 2010.

Arduino-Getting Started. (2017, October 10). Retrieved April 29, 2019, from https://www.arduino.cc/en/Guide/HomePage

Awwa Research Foundation (Awwa RF), & New York State Energy Research and Development Authority (NYSERDA). (2007). *Optimization of UV Disinfection* (NYSERDA Report Number 07-07 1P-4C-91184-11/07-NH). Retrieved from https://www.nyserda.ny.gov/Optimization-of-UV-Disinfection

Badamasi, Y. A. (2014). The Working Principle of An Arduino. In *2014 11th International Conference on Electronics, Computer and Computation (ICECCO)*. doi:10.1109/ICECCO.2014.6997578

Blatchley, E. R. (1997). Numerical modelling of UV intensity: Application to collimated-beam reactors and continuous-flow systems. *Water Research*, *31*(9), 2205-2218. doi:10.1016/s0043-1354(97)82238-5

Bloem, J., Bouwknegt, A., & Wesselink, G. A. (1977). Some new mercury alloys for use in fluorescent lamps. *Journal of the Illuminating Engineering Society*, *6*(3), 141-147. Doi:10.1080/00994480.1977.10747809

Bohrerova, Z., & Linden, K. G. (2007). Standardizing photoreactivation: Comparison of DNA photorepair rate in Escherichia coli using four different fluorescent lamps. *Water Research*, *41*(12), 2832-2838. doi: 10.1016/j.watres.2007.03.015

Bolton, J.R. 2002. New Developments in UV Photolysis and Advanced Oxidation, Proc. First Asia Regional Conference of Ultraviolet Technologies for Water, Wastewater & Environmental Applications, CDROM, International Ultraviolet Association, PO Box 1110, Ayr, ON, Canada N0B 1E0.

Bolton, J.R. and Cater, S.R. 2004. Homogeneous photodegradation of pollutants in contaminated water: An introduction, In Aquatic and Surface Photochemistry, Helz, G. R., Zepp, R. G. and Crosby, D. G., Eds., Lewis, Boca Raton, FL, pp. 467-490.

Bolton, J. R., & Cotton, C. (2008). *The Ultraviolet Disinfection Handbook* (1st ed.). Denver, CO: American Water Works Association.

Borsuk, J., & Armitage, D. (2010). UV Spectral Stability as it relates to the UV Bulb Temperature. In 2010 *UV & EB Technical Conference Proceedings*. Retrieved from https://www.radtech.org/proceedings/2010/papers/1497.pdf

Brandt, C. L., Giese A.C., (1956). Photoreversal of nuclear and cytoplasmic effects of short ultraviolet radiation on paramecium caudatum. *The Journal of General Physiology*, *39*(5), 735-751. doi:10.1085/jgp.39.5.735

Calvert, J. G., & Pitts, I. (1966). Photochemistry. *Journal of Chemical Education*, *43*(10), 564. doi:10.1021/ed043p564.2

Chadysiene, R., & Girgzdys, A. (2009). Assessment of ultraviolet (UV) radiation from technical sources. *Journal Of Environmental Engineering and Landscape Management*, *17*(3), 164-170. doi:10.3846/1648-6897.2009.17.164-170

Chan, Y., & Killick, E. (1995). The effect of salinity, light and temperature in a disposal environment on the recovery of E.coli following exposure to ultraviolet radiation. *Water Research*, *29*(5), 1373-1377. doi:10.1016/0043-1354(94)00226-w

Chevrefils, G., Caron, E., Malayeri, A. H., Mohseni, M., Cairns, B., Bolton, J., & Barbeau, B., Wright, H., Linden, K. G. (2006). Fluence (UV Dose) Required to Achieve Incremental Log Inactivation of Bacteria, Protozoa, Viruses and Algae. *IUVA News*, (8), 38-45. Retrieved from https://www.iuvanews.com/stories/pdf/archives/180301_UVSensitivityReview_full.pdf

Clinical Laboratory Evaluation Program, Laboratory Standards. Quality Assurance Standard 21 Guidance. Wadsworth Center, New York State Department of Health. Available at: www.wadsworth.org/labcert/clep/Survey/ standardsmenu.htm. Accessed August 28, 2006.

Christiano, M. (2015, December 28). *An Intro to Labview and Graphical Programming Languages*. Retrieved from All about Circuits website: https://www.allaboutcircuits.com/technical-articles/graphical-programming-languages-labview/

Dai, T., Vrahas, M. S., Murray, C. K., & Hamblin, M. R. (2012). Ultraviolet C irradiation: an alternative antimicrobial approach to localized infections? *Expert Review of Anti-infective Therapy*, *10*(2), 185-195. doi:10.1586/eri.11.166

Darby, J. L., Snider, K. E., & Tchobanoglous, G. (1993). Ultraviolet disinfection for wastewater reclamation and reuse subject to restrictive standards. *Water Environment Research*, *65*(2), 169-180. doi:10.2175/wer.65.2.10

Downes, A., & Blunt, T. P. (1877). Researches on the effect of light upon bacteria and other organisms. *Proceedings of the Royal Society of London*, *26*(179-184), 488-500. doi:10.1098/rspl.1877.0068

Druyvesteyn, M. J., & Penning, F. M. (1941). Errata: Mechanism of Electrical Discharges in Gases of Low Pressure. *Reviews of Modern Physics*, *13*(1), 72-73. doi:10.1103/revmodphys.13.72

Dulbecco, R. (1952). Experiments on photoreactivation of inactive bacteriophages. *Journal of Cellular and Comparative Physiology*, *39*(S1), 125-128. doi:10.1002/jcp.1030390413

Drinking Water Inspectorate, DWI guidance on the use of ultraviolet (UV) irradiation for the disinfection of public water supplies. (2016). Retrieved from Drinking Water Inspectorate website: http://www.dwi.gov.uk/stakeholders/guidance-and-codes-of-practice/uv-irradiation.pdf

Emerick, R. W., Loge, F. J., Thompson, D., & Darby, J. L. (1999). Factors Influencing Ultraviolet Disinfection Performance Part II: Association of Coliform Bacteria with Wastewater Particles. *Water Environment Research*, *71*(6), 1178-1187. doi:10.2175/106143097x122004

Emerick, R. W., Loge, F. J., Ginn, T., & Darby, J. L. (2000). Modeling the Inactivation of Particle-Associated Coliform Bacteria. *Water Environment Research*, *72*(4), 432-438. doi:10.2175/106143000x137969

Erturk, F., Ugur, E., Olson, J., & Akin, B. (2019). Real-Time Aging Detection of SiC MOSFETs. *IEEE Transactions on Industry Applications*, *55*(1), 600-609. doi:10.1109/tia.2018.2867820

Franke, S., Lange, H., Schoepp, H., & Witzke, H. (2006). Temperature dependence of VUV transmission of synthetic fused silica. *Journal of Physics D: Applied Physics*, *39*(14), 3042-3046. Doi:10.1088/0022-3727/39/14/025

Friedberg, E. R., Walker, G. C. and Siede, W. (1995). DNA Repair and Mutagenesis, p. 92-107. ASM Press, Washington, D.C.

Friedberg, E.C., Walker, G.C., Siede, W., Wood, R.D., Schultz, R.A. and Ellenberger, T. (2006) DNA Repair and Mutagenesis. 2nd Edition, ASM Press, Washington DC

Garipov, G. K., Khrenov, B. A., Klimov, P. A., Morozenko, V. S., Panasyuk, M. I., Petrova, S. N., … Cotsomi, J. P. (2010). Program of transient UV event research at Tatiana-2 satellite. *Journal of Geophysical Research: Space Physics*, *115*(A5). doi:10.1029/2009ja014765

Gates, F. L. (1929). A study of the bactericidal action of ultra violet light: i. The reaction to monochromatic radiations. *The Journal of General Physiology*, *13*(2), 231-248. doi:10.1085/jgp.13.2.231

Germicidal Lamp Basics, Light Sources Inc., 2013.

Goin, J., Skirda, A., & Tohktuev, E. (2004). Understanding UV monitoring for air and water UV treatments. *IUVA News, 6(1): 29–35*, *6*(1), 29-35. Retrieved from https://iuvanews.com/stories/pdf/archives/060102Goin%20Paper.pdf

Gonzalez, M. C., & Braun, A. M. (1995). VUV photolysis of aqueous solutions of nitrate and nitrite. *Research on Chemical Intermediates*, *21*(8-9), 837-859. doi:10.1163/156856795x00512

Hammoumi, A. E., Motahhir, S., Chalh, A., Ghzizal, A. E., & Derouich, A. (2018). Real-time virtual instrumentation of Arduino and LabVIEW based PV panel characteristics. *IOP Conference Series: Earth and Environmental Science*, *161*, 012019. doi:10.1088/1755-1315/161/1/012019

Hanzon, B. D., & Vigilia, R. (1999). Two Experts Offer Practical Guidance in Designing and Operating Ultraviolet Disinfection Systems. *Water Environment and Technology*, 35-42.

Hanawalt, P. C., Cooper, P. K., Ganesan, A. K., & Smith, C. A. (1979). DNA Repair in Bacteria and Mammalian Cells. *Annual Review of Biochemistry*, *48*(1), 783-836. doi:10.1146/annurev.bi.48.070179.004031

Harley, S., Schuba, B., & Corkal, D. (2008). Ultraviolet Disinfection of Private Water Supplies for Household or Agricultural Uses. Retrieved from Agriculture and Agri-food Canada website: http://www5.agr.gc.ca/resources/prod/doc/terr/pdf/uv_tech_bull_e.pdf

Harrington, B., & Valigosky, M. (2007). Monitoring Ultraviolet Lamps in Biological Safety Cabinets with Cultures of Standard Bacterial Strains on TSA Blood Agar. *Laboratory Medicine*, *38*(3), 165-168. doi:10.1309/wa952bxgdr2uqxna

Havelaar, A. H. Nieuwstad, Th. J., Meulemans, C. C. E. and van Olphen. M. (1991). F-specific RNA bacteriophages as model viruses in UV disinfection of wastewater. *Water Science Technology*, *24*(2), 347-352.

Heath, M., Wright, H., & Schmalwieser, A. W. (2013). UV lamp aging is predicted by direct measurement of UV transmittance. *International Ozone Association, International Ultraviolet Association Proceedings of the World Congress and Exposition, September 22-26, 2013, Las Vegas, Nevada*

Heberlein, J., Mentel, J., & Pfender, E. (2009). The anode region of electric arcs: a survey. *Journal of Physics D: Applied Physics*, *43*(2), 023001. doi:10.1088/0022-3727/43/2/023001

Heering, W. (2004). UV SOURCES – Basics, Properties and Applications. *IUVA NEWS*, *6*(4), 7-13. Retrieved from https://iuvanews.com/stories/pdf/archives/060401Heering_2004.pdf

Henry, V., Helbronner, A., and Recklinghausen, M., Nouvelles recherches sur la sterilization de grandes quantited d'eau par les rayons ultraviolets, *Comptes Rendus des Scéances de l'Academie des Sciences* 151: 677–680.

Jacob, S. M., & Dranoff, J. S. (1970). Light intensity profiles in a perfectly mixed photoreactor. *AIChE Journal*, *16*(3), 359-363. doi:10.1002/aic.690160309

Jena, S. P., Aman, S., & Das, R. (2015). Computerized Green House Data Acquisition System Using Arduino with LabVIEW. *International Journal of Advanced Research in Electrical, Electronics and Instrumentation Engineering*, *4*(4), 2350-2357. doi:10.15662/ijareeie.2015.0404046

Jin, S., Sharpless, C., Linden, K., Kelly, R., & Ferran, B. (2007). Aging evaluation of medium-pressure mercury lamps under typical operating conditions for drinking water disinfection applications. *Proceedings of the Water Environment Federation*, *2007*(1), 276-292. doi:10.2175/193864707787932171

Jolis, D., Lam, C., & Pitt, P. (2001). Particle Effects on Ultraviolet Disinfection of Coliform Bacteria in Recycled Water. *Water Environment Research*, *73*(2), 233-236. doi:10.2175/106143001x139218

Kuhn, H. J., Braslavsky, S. E., & Schmidt, R. (2004). Chemical actinometry (IUPAC Technical Report). *Pure and Applied Chemistry*, *76*(12), 2105-2146. doi:10.1351/pac200476122105

Lankhorst, M. H., & Niemann, U. (2000). ChemInform Abstract: Amalgams for Fluorescent Lamps. Part 1. Thermodynamic Design Rules and Limitations. *ChemInform*, *31*(48), no-no. doi:10.1002/chin.200048008

Lau, J., Bahnfleth, W., Kremer, P., & Freihaut, J. (2008). Investigation of surface temperature distributions of UVC lamps under variable flow conditions using infrared camera measurements. In *Indoor Air 2008, Copenhagen, Denmark*. Retrieved from https://www.isiaq.org/docs/papers/133.pdf

Lin, C. R., Wei, D. H., BenDao, M. K., Chen, W. E., & Liu, T. Y. (2014). Development of High-Performance UV Detector Using Nanocrystalline Diamond Thin Film. *International Journal of Photoenergy*, *2014*, 1-8. doi:10.1155/2014/492152

Lin, W. G., Wang, Y. F., & Yang, M. Z. (2011). The Measurement of LED Domain Wavelength Based on LabVIEW. *Advanced Materials Research*, *228-229*, 759-763. doi:10.4028/www.scientific.net/amr.228-229.759

Lindenauer, K. G., & Darby, J. L. (1994). Ultraviolet disinfection of wastewater: Effect of dose on subsequent photoreactivation. *Water Research*, *28*(4), 805-817. doi:10.1016/0043-1354(94)90087-6

Linden, K. G., Shin, G., Faubert, G., Cairns, W., & Sobsey, M. D. (2002). UV Disinfection of Giardia lamblia Cysts in Water. *Environmental Science & Technology*, *36*(11), 2519-2522. doi:10.1021/es0113403

Lindsey, J. L. (1997). *Applied Illumination Engineering* (2nd ed.). The Fairmont Press, Inc.

Loge, F. J., Emerick, R. W., Thompson, D. E., Nelson, D. C., & Darby, J. L. (1999). Factors Influencing Ultraviolet Disinfection Performance Part I: Light Penetration to Wastewater Particles. *Water Environment Research*, *71*(3), 377-381. doi:10.2175/106143097x122176

Lorch, W. (1987). *Handbook of Water Purification 2nd Edition.* Ellis Horwood Limited, Chichester, United Kingdom.

MA Lamp Electrodes. (2003, August 25). Retrieved April 22, 2019, from http://www.lamptech.co.uk/Documents/M8G%20MA%20Electrodes.htm

Madge, B. A., & Jensen, J. N. (2006). Ultraviolet Disinfection of Fecal Coliform in Municipal Wastewater: Effects of Particle Size. *Water Environment Research*, *78*(3), 294-304. doi:10.2175/106143005x94385

Malley, J. P., Ballester, N. A., Margolin, A. B., Linden, K. G., Mofidi, A., Bolton, J. R., Crozes G., Cushing B., Mackey, E., Laine J. M. and Janex M. L. (2004). Inactivation of Pathogens with Innovative UV Technologies. American Water Works Association Research Foundation, USA.

Mamane, H. (2011). Impact of Particles on UV Disinfection of Water and Wastewater Effluents: A Review. *Reviews in Chemical Engineering*, 24(2-3), pp. 67-157. Retrieved 14 May. 2019, from doi:10.1515/REVCE.2008.24.2-3.67

Margolis, M. (2011). *Arduino Cookbook*. Sebastopol, CA: O'Reilly Media.

Martin, N., & Gehr, R. (2007). Reduction of Photoreactivation with the Combined UV/Peracetic Acid Process or by Delayed Exposure to Visible Light. *Water Environment Research*, *79*(9), 991-999. doi:10.2175/106143007x214010

Masschelein, W. J. (2002). *Ultraviolet Light in Water and Wastewater Sanitation*. R. G. Rice (Ed.). Boca Raton, FL: Lewis Publishers CRC Press Company

McLeod, A., Hovde Liland, K., Haugen, J., Sørheim, O., Myhrer, K. S., & Holck, A. L. (2017). Chicken fillets subjected to UV-C and pulsed UV light: Reduction of pathogenic and spoilage bacteria, and changes in sensory quality. *Journal of Food Safety*, *38*(1), e12421. doi:10.1111/jfs.12421

Minns, P. D. (2013). *C Programming For the PC the MAC and the Arduino Microcontroller System*. Bloomigton, IN: Author House.

Mohamed, S., Minhat, M., Kasim, M., Adam, M., Sulaiman, M., & Rizman, Z. (2018). An Intelligent Lighting Control System (ILCS) using LabVIEW. *Journal of Fundamental and Applied Sciences*, *9*(2S), 602. doi:10.4314/jfas.v9i2s.38

National Instruments. (2019). Dataflow Programming Basics in NI LabVIEW – National Instruments. Retrieved April 26, 2019, from http://www.ni.com/getting-started/labview-basics/dataflow

National Instruments. (2019, January 10). Installing LabVIEW Interface for Arduino Toolkit Using VI Package Manager. Retrieved April 29, 2019, from https://knowledge.ni.com/KnowledgeArticleDetails?id=kA00Z000000PAS1SAO&l=en-CA

Nessim, Y., & Gehr, R. (2006). Fouling Mechanisms in a Laboratory-Scale UV Disinfection System. *Water Environment Research*, *78*(12), 2311-2323. doi:10.2175/106143006x95474

Newsome, D. (2006). *UV Lights & Lamps – A Manufacturer's Perspective* (FMS#14). Retrieved from UV SYSTEMS, Inc website: https://uvsystems.com/wp-content/uploads/uv_lights_lamps_1-27-2006_5.pdf

Oguma, K., Katayama, H., & Ohgaki, S. (2005). Spectral impact of inactivating light on photoreactivation ofEscherichia coli. *Journal of Environmental Engineering and Science*, *4*(Supplement 1), S1-S6. doi:10.1139/s04-048

Omnès, F., Monroy, E., Muñoz, E., & Reverchon, J. (2007). Wide bandgap UV photodetectors: a short review of devices and applications. *Gallium Nitride Materials and Devices II*, *6473*I. doi:10.1117/12.705393

Pan, A., & Zhu, X. (2015). Optoelectronic properties of semiconductor nanowires. In J. Arbiol & Q. Xiong (Eds.), *Semiconductor Nanowires Materials, Synthesis, Characterization and Applications* [Woodhead Publishing Series in Electronic and Optical Materials] (pp. 327-363). Retrieved from doi.org/10.1016/B978-1-78242-253-2.00012-8

Photoelectric effect. (2018). In E. Gregersen (Ed.), *Encyclopaedia Britannica*. Retrieved from https://www.britannica.com/science/photoelectric-effect

Ponce, E. (2017). Ultraviolet radiation detector to obtain the energy and rate of particles at different heights. *Proceedings of 35th International Cosmic Ray Conference — PoS(ICRC2017)*. doi:10.22323/1.301.0236

Qualls, R. G. and Johnson, J. D. (1983). Bioassay and dose measurement in UV disinfection. *Applied Environmental Microbiology, 45*, 872-877.

Razeghi, M., & Rogalski, A. (1996). Semiconductor ultraviolet detectors. *Journal of Applied Physics*, *79*(10), 7433-7473. doi:10.1063/1.362677

Redwitz, M., Dabringhausen, L., Lichtenberg, S., Langenscheidt, O., Heberlein, J., & Mentel, J. (2006). Arc attachment at HID anodes: measurements and interpretation. *Journal of Physics D: Applied Physics*, *39*(10), 2160-2179. doi:10.1088/0022-3727/39/10/028

Reed, N. G. (2010). The history of ultraviolet germicidal irradiation for air disinfection. *Public Health Reports*, *125*(1), 15-27. doi:10.1177/003335491012500105

Şahin, Ö., Tapan, İ., Özmutlu, E. N., & Veenhof, R. (2010). Penning transfer in argon-based gas mixtures. *Journal of Instrumentation*, *5*(05), P05002. doi:10.1088/1748-0221/5/05/p05002

Samah, A. H., Rahman, M. F., Omar, A. F., Ahmad, K. A., & Yahaya, S. Z. (2017). Sensing mechanism of water turbidity using LED for in situ monitoring system. *2017 IEEE 7th International Conference on Underwater System Technology: Theory and Applications (USYS)*. doi:10.1109/usys.2017.8309443

Scheible, O.K. and Bassell, C.D. (1981). Ultraviolet Disinfection of a Secondary Wastewater Treatment Plant Effluent EPA-600/S2- B1-152. United States Environmental Protection Agency,Cincinnati, OH, USA.

Scheible O. K., Casey M. C. and Forndran A. (1985). Ultraviolet disinfection of wastewaters from secondary effluent and combined sewer overflows. Report No. EPA/ 600/2-86/005. US Environmental Protection Agency, National Technical Information Service, Spring®eld, VA.

Schmalwieser, A. W., Wright, H., Cabaj, A., Heath, M., Mackay, E., & Schauberger, G. (2014). Aging of low-pressure amalgam lamps and UV dose delivery. *Journal of Environmental Engineering and Science*, *9*(2), 113-124. doi:10.1680/jees.13.00009.

Schöpp, H., & Steffen, F. (2016). Mercury Vapour Lamps. In R. Karlicek, C. Sun, G. Zissis, & R. Ma (Eds.), *Handbook of Advanced Lighting Technology* (pp. 1080-1093). doi:10.1007/978-3-319-00176-0

Sheriff, M., & Gehr, M. (2001). Laboratory investigation of inorganic fouling of low pressure UV disinfection lamps. *Water Quality Research Journal*, *36*(1), 71-92. doi:10.2166/wqrj.2001.00

Sommer, R. and Cabaj. A. (1993). Evaluation of the efficiency of a UV plant for drinking water disinfection. *Water Science Technology 27*(3-4),357-362.

Sommer, R., Cabaj, A., Haider, T., & Hirschmann, G. (2004). UV Drinking Water Disinfection – Requirements, Testing and Surveillance: Exemplified by the Austrian National Standards M 5873-1 and M 5873-. *IUVA News*, *6*(4), 28-35. Retrieved from https://www.iuvanews.com/stories/pdf/archives/060404SommerEtAl_2004.pdf

Sommer, R., Cabaj, A., Pribil, W., & Haider, T. (1997). Influence of lamp intensity and water transmittance on the UV disinfection of water. *Water Science and Technology*, *35*(11-12), 113-118. doi:10.1016/s0273-1223(97)00244-8

Stefan, M., Kruithof, J. and Kamp, P. 2005. Advanced oxidation treatment for herbicides: From bench-scale studies to full-scale installation, Proceedings of the Third International Congress on Ultraviolet Technologies, Whistler, BC, Canada, International Ultraviolet Association, Ayr, ON, Canada.

Sun, B. Z., Blatchley, E., Oliver, M., Zheng, C., & Jennings, K. (2008). Chemical effects on UV irradiation absorption of fouled quartz sleeves in ultraviolet disinfection. *Water Science and Technology: Water Supply*, *8*(2), 217-222. doi:10.2166/ws.2008.064

Takahashi, S., Abe, T., Nakagawa, A., Kamata, S., Chiba, T., Nakagawa, M., … Osada, H. (2014). Applicability of nitrogen-doped ZnO single crystals for photoconductive type UV sensors. *Physica status solidi I*, *11*(7-8), 1304-1307. Doi:10.1002/pssc.201300625

Tamilvarshini, R. (2018, May 29). Getting Started with LabVIEW: Glow LED with Button. Retrieved March 21, 2019, from https://circuitdigest.com/tutorial/getting-started-with-labview

Templeton, M. R., Andrews, R. C., & Hofmann, R. (2008). Particle-Associated Viruses in Water: Impacts on Disinfection Processes. *Critical Reviews in Environmental Science and Technology*, *38*(3), 137-164. doi:10.1080/10643380601174764

Travis, J., & Kring, J. (2007). *LabVIEW for Everyone: Graphical Programming Made Easy and Fun* (3rd ed.). Retrieved from thesherwoodgang.com/FIRST/Programming/LabVIEW%20For%20Everyone.pdf

U.S. Army Public Health Command (USAPHC). (2004). Ultraviolet Light Disinfection in the Use of Individual Water Purification Devices. Technical Information Paper #31-006-0211

U.S. Environmental Protection Agency (USEPA) (2003). *Ultraviolet Disinfection Guidance Manual*. D.C. Office of Water.

United States Environmental Protection Agency (USEPA) (2006). *Ultraviolet disinfection guidance manual for the final long term 2 enhanced surface water treatment rule (EPA 815-R-06-007).* Retrieved from U.S. Environmental Protection Agency, Office of Water website: https://nepis.epa.gov

Vasils'ev, A. I., Vasilyak, L. M., Kostyuchenko, S. V., Kudryavtsev, N. N., Kuzs'menko, M. E., & Pecherkin, V. Y. (2006). Effect of a protective layer on the lifetime and output radiation intensity decay rate of quartz low-pressure gas discharge lamps. *Technical Physics Letters*, *32*(1), 42-44. doi:10.1134/s1063785006010147

Wait, I. W., & Blatchley, E. R. (2010). Model of Radiation Transmittance by Inorganic Fouling on UV Reactor Lamp Sleeves. *Water Environment Research*, *82*(11), 2272-2278. doi:10.2175/106143010x12681059116491

Wait, I. W., Johnston, C. T., & Blatchley III, E. R. (2007). The Influence of Oxidation Reduction Potential and Water Treatment Processes on Quartz Lamp Sleeve Fouling in Ultraviolet Disinfection reactors. *Water Research*, *41*(11), 2427-2436. doi:10.1016/j.watres.2007.02.057

Water Environment Federation 2004. Water Environment Federation Disinfection Process Survey Summary. *Water Environment Technology 16*(7): 47 and 49.

What is ultraviolet radiation? (2017, November 7). Government of Canada. Retrieved from https://www.canada.ca/en/health-canada/services/sun-safety/what-is-ultraviolet-radiation.html

Whitby, G.E., Palmateer, G., Cook, W. G., Boon, F., and Janzen, E. 1985. The Effects of Wastewater Quality on Ultraviolet Light Disinfection. *Proceedings of Technology Transfer Conference No. 6, Part 2 Water Quality Research*. Ontario Ministry of Environment, Toronto, Ontario, Canada.

Wright, N. G., & Horsfall, A. B. (2007). SiC sensors: a review. *Journal of Physics D: Applied Physics*, *40*(20), 6345-6354. doi:10.1088/0022-3727/40/20/s17

Zimmer, J. L., & Slawson, R. M. (2002). Potential Repair of Escherichia coli DNA following Exposure to UV Radiation from Both Medium- and Low-Pressure UV Sources Used in Drinking Water Treatment. *Applied and Environmental Microbiology*, *68*(7), 3293-3299. doi:10.1128/aem.68.7.3293-3299.2002

Zou, Y., Zhang, Y., Hu, Y., & Gu, H. (2018). Ultraviolet Detectors Based on Wide Bandgap Semiconductor Nanowire: A Review. *Sensors*, *18*(7), 2072. doi:10.3390/s18072072

NOTES

CHAPTER 3

MATERIALS AND METHODOLOGY

This chapter elaborates the information about the arrangement of the direct measurement setup and its components, the functioning of the components and the method followed to perform the analysis of the UV output from the lamp. Furthermore, this chapter contains the schematic diagram of the setup arrangement and the images illustrating the setup components. The idea of the setup arrangement was referred from the previously reported experimental studies by the numerous researchers; however, the setup was modified after confirming the research gaps in previously reported studies. Chapter 2 describes the comprehensive review of the refereed literature to design and develop the experimental setup to conduct the experimental analysis of the UV lamp output for this research. Moreover, the literature review allowed to identify the research gap to modify and advance the setup arrangement with the automation followed by Arduino LabVIEW interface. Furthermore, the setup was modified by the addition of an external Thermal IR camera to observe the non-uniform temperature profile along the length of the lamp.

3.1 Overview of the experiment

The experimental analysis of UV lamp output was performed by direct measurement techniques followed by the horizontal optical bench arrangement. The experiment was performed by measuring irradiance of new LP lamp at 254 nm using narrowband radiometer and photovoltaic sensor. The measurements were logged into a computer by the developed software using LabVIEW programming, interfaced with Arduino microcontroller to control the functioning of the setup through automation. The developed experimental setup and measurements of the UV lamp output was performed at Lakehead University, Thunder Bay, Canada. The experimental analysis was performed for an initial 5% lifetime of the LP lamp, i.e. initial 450 burn-in hours approximately for 2 months on a daily basis. The experimental analysis was performed along the axial length of the lamp in one radial direction, consistently for 450 hours of analysis. The measurement also includes initial output drop by the LP lamp, before the initial drop occurred, i.e. during the first 100 hours before the lamp reached to its stable output.

The observations were logged automatically into the computer by developed program, for every measurement run on an hourly basis for 450 operating hours. During experiment, log of ambient temperature and humidity was maintained. Moreover, along with the radiometry technique to observe UV lamp intensity measurement along the axial length of the lamp; a thermal analysis was performed for the lamp section at the electrode and at the central part to verify the non-uniform temperature profile of the lamp quartz sleeve. The fully functional setup was consisting of UV LP lamp, horizontal optical bench arrangement, UV sensor and research radiometer, LabVIEW based software for data logging, Arduino-LabVIEW interfaced program for automated setup control and thermal IR camera to record the thermal images of the lamp during the lamp operating hours.

As mentioned earlier, in Chapter 1 (section 1.4), one of the objectives of this research was to develop experimental setup and test the functionality of the setup components, for anticipated research outcomes. Furthermore, the final goal of this research was to submit a fully developed and customized setup to Thunder Bay WPCP. In this research, the fully functional and automated direct measurement set up was developed and tested by using LP lamp. The findings of LP lamp output performance and variation in UV intensity has been reported in Chapter 4.

3.2 Experimental arrangement and working mechanism

The experiment was performed with an optical bench horizontal arrangement. The orientation of the measurement setup must be horizontal, as mentioned by the International Ultraviolet Association (IUVA). The measurement was taken in the still room air and at room temperature ~ 20 to 22°C. The setup was covered with the box painted with black heat resistant paint to avoid reflected light. The black box was an additional component to the setup, which was constructed to avoid direct exposure to the UV-C radiation of LP lamp. The LP lamp was mounted on the solid metal frame (aluminum rail) inside the black box. The aluminum rail, sensor adapter housing and IR camera were inside the black box during the experiment. The sensor was configured with the radiometer through sensor input slot on the radiometer (radiometer sensor input has shown in figure 3.13). The functioning of the radiometer was controlled with the LabVIEW based program (i.e. signal receiving on and off).

The UV sensor was mounted on the 3-D printed adapter housing. The linear movement of the adapter housing along the axial length of the UV lamp was enabled with the stepper motor motion controlled by the signal input through the Arduino circuit board via computer supervised program. The sensor adapter housing was assembled with the linear encoder to tract the position of the sensor across the length of the lamp on the aluminum rail. The 3-D printed adapter housing was mounted on the aluminum rail profile for the smoother movement of the sensor on the rail the linear encoder was attached to the aluminum rail from rare side. The linear encoder and the sensor housing were mounted on the lead screw at the ball nut to allow backward and forward movement of the sensor housing and linear encoder, as a result of clockwise and counterclockwise rotation of the stepper motor.

The movement of the sensor housing along with the linear encoder, was controlled with the stepper motor, configured with the Arduino LabVIEW interface. The setup and radiometer functions were controlled with the developed software using LabVIEW programming; however, UV lamp and radiometer were switched on and off manually. The details about the setup components are explained in the following section (section 3.3).

The following figure 3.1 illustrates the arrangement of the measurement setup.

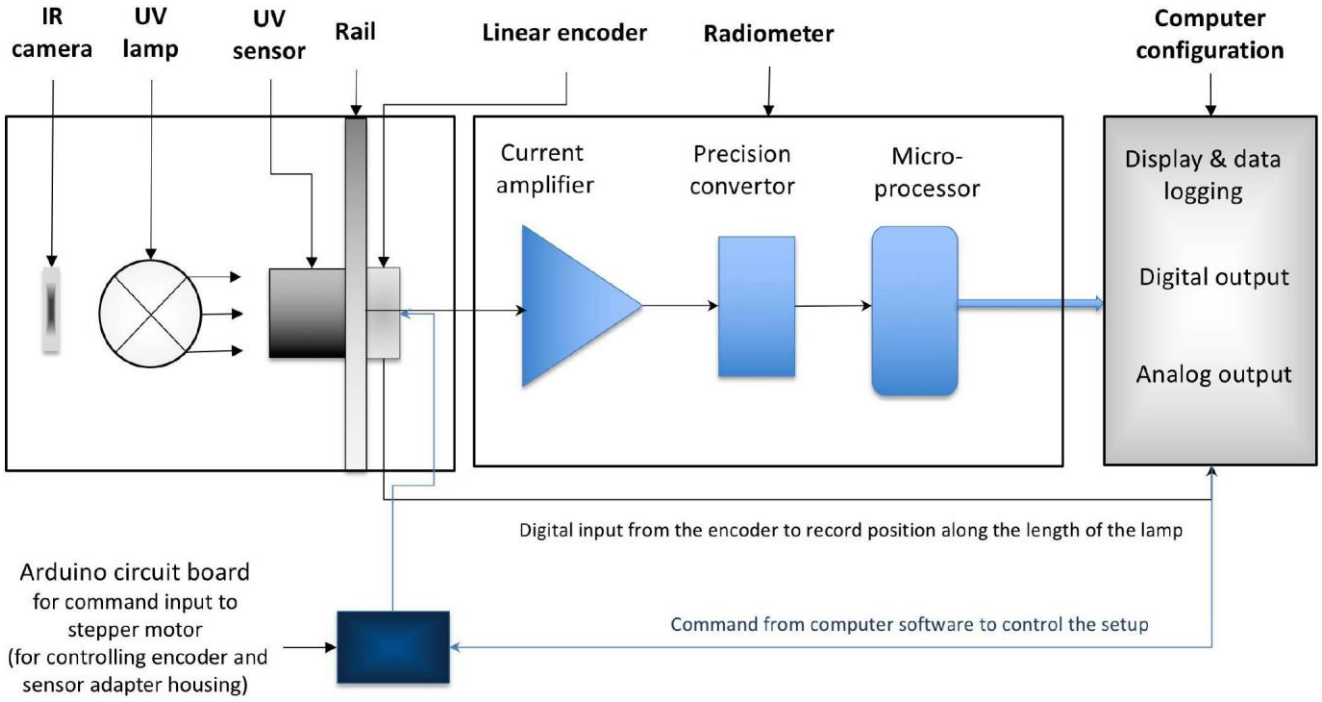

Figure 3. 1 Schematic diagram of the setup

3.3 Setup components

The experimental setup for UV lamp output measurement was comprising of, a mechanical system component (i.e., rail, encoder and sensor housing, stepper motor), electric components (i.e., sensor, radiometer, and circuit board), software for collecting and data logging and thermal imaging camera. The figure 3.2, illustrates the overview of the experimental setup arrangement.

In this section, the setup components are listed, and detailed information of the setup components has described.

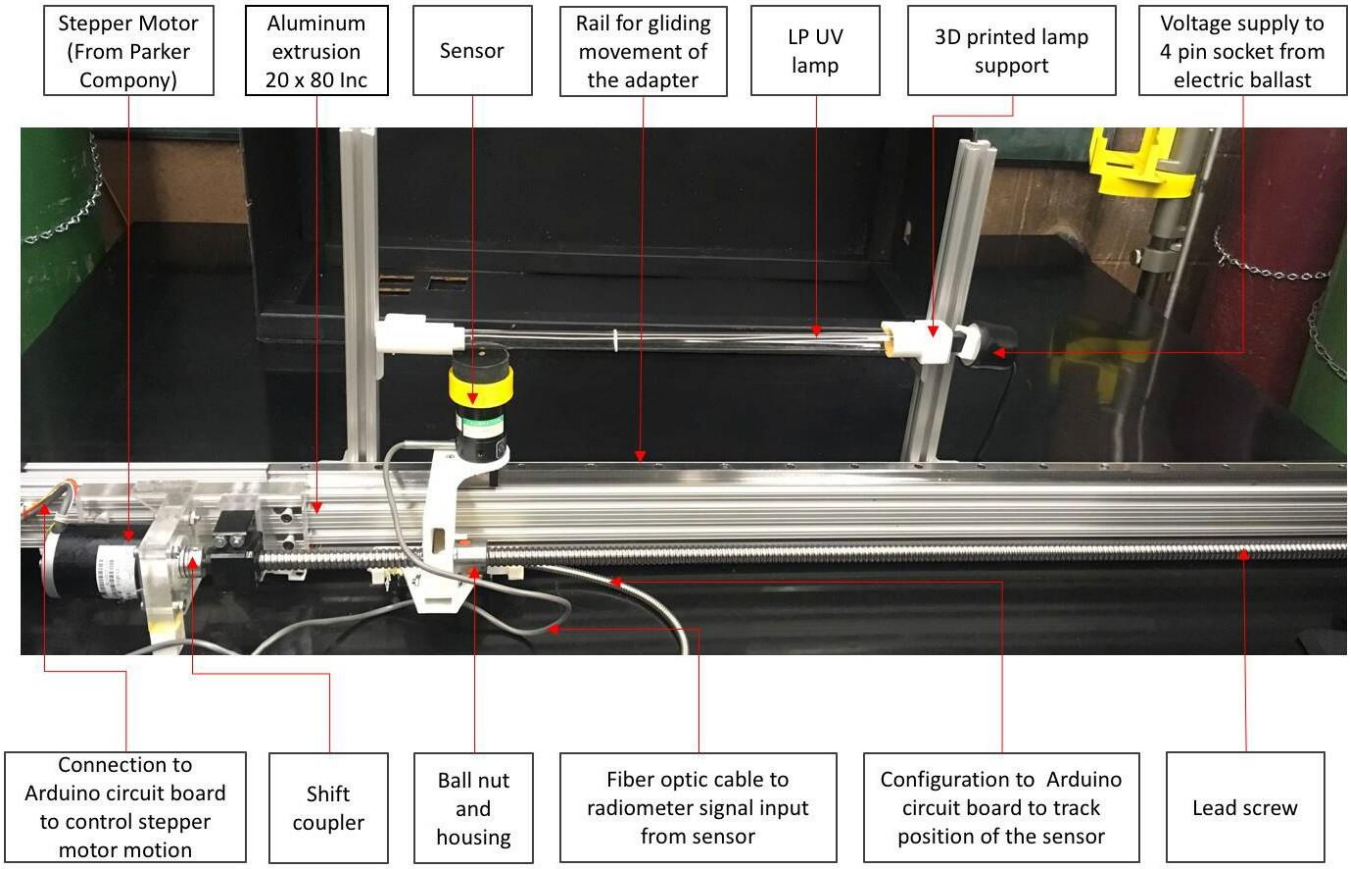

Figure 3. 2 Setup arrangement

3.3.1 UV lamp

To perform the experiment, LP lamp was used model #GPH436T51/4 (4 pin). The lamp base was 4 pins, single ended (B16). The lamp had preheated category for 2 electrodes (wires) with ~ 25 watts lamp wattage and a monochromatic spectrum at 254 nm wavelength. The lamp sleeve was consisting of the fused quartz glass specifically designed for 254 nm wavelength transmission from the glass sleeve. The lamp life expectancy declared by the lamp manufacturer was ~ 9000 hours. The lamp was 436 mm long, and the distance between electrode 400 mm (from cathode to anode distance) and the diameter of the lamp sleeve was 15mm. Based on observation during the 5% lifetime of the lamp, it took ~20 to 30 min to get warm up and emit stable output. However, the lamp was turned on for 30 min before proceeding the experiment. The figure 3.3, illustrates the components of the UV lamp.

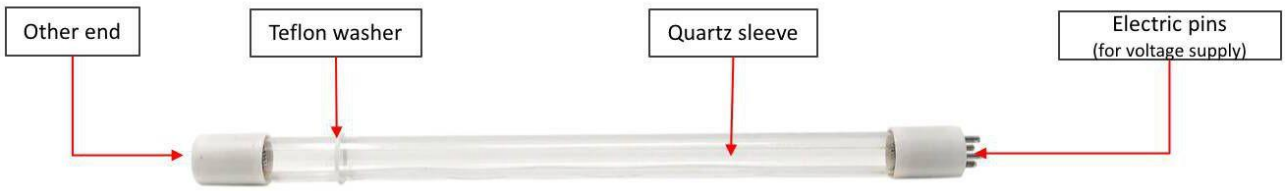

Figure 3. 3 Components of the LP UV lamp

The figure below illustrates the LP UV lamp after proper warm up. The image was clicked from a small window constructed at one side of the black box with UV absorbing glass. (The image has mirror reflection formed at the middle due to glass window).

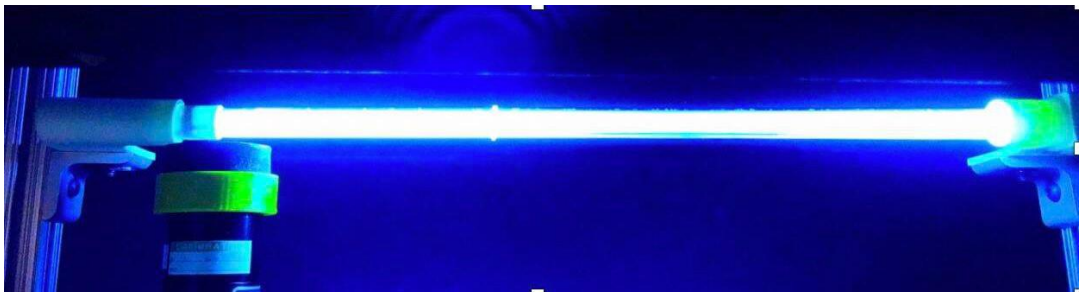

Figure 3. 4 Illumination of the UV lamp after preheating

3.3.2 Power feed, ballast and electric assembly

The lamp was framed on the 3D printed support structure and was mounted on the vertical aluminum extrusion. The vertical extrusion was then attached to set up. However, it was fixed to the rare side of the horizontal aluminum extrusion, to provide rigid support to the elevated lamp arrangement. The arrangement of the UV lamp has shown in the following figure.

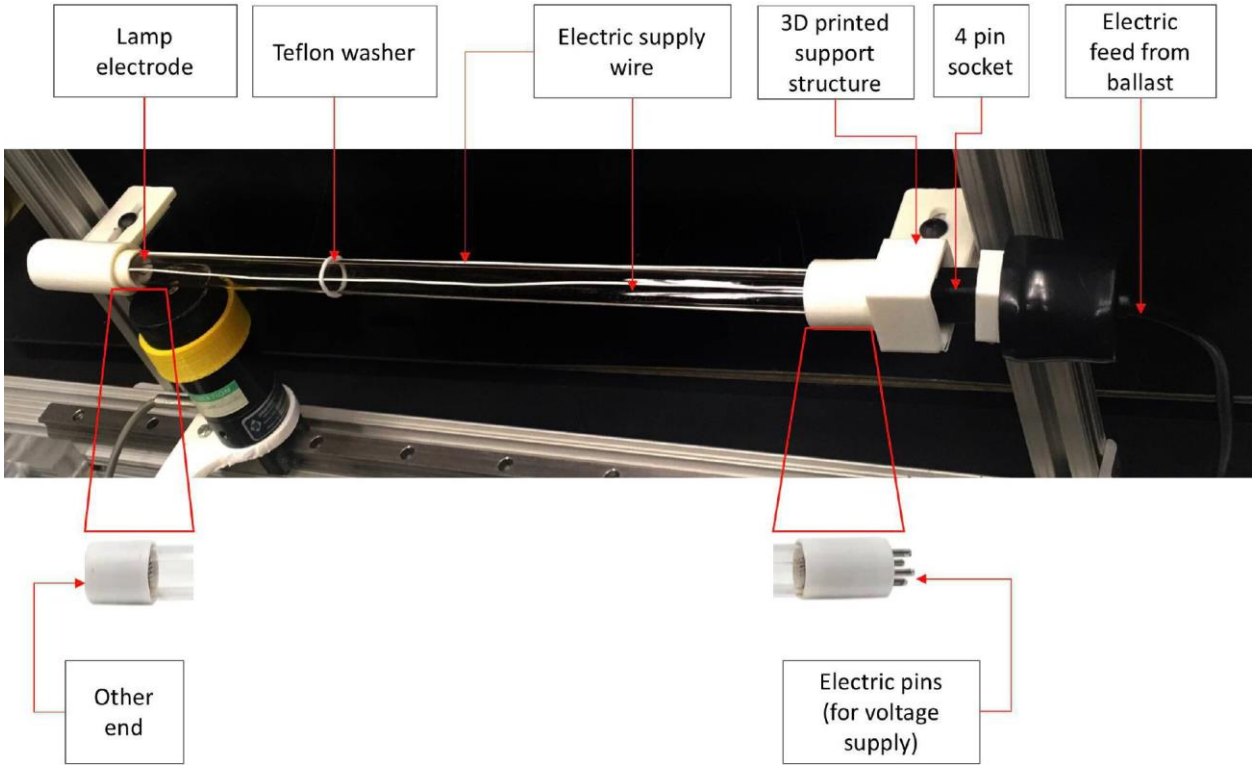

Figure 3. 5 Power supply to UV lamp

The lamp was operated at room temperature and with an electric feed of 120 volts at 55 Hz frequency, and the lamp was operated at 40 watts. The electric feed to the UV lamp was provided thought the three-pin plug electronic ballasts from HQUA company model # HQUA-OWS-455EB (HQUA- 4 ~ 55 watts) for 25 watts output. The electric supply to ballast was provided through surge protected power outlet. The lamp had supplementary electric wires, which were attached to the other end electrode (lamp end without the 4 pins).

The purpose behind the providing electronic ballast was to regulate the electric input the UV lamp by preventing the UV lamps from drawing an excessive amount of electric current and ultimately

damaging internal components. The following figure 3.6 illustrates an electric ballast that was used to provide electric supply to the lamp.

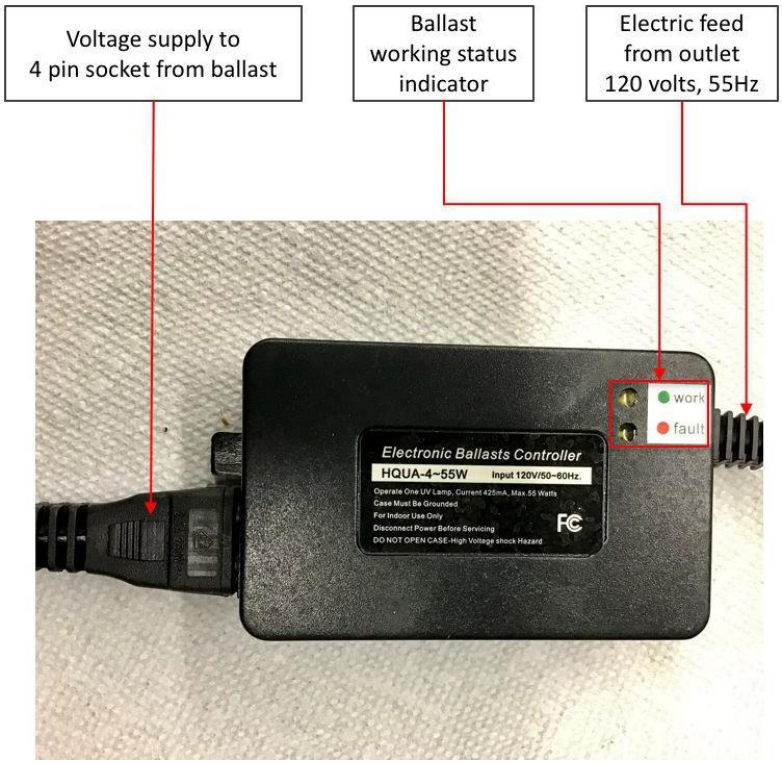

Figure 3. 6 Electronic ballast and power feed to UV lamp

(image was taken when ballast was inactive to avoid any interference with the radio frequency)

3.3.3 Aluminum rail profile

The experimental setup was built by using aluminum extrusion 20” x 80” dimensions, to provide rigid support to the structure. The following figure illustrates the arrangement by using aluminium extrusion. The image below has taken prior to build complete setup as few components are extremely delicate and could have damaged as consequence of the consistent disruption to external setup components.

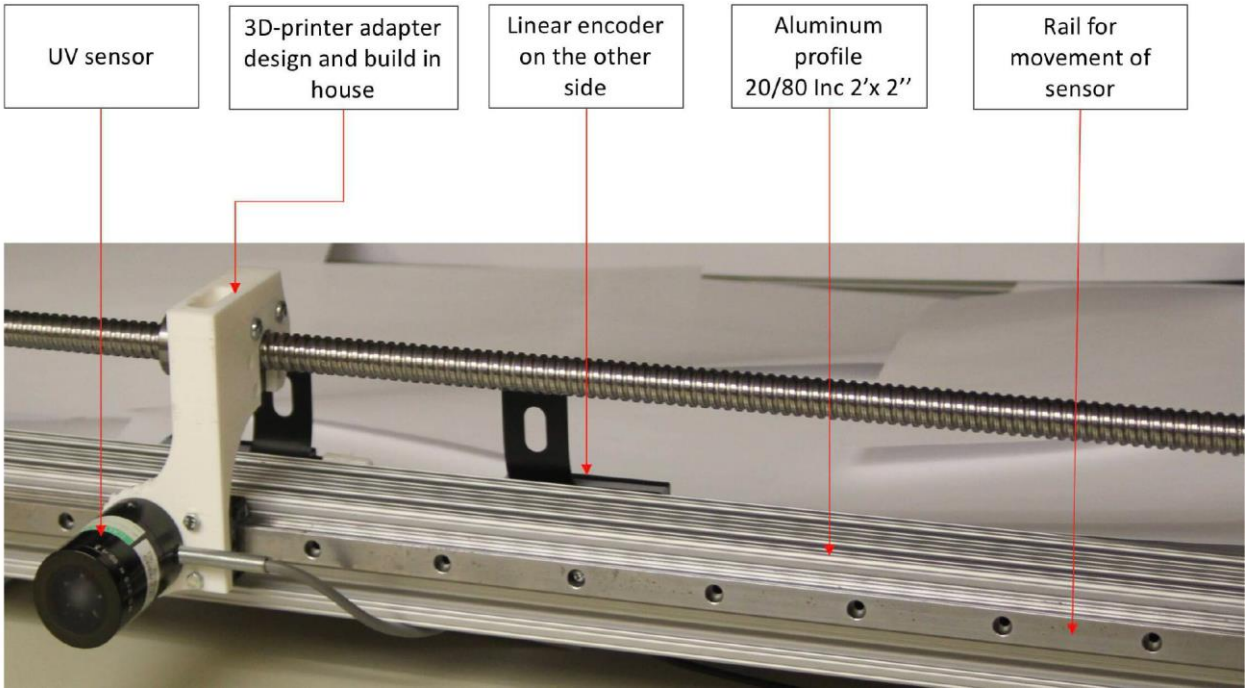

Figure 3. 7 Aluminium profile and assembled setup components

The setup arrangement with the inclusion of aluminum extrusion enabled the enactment of the auxiliary setup components such as stepper motor, encoder and sensor mount. Furthermore, it enabled an elevated horizontal lamp arrangement by the addition of a vertical support structure from the rare side of the extrusion. The aluminum extrusion provided rigid structure, that was unwavering during the movement of the sensor mounted adapter, across the lamp through the gliding movement on the rail causing no disturbance to lamp or sensor.

The aluminum rail is a linear motion bearing allowing backward and forward motion of the sensor mounted adapter. The purpose of the rail is to guide, support, locate and accurately move the sensor mounted adapter along the aluminum extrusion of the setup.

3.3.4 Stepper motor, lead screw and DC supply to compumotor

As mentioned earlier in section 3.2, the linear motion of the sensor was regulated with the stepper motor from Parker company. The stepper motor was fixed to the aluminum extrusion horizontally by providing 3D printed support assembly at both ends of the stepper motor. The rear end of the stepper motor is also known as support bearing. The figure below illustrates the aluminum rail, stepper motor and power supply arrangement.

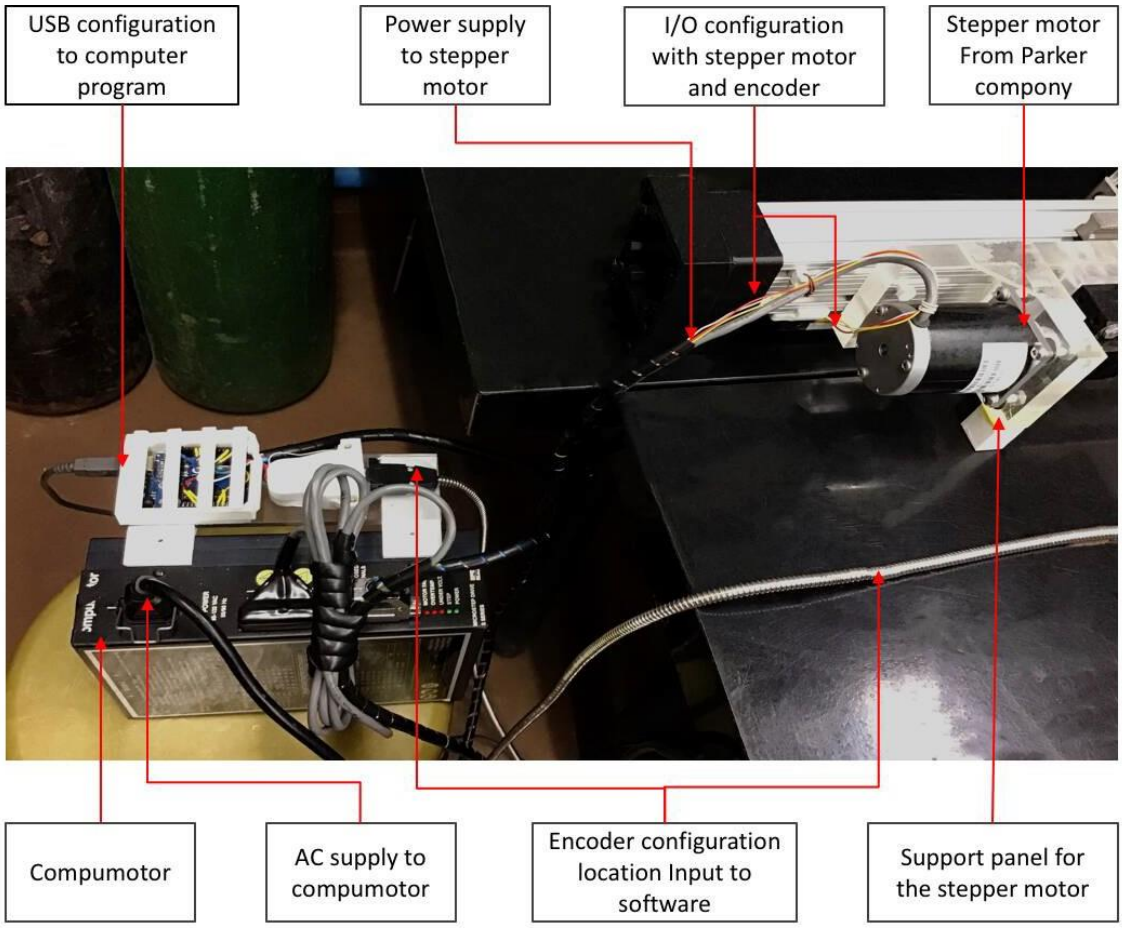

Figure 3. 8 Steeper motor components and power feed

The stepper motor is an electromechanical device which transfigures the electric pulses applied to their excitation windings into precisely outlined mechanical shaft rotation. The shaft of the motor rotates with a fixed angle for each discrete pulse for linear or angular motion (Electrical Technology, 2019). The mechanical shaft rotation enabled the rotatory movement of the lead screw (i.e. clockwise and counterclockwise rotation). The UV sensor was mounted on the 3D printed adapter housing and was fixed next to the ball nut on the nut housing. The rotating mechanism of the stepper motor was controlled by the signal input from the Arduino circuit board through the LabVIEW and Arduino interfaced program. As input was provided through the computer program, the stepper motor performed the rotatory motion of the leadscrew, which performed linear movement of the 3D printed adapter housing, allowing adapter housing to glide on the aluminum rail along with the encoder attached to the adapter housing from the rare side. As 3D printed adaptor housing travels in the linear direction, the UV sensor continuously scans the UV lamp with a specified distance interval.

In this experimental arrangement, the program was explicitly written to perform UV output measurement with 2000µm increments along the length of the lamp, i.e. 0 mm to 400mm or 0 µm 40000µm. The program controlled, the rotatory motion of the stepper motor, consequently controlling the movement of the sensor mounted adapter across the axial length of the UV lamp. The program was designed to control the rotatory motion of the stepper motor to that can enable scanning of the UV lamp with 2000µm increment with a complete stop at each measurement point i.e., 0µm, 2000µm, 4000µm…. 38000µm, 40000µm etc. The program allowed, control over the linear motion of the sensor adapter through stepper motor with a specific stop point to forward linear motion towards 40000 µm location, i.e., electrode, by inputting desired scanning range across the length of the lamp by putting numeric input in the developed supervisory program. During each experiment the measurements had taken twice, the first measurement when sensor mounted adapter housing moves from one electrode of the lamp, i.e. 0 µm position towards the other electrode of the lamp, i.e. 40000µm position. After that the stepper motor halts and reverses the rotatory motion, i.e. it rotates contraclockwise to bring back the sensor mounted adapter housing at its initial position, i.e. at 0 µm. During this sensor mounted adapter housing, reverses the scanning mechanism by stopping at 2000µm intervals; but with decrementing length units as it reverses towards the 0µm position from the 40000µm.

During this second measurement is proceeded for the same position along the length of the lamp. The measurement sample 0, 2000, 4000, 6000…. 38000, 40000 (halt)38000…. 6000, 4000, 2000, 0µm. The power supply to stepper motor and encoder was supplied through the compumotor from Parker company, which was connected to AC power supply as shown in following figure.

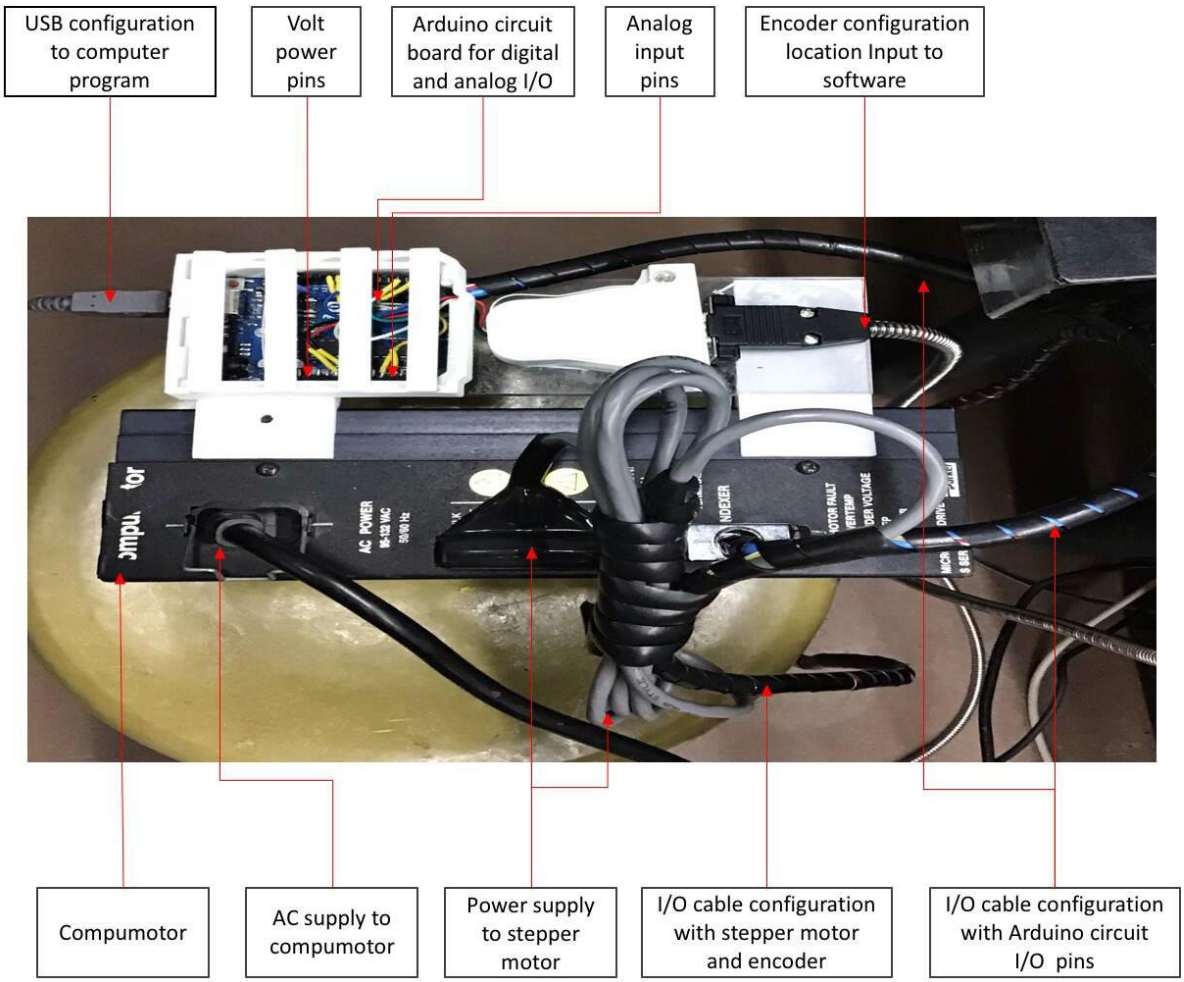

Figure 3. 9 Compumotor and Arduino circuit board

3.3.5 UV sensor and location encoder

The irradiance of LP lamp at 254 nm wavelength was measured with narrowband UV sensor from International Light Inc. detector model # SED 240. The UV sensor was mounted on the 3-D printed adapter housing, and further, it was fixed on the ball nut housing of the lead screw, to perform the linear motion of the sensor across the length of the lamp. The following figure illustrates the UV sensor arrangement and the assembly of the modules.

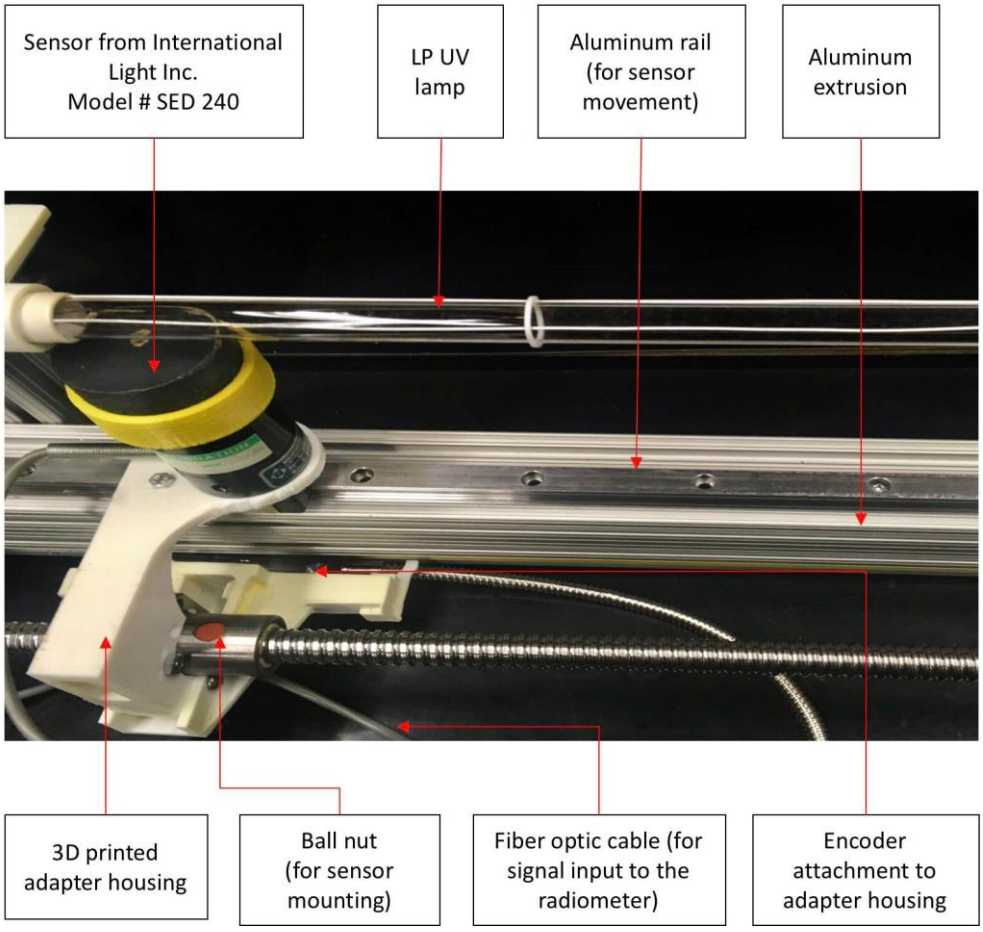

Figure 3. 10 UV sensor configuration with the setup

As mentioned in the preceding section (section 3.3.4), the linear motion of the sensor adapter housing was controlled with the stepper motor. The sensor adapter housing was fabricated and fixed on the aluminum rail to allow smooth gliding of the sensor along the axial direction of the

lamp during the experiment. All components were arranged and fixed on the aluminum extrusion to maintain rigid support to the setup configurations. The UV sensor was fabricated using a diffuser #7037, a filter NS 313 # 8543 and the UV detector SED 240 from the International Light Inc. The figure below illustrates the internal arrangement of the sensor components.

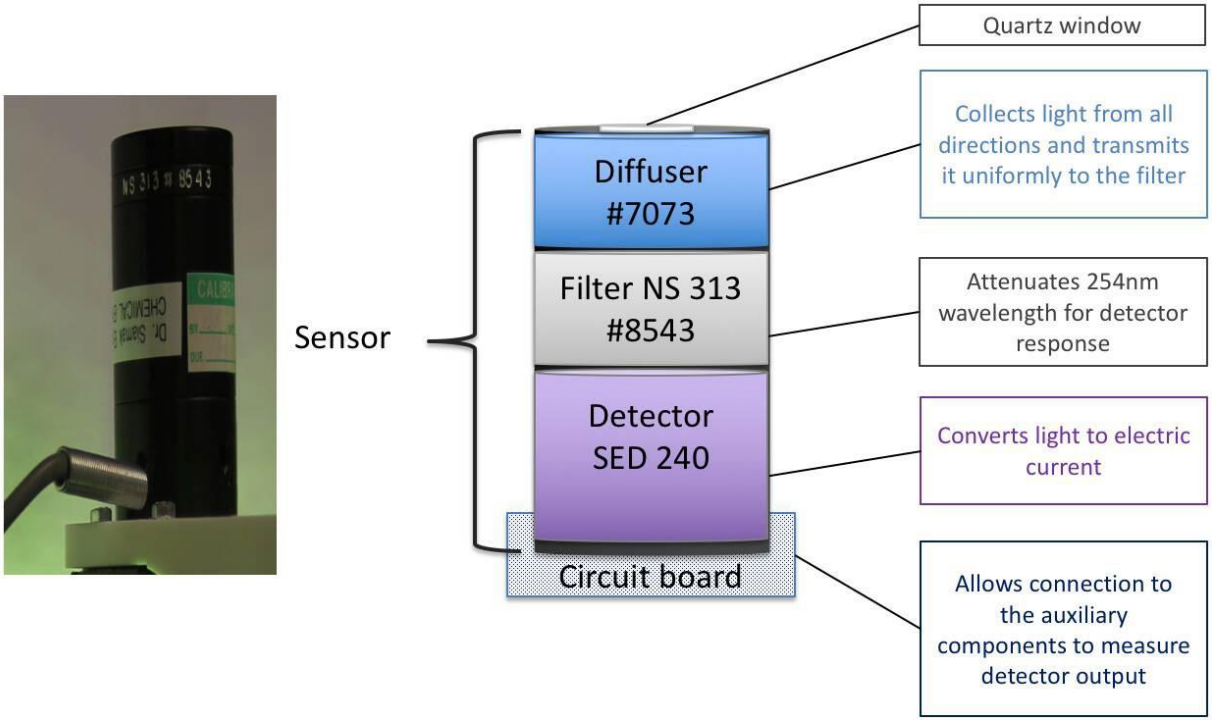

Figure 3. 11 Internal components of the UV sensor

The UV sensor was fixed on the lead screw at the ball nut with the use of 3D printed adapter housing to hold and support the sensor, as shown in the following figure.

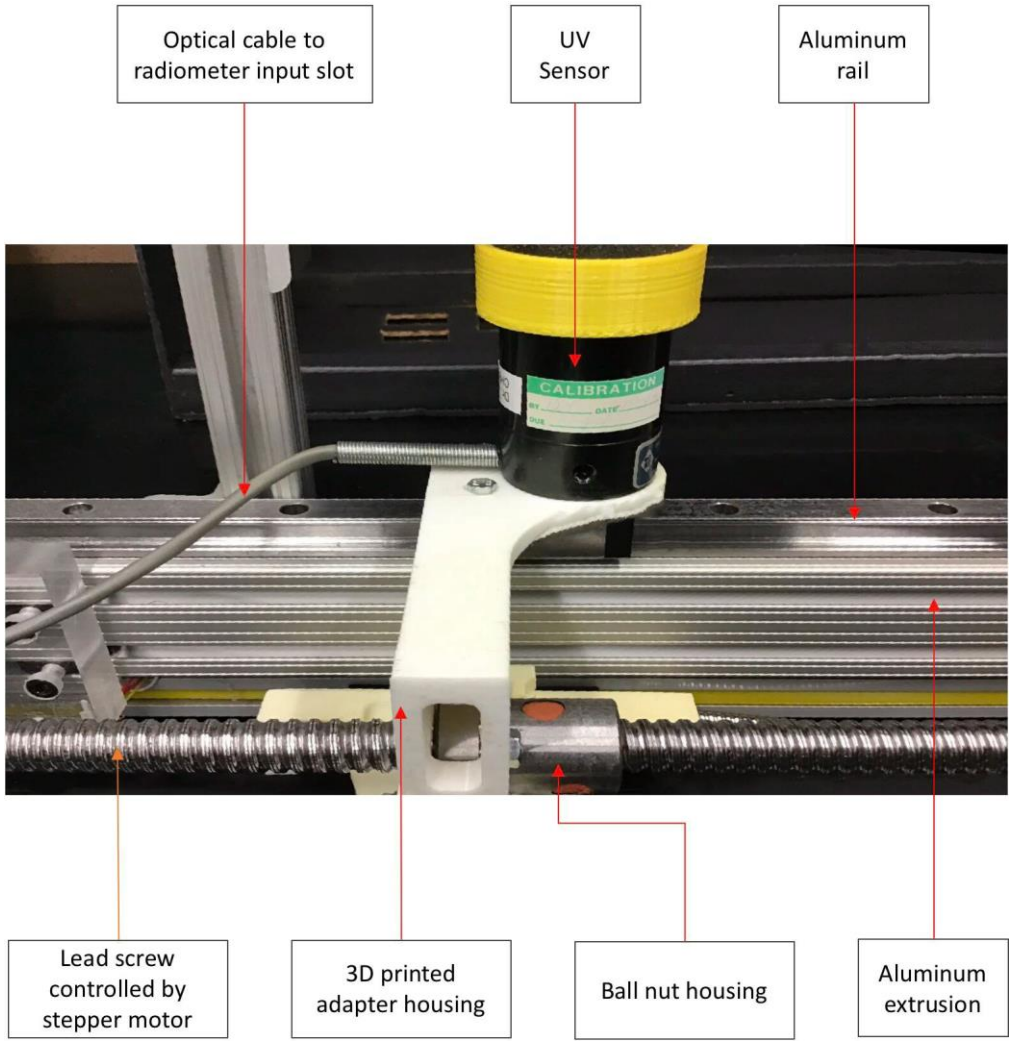

Figure 3. 12 Sensor arrangement and motion mechanism

The following figure illustrates the radiometer configuration for sensor signal input.

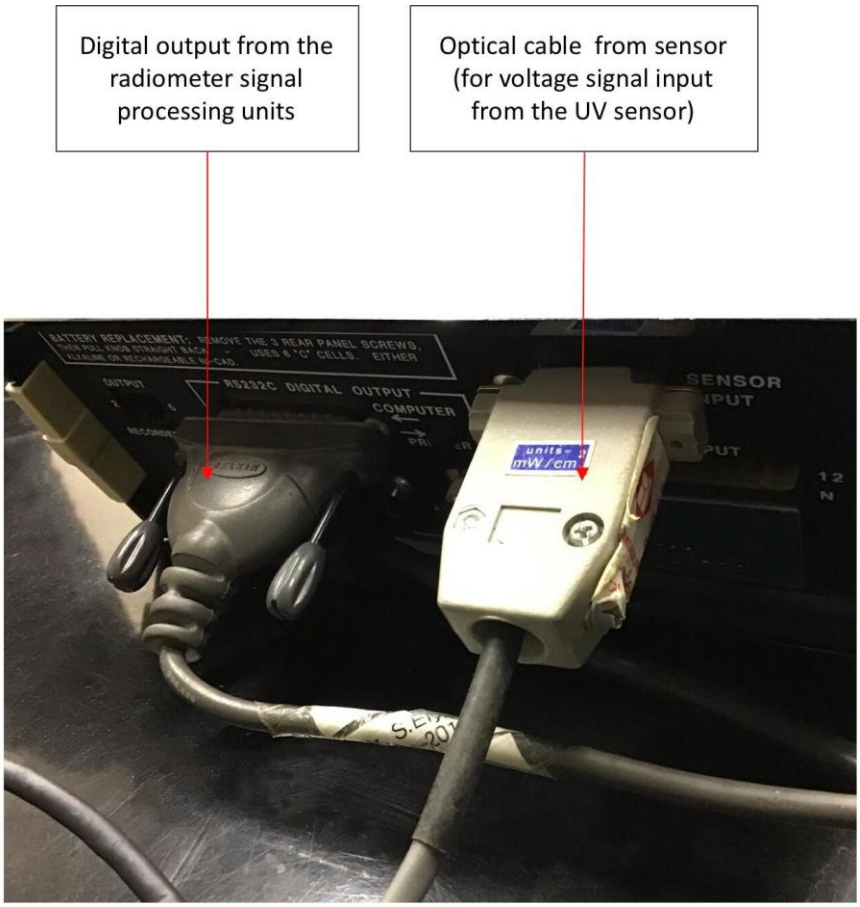

Figure 3. 13 Signal input to the radiometer

The sensor was connected to the research radiometer IL1700 by fiber optic cable to transfer the small voltage detected by the detector SED 240 to the signal processing elements of the research radiometer. Further, the signal output was recorded and logged by the developed computer program.

3.3.6 Radiometer and signal measurement

The UV intensity was measured with pre-calibrated research radiometer IL 1700 from International Light Inc. The following figure illustrates the front panel modules of research radiometer IL 1700 from International Light Inc.

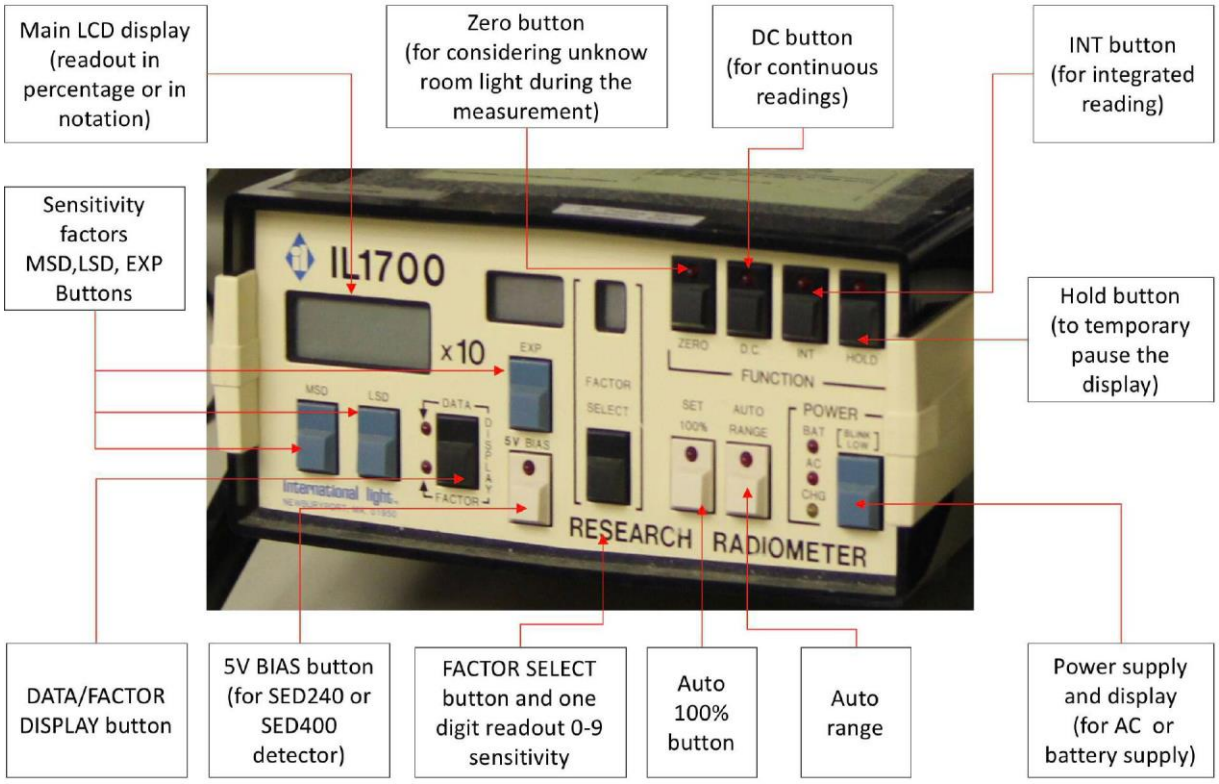

Figure 3. 14 Front panel of the radiometer

The measurement of UV lamp intensity was performed across the axial length of the UV lamp at multiple measurement points. During the measurement when filtered UV light of 254 nm wavelength was irradiated on the detector part of the sensor, a small voltage was generated during the irradiation. Further, generated electric voltage was conveyed for amplification and processing to the radiometer, to obtain the UV intensity of the incident UV radiation.

The figure below illustrates the back-panel components of research radiometer IL 1700, for signal input, auxiliary output ports and PC configuration to record and store the data in the developed computer program.

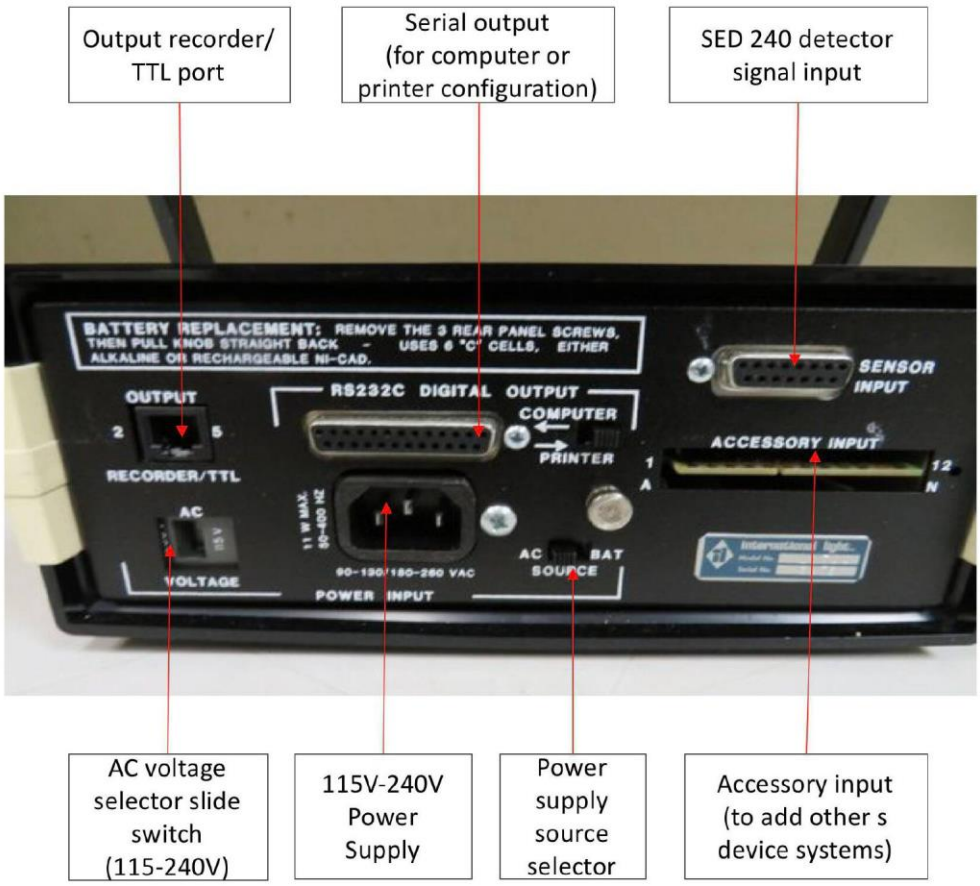

Figure 3. 15 Back panel of the radiometer IL 1700

During the experiment, the sensor adapter housing was moved in the linear motion across the axial length of the lamp with the help of the stepper motor motion. The collaboration among the setup components was performed and controlled by the LabVIEW interfaced computer program. As illustrated in figure 3.13 in section 3.3.5, the detector signal output was transferred to radiometer through the fiber optic cable by the sensor input port at the back panel of the radiometer. Further, this signal gets amplified by the propriety current amplifier and converted with the help of precision I/F converter to be processed by the internal microprocessor. The reading (UV intensity) obtained by the radiometer was displayed on the radiometer display and was recorded in the

computer program for each measurement point. The UV lamp intensity measurement was accomplished at multiple measurement points with the provision of the specific increment in a distance when sensor adapter housing was allowed to move forward 0 µm towards 40000µm (from left/ initial location to the right), and with specified decrement for movement from 40000µm towards 0 µm (from right to left/initial location). Each experiment was programmed to run, two measurements across the axial length of the lamp at multiple measurement points, the first measurement, when sensor adapter housing moves from 0µm location towards the 40000µm location and second measurement when sensor adapter housing moves from 40000µm towards 0µm location. The program was designed in such a way that, the sensor will be allowed to move with specified increment and then it was allowed to halt at measurement position for ~1 to 2 seconds to detect the UV intensity and, then sensor was allowed to move towards next measurement point. The same mechanism was followed for both the measurements i.e. measurement # 1, linear movement from left electrode to right electrode (with increment units) and measurement # 2, right electrode to left electrode (with decrement units).

The implementation of the twice the measurement (per experiment) for both linear directions (i.e. backward and forward) verified the UV output twice at every measurement point and confirmed accuracy of the obtained readings of the UV intensity at corresponding measurement point.

The signal i observed from by the radiometer is the integral of the product of the instrument responsivity S (λ) and the irradiance distribution of the light source E(λ).

$$2 = \int_{\sim} E(\lambda) \cdot S(\lambda) d\lambda \qquad \text{Equation 2. 14}$$

i- signal observed by detector (W)

E(λ) - irradiance distribution of UV light source (W/cm^2 , mW/cm^2)

S(λ) – instrument responsivity (Area/W)

In this experiment λ is 254 nm

The instrument responsivity is a function of the responsivity of the detector as well as the transmittance of the diffuser and the optical filter.

3.3.7 Arduino circuit board and configuration with setup modules

The mechanical components of the UV lamp measurement setup (i.e. stepper motor, lead screw) were controlled with the use of the Arduino UNO circuit board to provide a signal to the configured setup modules, and LabVIEW interfaced computer program to input the command to be processed by the Arduino circuit board. The command was provided through the Arduino-LabVIEW interfaced program, was used to regulate the rotation of the mechanical shaft of the stepper motor, allowing linear movement of the UV sensor adapter housing which was fixed on the lead screw and mounted on the ball nut. The Arduino UNO circuit board was consisting of the 14 digital I/O pins to allow signal input and output using the pin mode, digitalwrite (), digitalread () functions, which works on the 5V supply at the opposite of the digital pins.

The serial 0 (RX) was used to receive TTL serial data, and serial 1(TX) was used to transmit the serial data. These pins are connected to corresponding pins of the Atmega328 Microcontroller USB to TTL serial chip. Figure 3.17 illustrates the circuit board and pin assembly.
The digital pin 2 and 3 are also known as external interrupts configured to trigger an interrupt a low value or change in the value.
The digital pins 3,5,6,9,10,11 provide 8-bit PWM output, with analogwrite function.
The digital pins 10,11,12,13 support the command communication using the Serial Peripheral Interface (SPI) library to perform two-way interaction between the setup modules. It is performed using the 4-types of the signal,
pin 10 Slave Select (SS),
pin 11 Master Out Slave In (MOSI),
pin 12 Master In Slave Out (MISO),
pin13 Serial Clock (SCK)
Master is a microcontroller, which controls the peripheral devices.
The pin 10 (SS) to enable and disable the devices, the pin 13 (SCK) to synchronize data transmission prepared by the microcontroller. The pin 11 (MOSI) to transfer the data/command to the peripheral devices (i.e. Stepper motor motion/ shaft rotation).
The pin 12 (MISO) to sending data to the master (e.g. encoder/sensor position)

The following figure illustrates the basic structure of the Arduino circuit board.

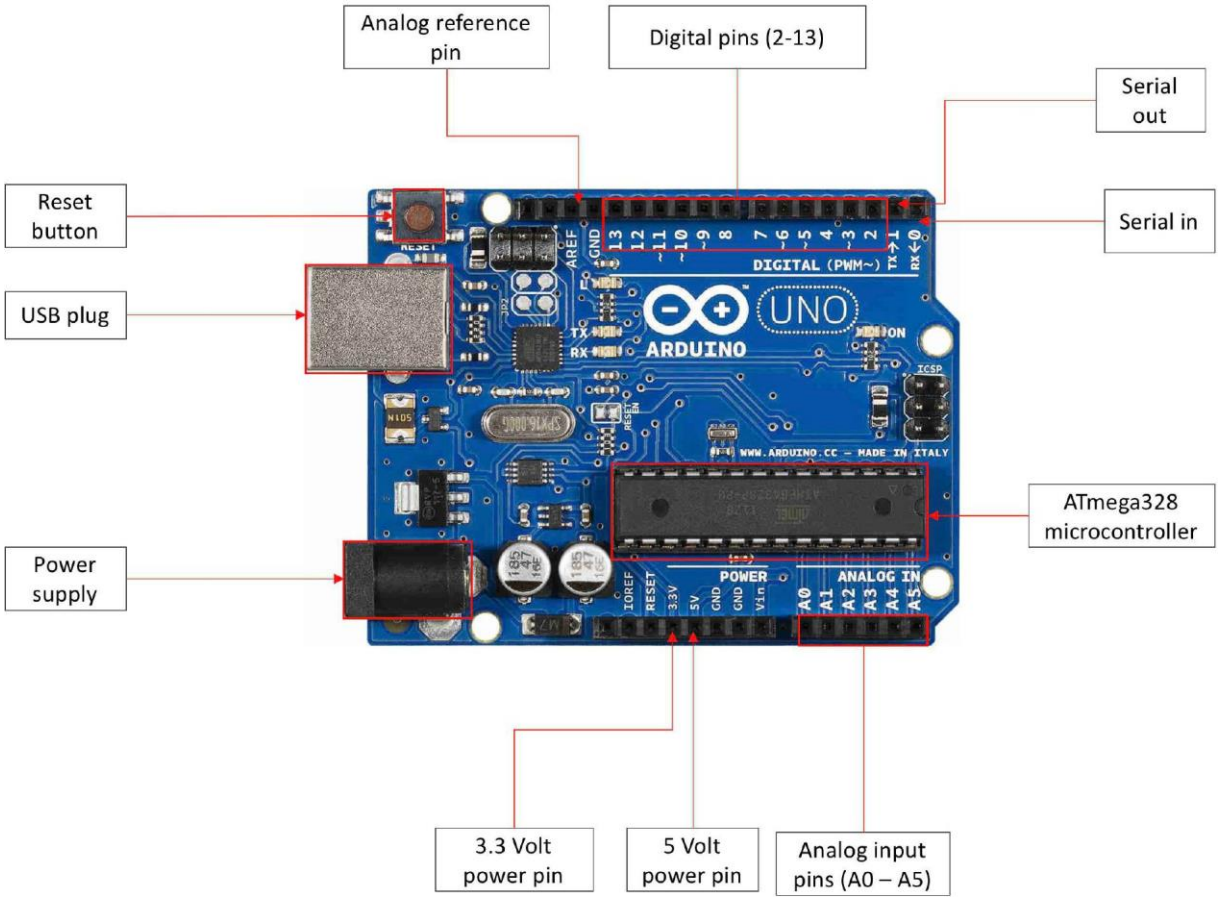

Figure 3. 16 Arduino circuit board modules

The circuit board also has 6 analog input pins, labelled as A0 to A5, which utilize ADC (Analog Digital Converter). ADC is used to convert the analog signal into the digital signal, which can be comprehended by the non-analog device. This process allows the processor or digital device to measure the signal and use it for the required purpose. ADC converts the voltage into bits, that microprocessor can understand. The pin 5V and 3.3. V regulated the power provided through the compumotor. The USB plug port was connected to a computer.

The Arduino circuit board microcontroller Atmega328 provides serial communication among the circuit modules. The data received back from the circuit modules to the circuit board was transmitted through the USB to Serial chip and USB to computer connection. The data received

from the circuit board to computer contained the information about the sensor adapter location, which was facilitated by the stepper motor motion and lead screw rotation, functioned by the input signal through the Arduino circuit board. The UV lamp intensity reading from radiometer was transferred directly to the computer input. The LabVIEW interface programmed allowed to log data, which included the information about the date, time, location of the sensor (input through Arduino circuit board) and UV intensity reading from the radiometer. The combined measurement data was recorded and logged in the textual file on the computer by the interfaced computer program.

The following figure illustrates the Arduino circuit board and I/O pin assembly.

Figure 3. 17 Arduino circuit board and I/O pin assembly

3.3.8 Thermal imaging camera

The experimental analysis also included observation of the non-uniform temperature profile of the UV lamp with the use of thermal imaging IR camera from FLIR Systems Inc. Model # FLIR ONE PRO iOS. The camera was compact, which allowed a suitable arrangement without interrupting the previous arrangement of the set-up. The camera model had revolutionary FLIR Vivid IRTM image processing technology, which had 3X speed than any another thermal camera from the FLIR and allowing measurement of the temperature up to 400°C (FLIR One Pro, 2019).

The FLIR thermal imaging camera was configured with the Apple iPad to cover a wider area of the experiment and obtain complete thermal images of the UV lamp. The thermal image collection and processing was performed with the software platform named as FLIR ONE (for iOS devices). The thermal imaging camera was used to observe uneven temperature profile at two electrodes and a central part of the lamp.

The figure below illustrates the FLIR IR thermal camera.

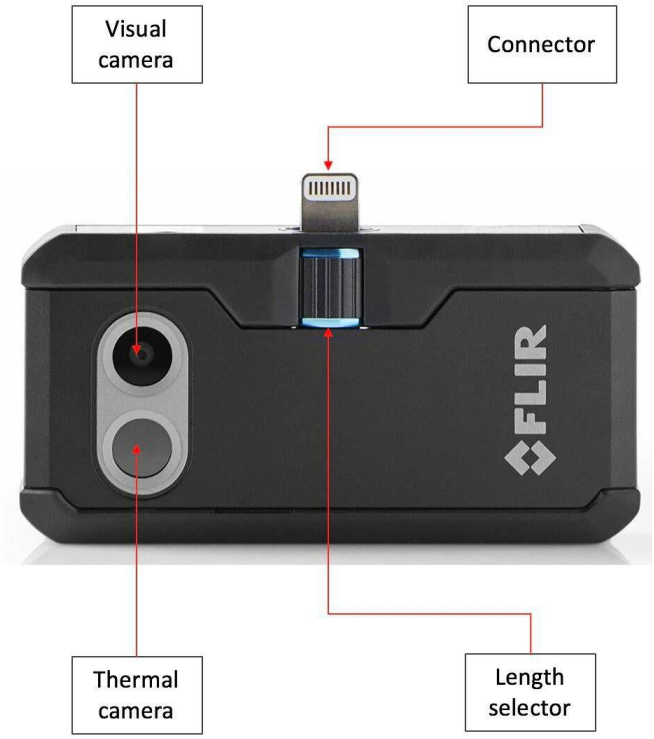

Figure 3. 18 Thermal imaging camera from FLIR Systems Inc.

The following figure 3.19 illustrates the thermal image of UV lamp.

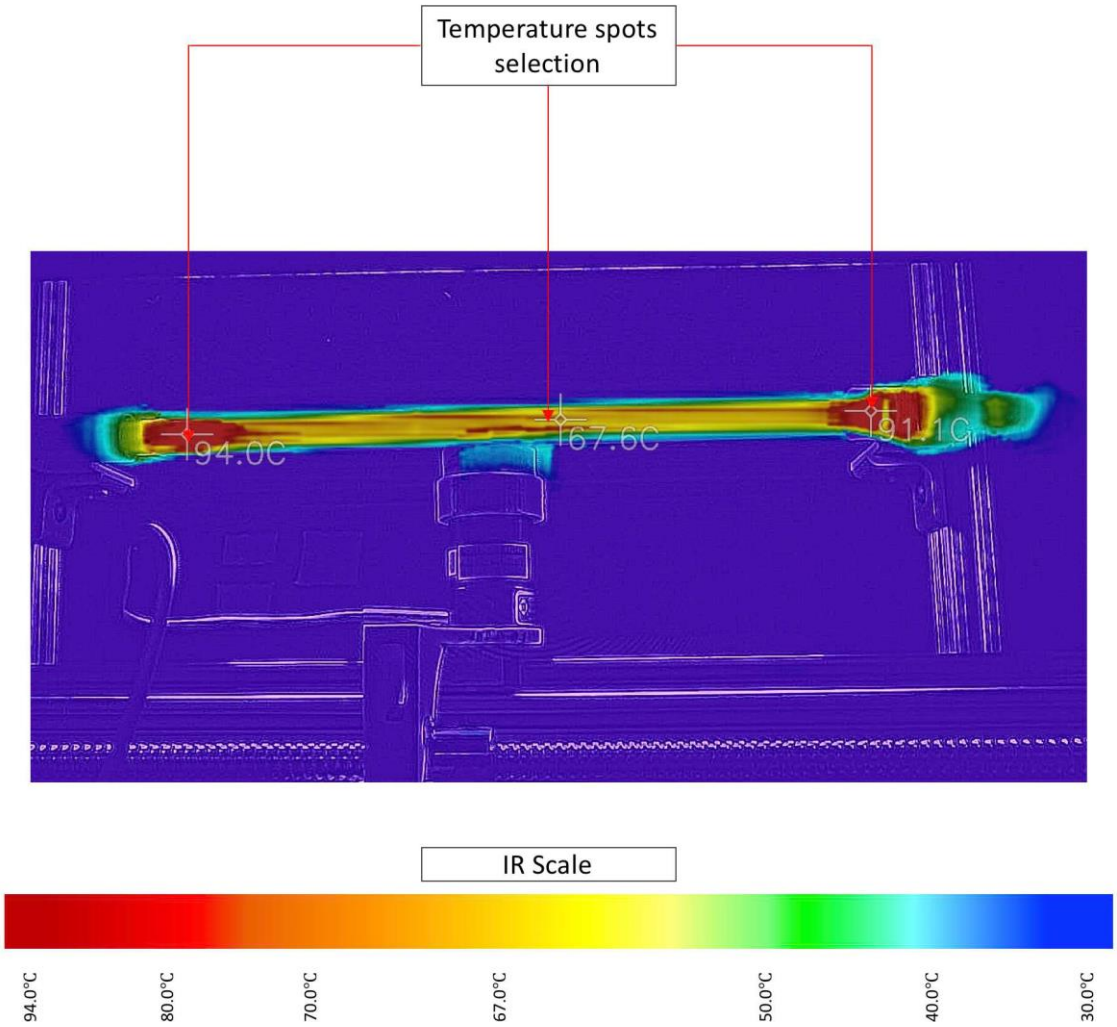

Figure 3. 19 Sample thermal image and IR scale

3.3.9 Digital hygrometer and thermometer

During the experiment, digital hygrometer and thermometer were used from company ThermoPro model # TP55. The purpose behind using the digital hygrometer and thermometer was to log the ambient air characteristics. The experiment was performed at room temperature ~ 20 to 22°C. During mid-winter to the late-winter season, the humidity was observed between 10 to 12 %, and by the early spring, the humidity was ~15%. The primary purpose of keeping a record of the room temperature and humidity was to assure there is stable room conditions during the experimental phases. The following figure illustrates the arrangement of the digital hygrometer and thermometer.

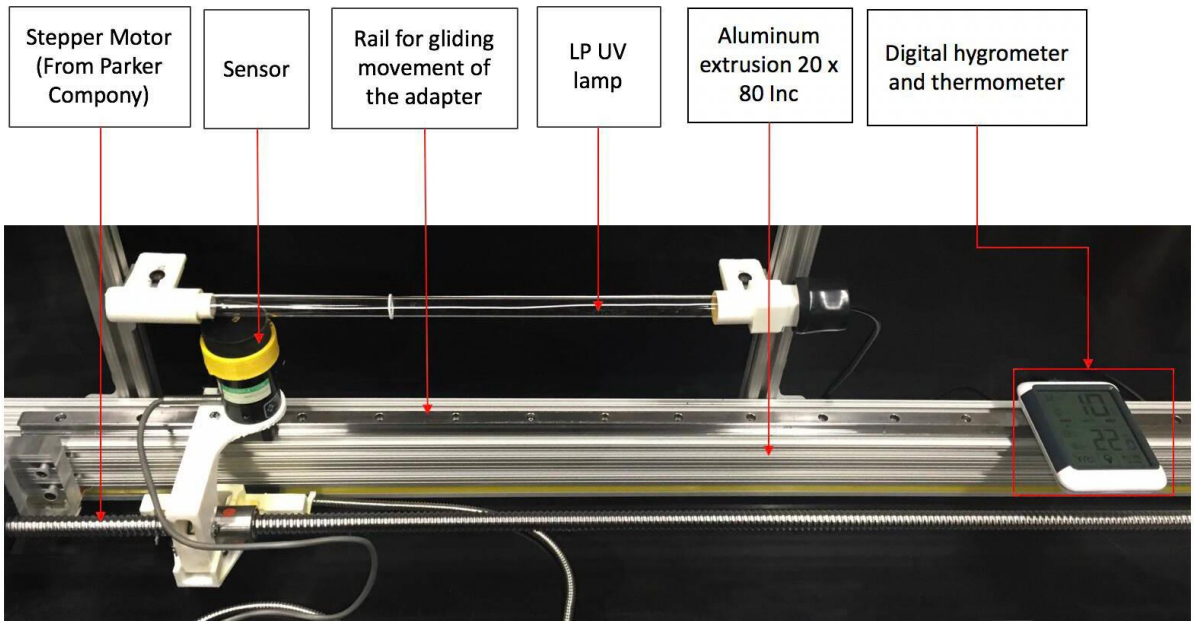

Figure 3. 20 Arrangement of the digital hygrometer and thermometer

3.4 Automated control of setup components

The experiment was performed using Arduino-LabVIEW interfaced computer program, which allowed control over the setup components by inputting the command. Figure 3.21 illustrates the front panel of the developed computer program, which allowed control over radiometer signal input, sensor movement and distance interval and digital readout for sensor location and UV intensity.

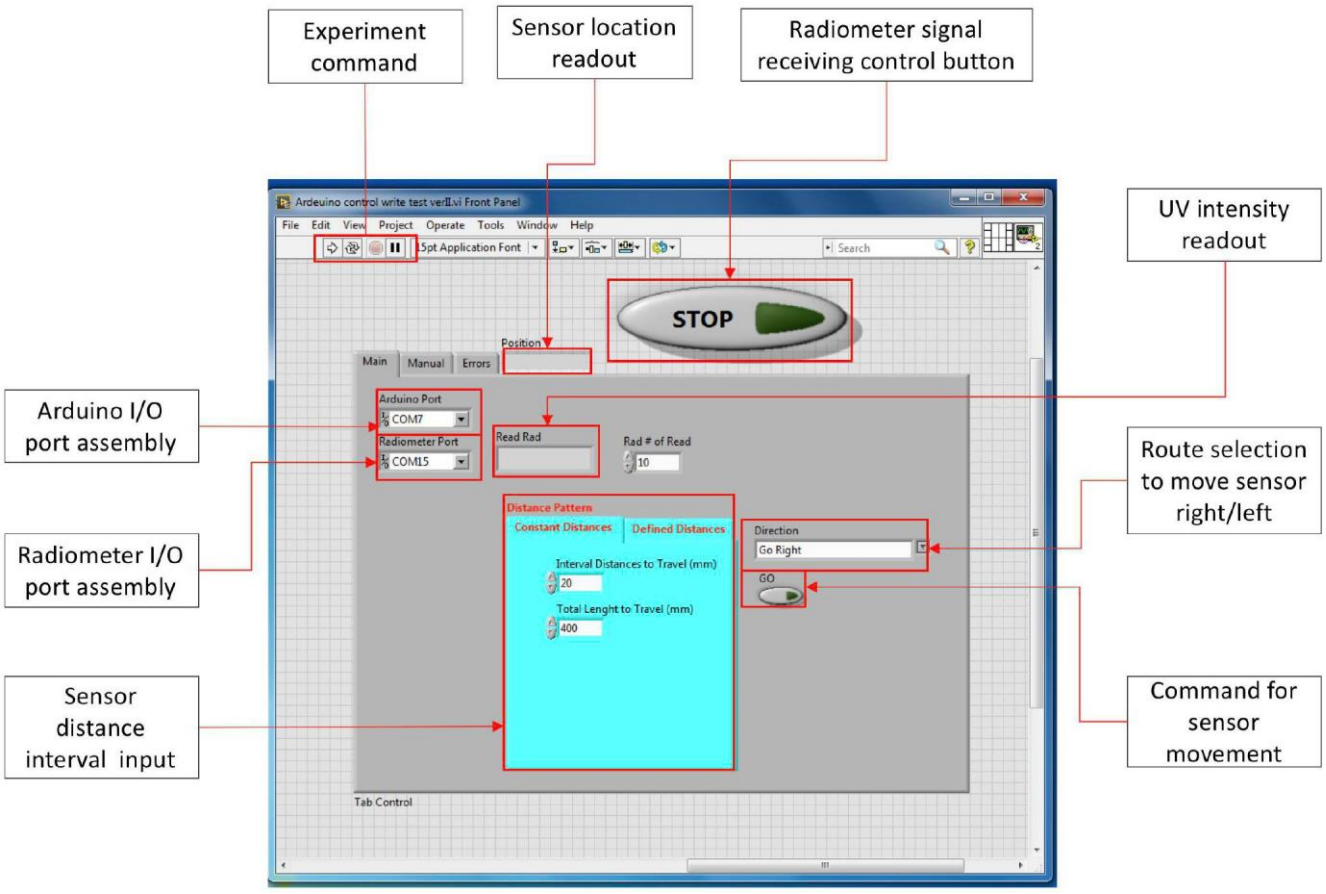

Figure 3. 21 Computer program to control setup components

At the beginning of the experiment, the command was given to generate the written file to log the data from the experimental command selector. The command named as the run was used to generate this written file on a computer.

Figure 3.22 illustrates the experimental command inputs to run, stop and pause the experiment. As shown in figure 3.22, the different commands that can be given through the program to perform the experiment.

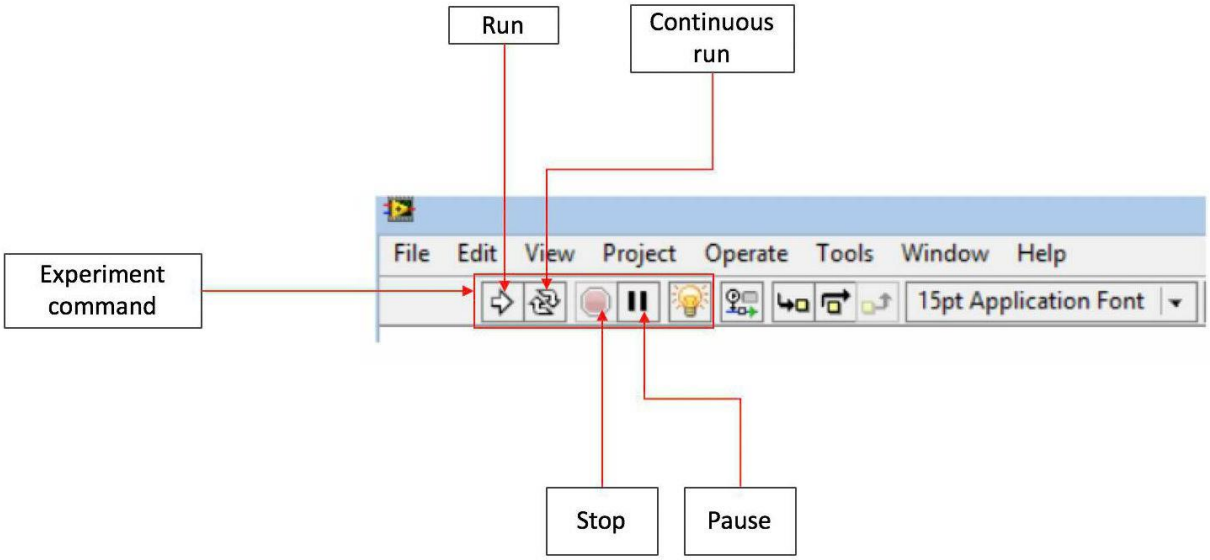

Figure 3. 22 Experimental commands

The program was designed to conduct multiple measurements by the sensor at predefined locations. During the experiment, the sensor was stopped at specified distance interval, i.e. after each 2000µm or 200mm or 2cm, to obtain the UV lamp intensity reading. During each experiment, the measurement was performed twice at 20 different points (x2) with constant distance increment, when the sensor was commanded to move right from 0µm location to the 40000µm. Then the second measurement was performed when the sensor was reverted with equal decrements towards left from the 40000µm point towards 0µm position. The designed program allowed constant increment and decrement based measurement of the UV lamp at every 2000µm or 2cm location precisely to obtain the reading while the sensor is motionless during at each measurement position across the length of the lamp the exact location of the sensor and the distance travelled by the sensor was tracked by the linear position encoder. The developed program was also provided with the manual control feature.

3.5 Data collection and logging

The developed program was designed to record and log the data in the written file, which was generated after the selection of the run command, as shown in figure 3.22. The generated file records the data for each measurement session, including the date, real-time, location of the sensor across the length of the lamp and UV intensity (through the radiometer input) for that point.
The program was designed to log the data, while the experiment is getting performed, which avoided flooding of unnecessary data. The experiment was performed every hour, for 20 measurement points (each point was measured twice) which included 39 measurements per one hour. The 20th point at 40000µm or 40cm position was measured only once.

To begin the experimentation, the run command was provided in the LabVIEW interface program, and after the generation of the log file, data was collected by commanding the setup to move the sensor with input distances. However, prior to every experiment UV lamp was turned on for at least 20 to 30 minutes and UV output data was collected during UV lamp warmup time to observe the lamp output stability and its variation for every operating cycle for 450 hours lifetime. The experimentation was implemented for ~10 to11 times a day on an hourly basis.
Each experiment took ~ 10 minutes to perform two measurements. At the end of the experimentation (at the end of the operating cycle), stop command was provided to the program to stop the data logging, radiometer signal receiving and, the experiment (for experimental command refer to figure 3.21 and 3.22).
The following figure illustrates a sample textual log, generated by the computer program.

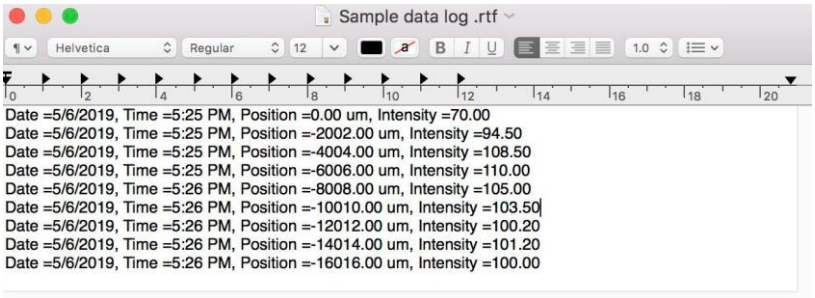

Figure 3. 23 Sample textual data log format (measurement #1sensor movement left to right)

3.6 Method and procedure sequence

In this section, the experimental method and collaboration sequence of the setup components has described. To measure the irradiance, the LP lamp was mounted horizontally with the support structure and covered with the black box enclosure during the experimentation, and the lamp support structure was fixed on the aluminum profile as shown in figure 3.2.

The lamp arrangement was motionless during the entire phase of experimentation and UV lamp was neither moved nor rotated during the experimental analysis (450 hours) to avoid disturbance to the inert gas and mercury fill inside the lamp sleeve. At the beginning of the experimentation, the UV lamp was turned on for ~20 to 30 minutes for the warm-up. During the warm-up phase, the UV intensity of lamp was measured by the sensor at a fixed location (at 0.00 cm) to observe the time taken by the UV lamp to emit stable output as well as to verify the stability range of the UV lamp during the 450 hours. After confirming the stable UV output, the experiment was performed with 2 scanning measurements with specified distance input in the computer program. Approximately 10 to 11 experiments were performed daily. The UV lamp performance was evaluated by measuring UV lamp intensity along the axial direction of the lamp with a fabricated UV sensor and narrowband radiometer. The sensor was fixed on the custom-made adapter housing and was mounted on the steeper motor-controlled leadscrew, which was controlled by the Arduino-LabVIEW interface computer program.

The setup components were collaborated with one another through two-way I/O signal communication using Arduino circuit board, to monitor and control the mechanical movement of the stepper motor, lead screw and, sensor adapter housing. The LabVIEW interface program allowed to regulate the setup functions, UV intensity measurements and data logging in a textual file based on the I/O signal interaction between the corresponding the devices. The detail about setup component and working mechanism in explained in preceding sections (section 3.2, 3.3, 3.4 and 3.5).

3.7 Result interpretation

The experiment was designed to acquire the data during each measurement and log into a textual file through a LabVIEW interfaced computer program. During each lamp operating cycle of LP UV lamp, the UV output data was collected, sorted and graphically arranged to observe the UV intensity of lamp for specified measurement point (i.e. 0, 2000, 4000…μm). The data was represented using a graphical arrangement of UV lamp intensity in terms of UV output at the multiple measurement points along the length of the lamp.

3.8 References

Arduino. (2019). Getting Started with Arduino and Genuino products. Retrieved May 24, 2019, from https://www.arduino.cc

Awwa Research Foundation (Awwa RF), & New York State Energy Research and Development Authority (NYSERDA). (2007). *Optimization of UV Disinfection* (NYSERDA Report Number 07-07 1P-4C-91184-11/07-NH). Retrieved from https://www.nyserda.ny.gov/About/...and.../Optimization-of-UV-Disinfection

Electric Technology. (2019, May 8). What is a Stepper Motor? Types, Construction, Operation and Applications. Retrieved May 11, 2019, from https://www.electricaltechnology.org/2016/12/stepper-motor-construction-types-and-modes-of-operation.html

FLIR ONE Pro. (2019). Retrieved May 14, 2019, from https://www.flir.ca/products/flir-one-pro/

National Instruments. (2019). LabVIEW Basics [LabVIEW MakerHub]. Retrieved May 26, 2019, from https://www.labviewmakerhub.com/doku.php?id=learn:tutorials:labview:basics

Parker Hannifin Corporation. (2005). Motion Control Systems - A Complete Family of Motion Control System Products from Parker Hannifin. Retrieved May 21, 2019, from http://www.parkermotion.com/

Schwartz, M., & Manickum, O., (2015). Programming Arduino with LabVIEW (1st ed.). Retrieved from http://s1.nonlinear.ir/epublish/book/Programming_Arduino_with_LabVIEW_1849698228. pdf

ThermoPro. (2014, December 18). Indoor Thermometers & Hygrometers. Retrieved May 18, 2019, from https://buythermopro.com/category/indoor-thermometers-hygrometers/

NOTES

CHAPTER 4

RESULTS AND DISCUSSIONS

This chapter elaborates the research findings of UV lamp performance during the preliminary 5% lifetime of the LP UV lamp. The experimental analysis was performed with the developed direct measurement setup for evaluating the variation in the UV intensity of the lamp during preliminary 450 hours. The detail about the direct measurement setup is described in chapter 3. This chapter includes a graphical representation of experimental results and, explanations framed based on the research findings.

4.1 Overview of the experimental results

The LP UV lamp used for the experimental analysis was new, hence part of observations also includes the findings during initial 100 hours burn-in time, i.e., experimental analysis has reported, UV lamp performance when LP lamp researched to maximum UV output phase and then, decreased to steady state output phase indicating LP lamp has passed through an optimum into an overheated condition. This initial dropped during approximately first 100-120 hours. The findings related to preliminary UV output drop, after a slightly overheated lamp condition allowed to generate a UV irradiance curve as a function of the time across the length of the lamp. After the preliminary UV output drop, LP lamp started to emit stable UV intensity across the length of the lamp for a short time, and after that lamp experienced uneven UV output across the length of the lamp.

The preliminary output drop occurred during week 3 between 102 to 109 operating hours.
The experimental observations noticed non-uniform UV output pattern across the length of the lamp and spotted multiple peaks and drop along the lamp length. For each operating cycle (i.e., for ~10-12 hours daily), collected measurement data was analyzed and plotted to identify the UV lamp ageing profile. The measurement data was collected through a LabVIEW interfaced computer program, and data was comprised of real-time monitoring of the UV lamp intensity at the specified positions across the lamp length. As previously mentioned in section 3.6, the experimentation included ~10 to 12 experiments for every lamp operating cycle (10 to12 hours

experiment run), with 2 measurements for each run. However, the result for each experimental run (i.e., hourly collected data) was generated through the averaging of the 2 measurements taken for each specified measurement point (total 20 points) during each run. At the end of each experimentation (i.e., after one lamp operating cycle), the results of every experimental run were generated through an averaging of the two measurements to diminish the error. The averaging method was selected to obtained more precise signal input and diminish the measurement error (National Instruments, 2006). For every lamp operating cycle, approximately 10 experimental runs were performed and at the end of every lamp operating cycle, concluding results were generated by the averaging of ~10 to 12 experimental runs, performed under corresponding lamp operating cycle. After every lamp operating cycle, the lamp was turned off for the next 10 hours, and the next experimentation was performed for followed by the same routine. The experimentation included 45 lamp operating cycles.

The experimental analysis was consisting of the observations of the UV lamp performance for every lamp operating cycle, which includes observations of UV lamp stability for warm-up phase after UV lamp was ignited (~20 to 30 minutes) and, UV output measurement for each operating cycle during stable output phase (~10 hours). During all phases of the experimentation, the ambient air temperate near setup was maintained ~21 to 22°C, in a still room. The experimental analysis also includes the detection of the non-uniform temperature profile at the lamp electrode and central part, observed by the thermal imaging camera. Furthermore, results were combined and represented by a UV output curve as a function of time. The final results were prepared by the unification of the experimental data of 45 lamp operating cycles to identify the change that occurred in the lamp output based on a weekly timeframe.

4.2 Visual observations of UV lamp ageing

UV lamps degrade with as they age, resulting in reduced and non-uniform UV output. As previously mentioned previously (section 1.1.3 and 2.7), the lamp ageing phenomenon depends on various parameters such as lamp operating cycles, electric feed system, ambient conditions and purpose of the application and can vary from one lamp to another (Heath et al., 2013; Lankhorst and Nilemann, 2000; Sigel 1995). However, in various studies the visual ageing signs of the lamp has been reported; such as darkening near the lamp electrode, fouling of the quartz sleeve, resonant darkening and discoloration of the lamp sleeve (AwwaRF and NYSERDA, 2007; Schmalwieser et al., 2014). The experimental analysis was performed for 450 burn-in hours for LP UV lamp to evaluate UV output and change occurred in irradiance output over time. During experimental analysis, visible ageing signs were noticed on the lamp sleeve especially darkening of the sleeve near the electrode, discoloration of the lamp sleeve, the random formation of the spot along the length of the lamp.

4.2.1 Darkening of the lamp end

Figure 4.1 illustrates the firsts visible ageing sign, that was identified during week 6 after 224 burn-in hours. The following figures illustrate the visual ageing signs, identified during the experimental analysis.

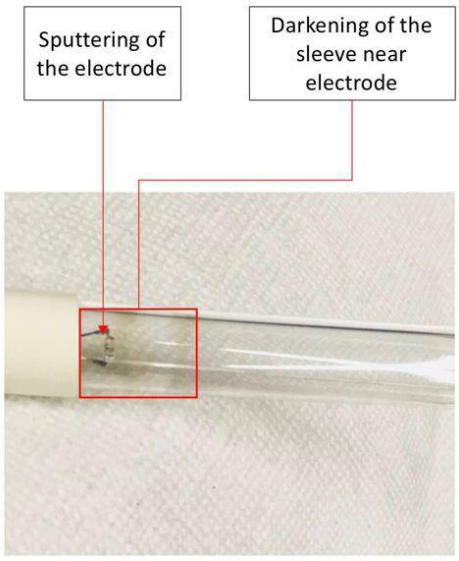

Figure 4. 1 Darkening of the lamp sleeve (occurred after 224 burn-in hours)

Initially, the appearance of the darker area at the end of the electrode was indistinguishable, however as the experiment was continued further, the darkening at the lamp end became denser as displayed in figure 4.2 and figure 4.3.

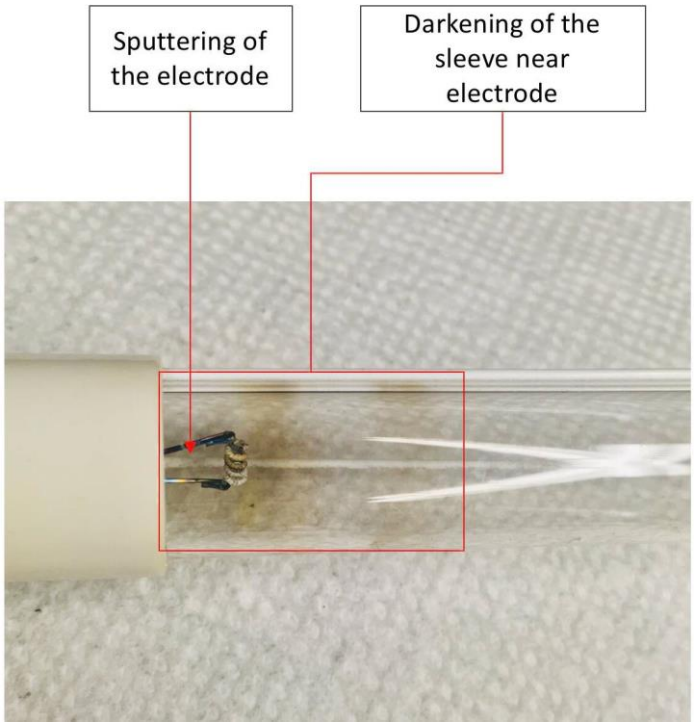

Figure 4. 2 Darkening of the lamp end after 328 hours

Figure 4.2 illustrates the darkening of the lamp edge became denser after 328 burn-in hours during week 8 though the lamp was functioned for the same operating conditions and schedule. Furthermore, by the end of the planned experimental schedule, i.e. after 450 burn-in hours, the darkening at the lamp end was much more blacken, than it was observed initially after 224 burn-in hours.

Figure 4.3 illustrates the darkening of the quartz envelope at the end of the lamp after 450 burn-in hours during week 10. The darkening at the lamp end can be caused by the sputtering of the lamp electrode material during the lamp start-up and operating span (AwwaRF and NYSERDA, 2007; USEPA 2006).

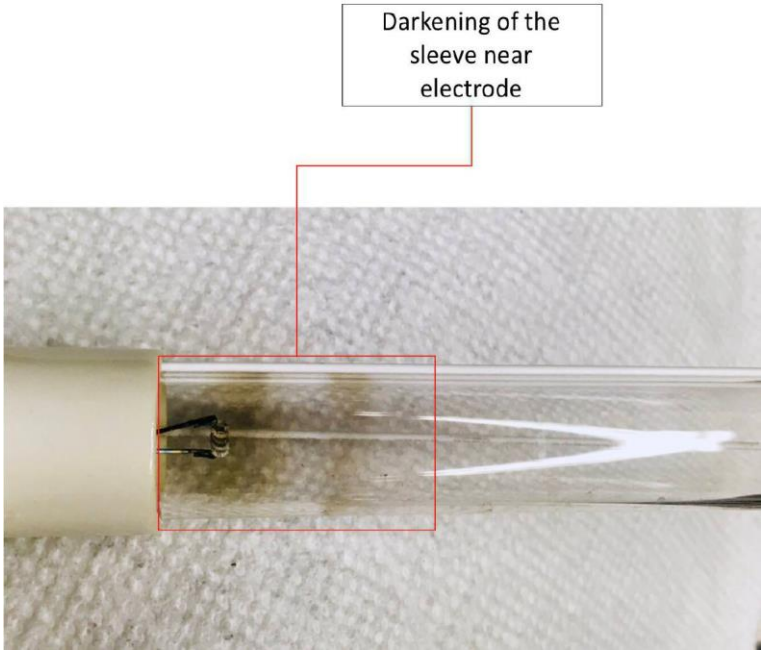

Figure 4. 3 Darkening of the lamp edge after 450 burn-in hours

Figure 4.4 displays the lamp end prior to the experimentation. This figure can be compared with the previous figures 4.1, 4.2 and 4.3 to justify the darkening of the lamp end as it has aged. The lamp electrode in figure 4.4 had uniform blackish colour without any glazing, which could not remain uniform and can be noticed in figure 4.3. After consistent lamp operation, it turned into a glossy blackish shade; this phenomenon is also known as electrode sputtering, which is caused due to excessive heating of the electrode. The overheating of the electrode results into deposition of the electrode material on the lamp sleeve from inside, and as the lamp ages, it becomes denser, and consequently, it triggers resonant darkening due to convection effects and deflection of the plasma.

In other similar studies by AwwaRF and NYSERDA (2007), the formation of the resonant darkening and distortion in the form of sinusoidal shape was reported for MP lamps.

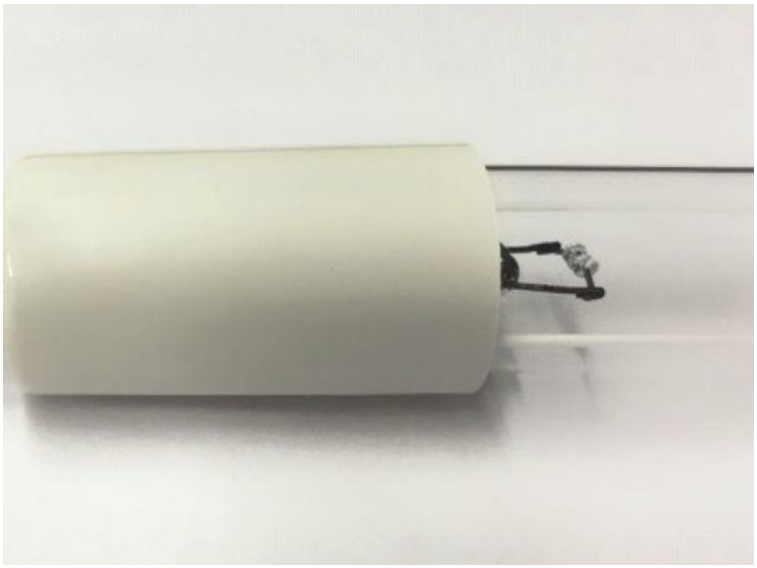

Figure 4. 4 Lamp electrode prior to begin experimentation

4.2.2 Discoloration and sleeve fouling of the lamp sleeve

The experimental analysis was performed for 450 hours and, during the experimentation, discolouration of the lamp sleeve was observed along the length of the lamp and, around lamps circumference. The discoloration along the length of the lamp was randomly formed and was grey. Initially, the sleeve fouling along the length of the lamp was indistinct; however, as lamp aged, it became more noticeable. Following figure 4.5 illustrates the clear lamp sleeve prior to the beginning of the experimentation.

Figure 4. 5 Lamp sleeve prior to begin experimentation

The discoloration along the length of the lamp is a consequence of the convention effect and the deflection plasma due to the electromagnetic field. The non-uniform plasma distribution leads to uneven UV irradiance along the length of the lamp and variation in the temperature profile of the quartz sleeve. Figure 4.6 displays, the fouled sleeved after 289 burn-in hours during week 6. Initially fouled sleeve was indistinguishable; however, as experimentation was carried further, sleeve fouling was more visible though the lamp was operated under same ambient conditions.

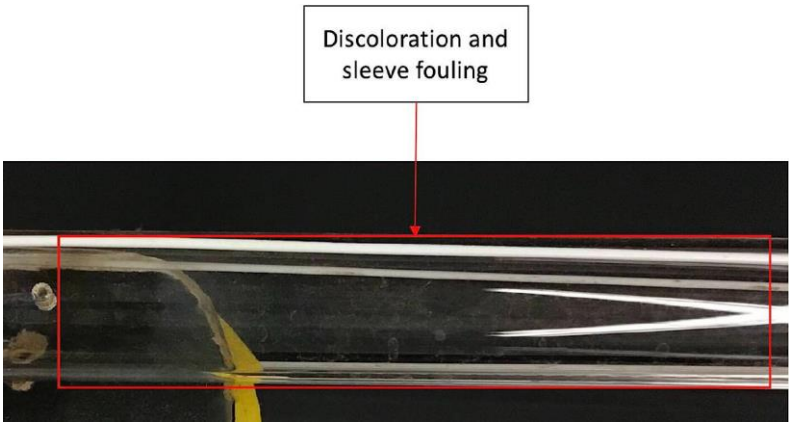

Figure 4. 6 Quartz sleeve fouling after 289 burn-in hours

The following figure 4.7 displays fouled quartz sleeve on the other end side of the lamp (two images were taken to provide a close view of the lamp sleeve, which could not be possibly shown in a single image).

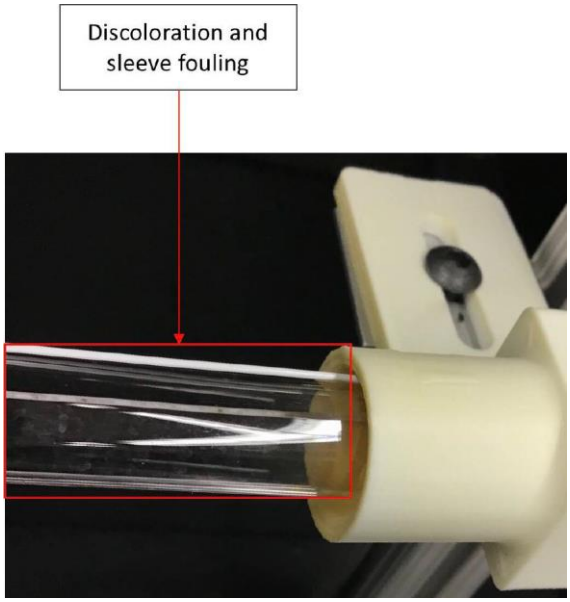

Figure 4. 7 Quartz sleeve fouling on other end of the lamp after 298 burn-in hours

The figure 4.8 and 4.9 displays the prevalent sleeve fouling after 419 hours during week 9 of the experimentation.

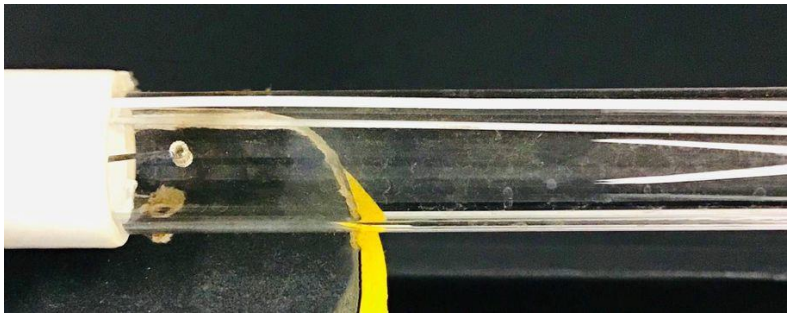

Figure 4. 8 Quartz sleeve fouling after 419 burn-in hours

The sleeve fouling and discoloration of quartz sleeve become predominant during week 9 and week 10. The reason behind the discoloration can be consistent operating of the UV lamp and

several scheduled operating cycles during the entire phase of the experimentation, which could have triggered the sleeve fouling.

Figure 4.9 displays the predominant sleeve fouling at another end of the UV lamp (right-sided electrode). The image was taken after 419 lamps burn-in hours. The difference can be perceived by comparing figure 4.7 (earlier image after 289 burn-in hours) and figure 4.5 (image prior to the beginning of the experiment).

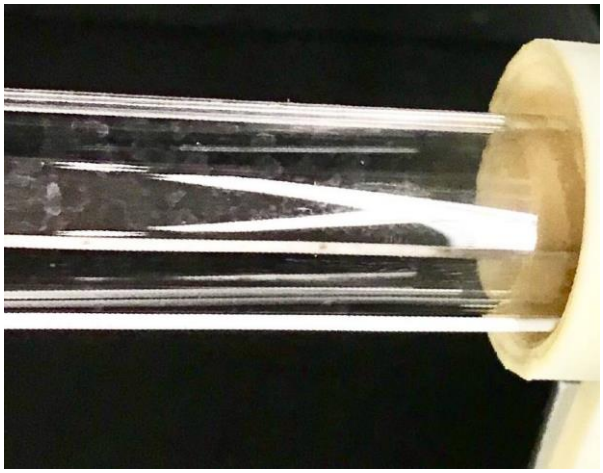

Figure 4. 9 Quartz sleeve fouling on other side of the lamp after 419 hours

Furthermore, the ambient air can be responsible for the quartz sleeve fouling. The surrounding air temperature has a direct influence on the UV lamp s it affects the surface temperature of the quartz sleeve, and it determines the stability of the inside mercury vapour. If the surrounding temperature is cooler than the temperature inside the quartz sleeve, mercury condenses on the quartz sleeve from inside, and process of reabsorption of mercury plasma radiation inside the quartz tube affects the wall temperature and eventually affecting the quartz sleeve characteristics (Franke et al., 2006; Schöpp and Steffen, 2017).

Figure 4.10 illustrates the temperature profile, for the temperature inside the quartz sleeve and at the surface of the quartz sleeve (image taken by FLIR thermal imaging camera). Figure 4.10 justifies the temperature difference between the quartz sleeve surface and the inside of the sleeve. The inside sleeve temperature was ~63°C, while surface temperate of the quartz sleeve was relatively cooler than the inside of the sleeve.

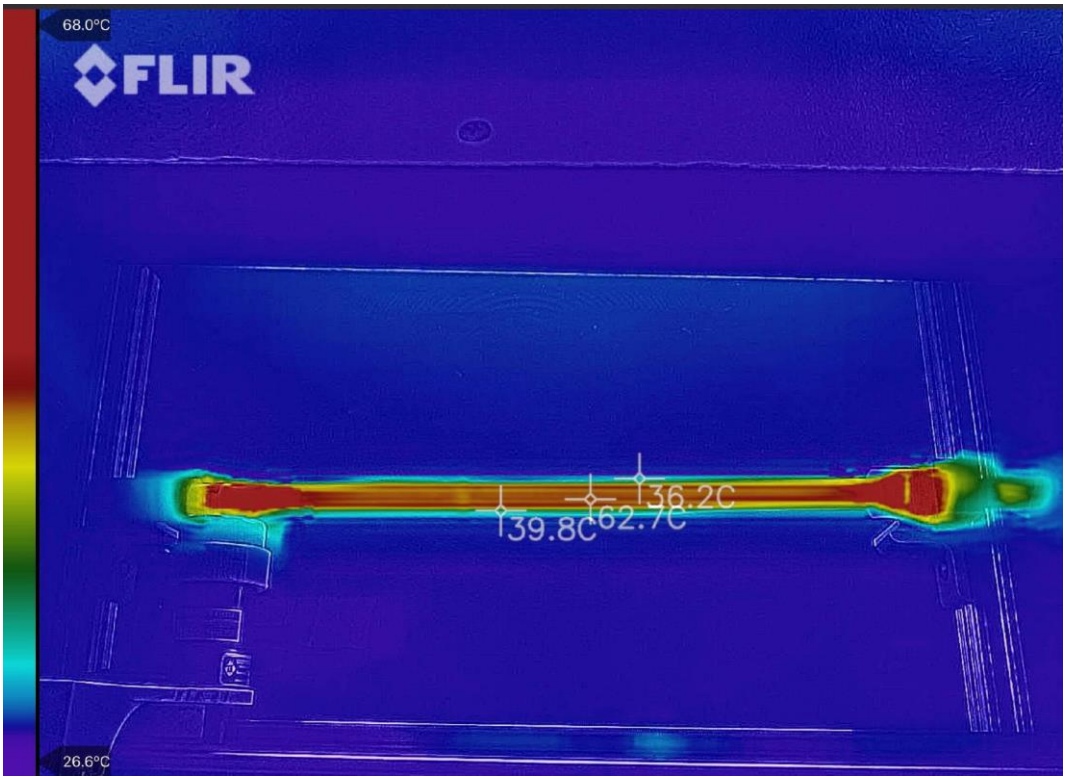

Figure 4. 10 Temperature profile inside and at a surface of the quartz sleeve

The inside temperature of the quartz sleeve ~ 60-70°C depending upon the hours of lamp operation under the corresponding lamp operating cycle (between ~1 to 10hours).

Figure 4.11 displays the temperature profile at the central part of the quartz sleeve after the lamp was warmed up. The ambient air temperature during the experiment was ~21 to 22°C; however, the temperature inside the black box (used to cover the set-up) was ~29 to 31 °C.

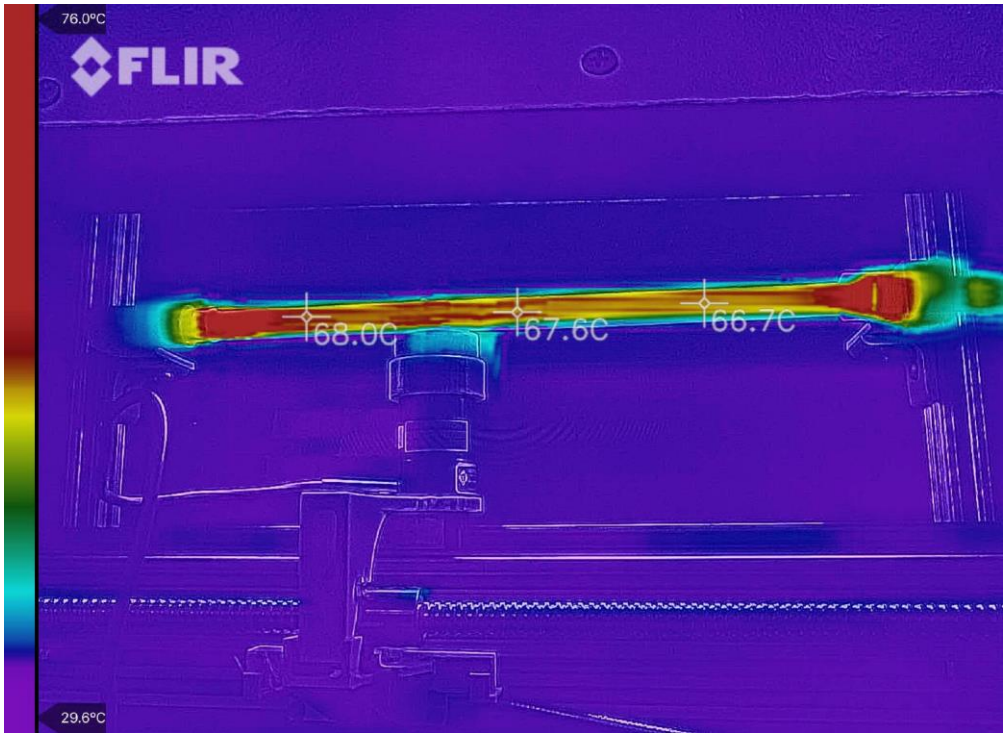

Figure 4. 11 Temperature profile at central part of the lamp

4.2.3 Solarization of the quartz sleeve material

Another visual ageing sign of the lamp was observed on the quartz sleeve due to the solarization of the lamp sleeve material in relation to the photochemical effect. It is very much similar to the sleeve fouling; however, it occurs as a result of the accumulation of the sputtered oxides of the electrode material on the lamp sleeve due to overheating of the electrode. Furthermore, in mercury pressure lamps the mercury can combine with the other constitutes present in the quartz sleeve, which results into the formation of the thin and non-uniform UV absorbing layer inside the quartz sleeve (USEPA, 2006). This effect leads to premature ageing of the quartz sleeve and results into decreased UV output due to affected UVT. Figure 4.8 in the previous section displays the formation of the thin layer inside the UV lamp sleeve. During experimentation, the formation of the spots on the quartz sleeve from inside was observed. The spots were formed near the mercury droplets and could be accountable photochemical degradation of the quartz sleeve material. Differential temperature zones inside the lamp sleeve and at the sleeve surface has shown in earlier figure (figure 4.10). The following figure displays the formation of the unusual spots at the central part of the lamp.

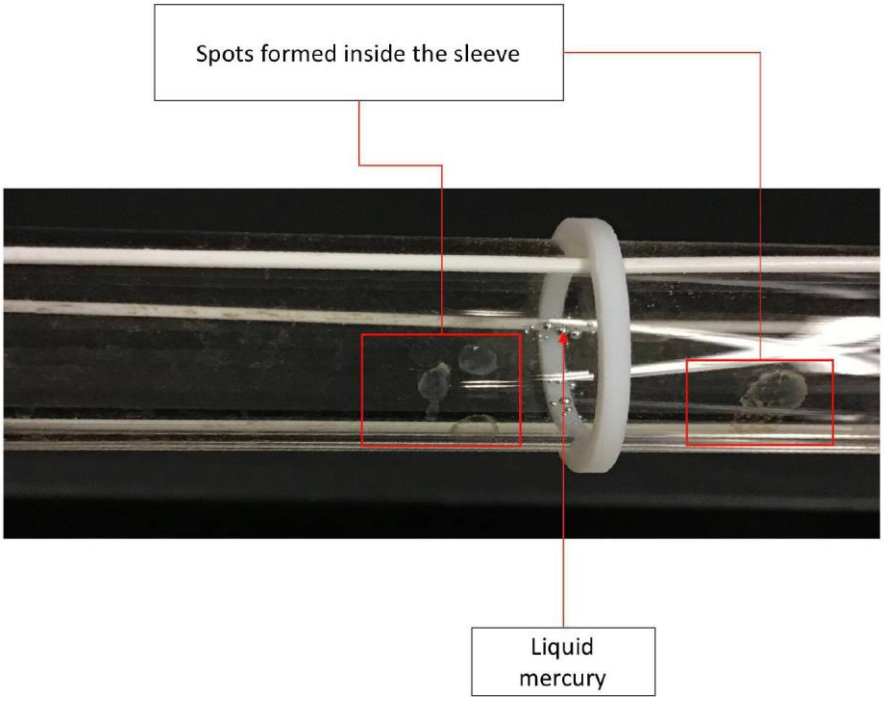

Figure 4. 12 Formation of the spots on lamp sleeve

4.2.4 Resonant darkening effect

The resonant darkening and distortion are driven by an effect of electric feed form the electronic ballast (AwwaRF and NYSERDA 2007). The resonant darkening of LP lamp used for the experimentation was characterized by the formation of the evenly spaced darken areas at the electrode from both the ends with the alternate region of peaks and lows. The resonant darkening gets particular shape by the formation of the standing waves within the plasma due to the variable operating frequency of the lamp ballast (AwwaRF and NYSERDA, 2007). The prolonged operation (~ after 6000 hours) of the UV lamp, leads to an intense resonant darkening and distortion of the lamp sleeve, it was narrated in the detail report by AwwaRF and NYSERDA (2007) for MP lamp. The following figure illustrates the formation of the preliminary alternate resonant darkening at the lamp electrode after 419 burn-in hours.

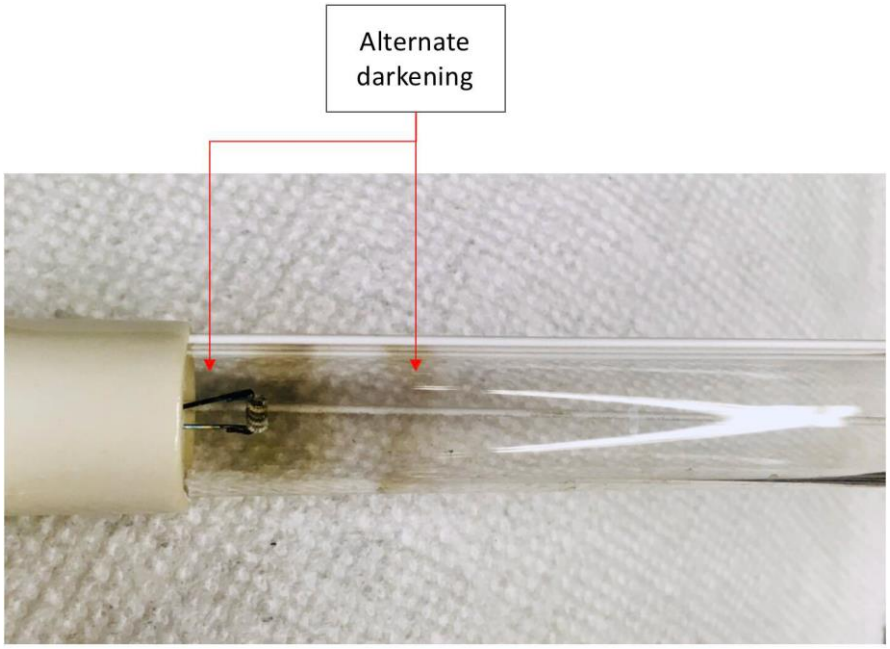

Figure 4. 13 Preliminary resonant darkening after 419 burn-in hours

4.3 UV lamp output stability test and results

The experimentation was performed for the initial 5% life span, i.e. 450 burn-in hours for the new LP UV lamp. The experimental analysis included the measurement of the UV lamp output for 254 nm irradiance along the length of the lamp with fully optimized direct UV measurement setup. The data collected, to study the UV lamp output comprised of the UV output stability during the warm-up phase for the corresponding lamp operating cycle (~10 hours). The UV output stability test was performed at one lamp electrode, i.e. opposite to the electrode feed pins. The following figure illustrates the setup arrangement and sensor position for the UV output stability test.

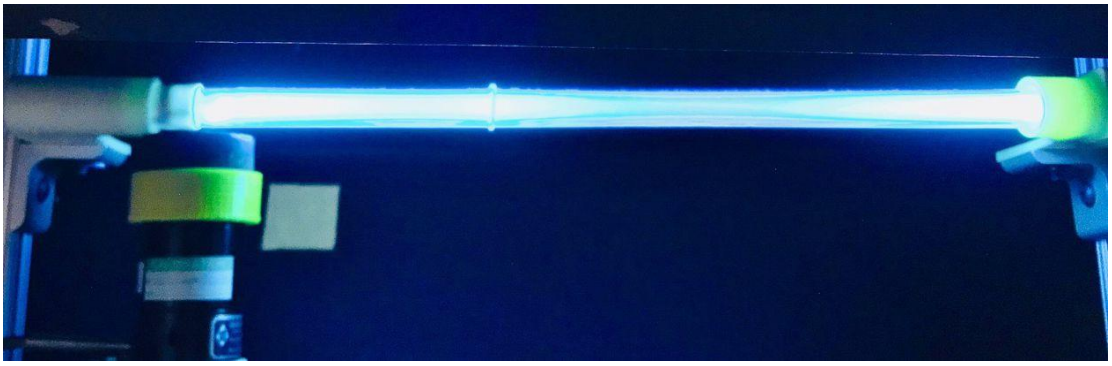

Figure 4. 14 Lamp UV output stability test arrangement at position 0.00

The stability test was performed for each operating cycle of the UV lamp prior to begin with the experimental run on an hourly basis, to observe any unexpected behaviour in lamp stability (i.e. for every lamp ignition ~ 45 tests). However, in this report, only one-line graph per week has been represented; especially the data collected at the beginning of the week and at the end of the week has been plotted for comparison (for stability test). The stability test was performed for the ~20 to 30 min at 0.00 cm position at the electrode. The UV output obtained during this test was plotted as a function of the time.

Figure 4.15 illustrates the UV output stability curve for position 0.00 cm, the UV irradiance for position 0.00 cm has plotted as a function of time. The data was collected during the lamp warm-up phase after every ignition at corresponding operating cycle. Following figure 4.15 was plotted at the beginning of every week when the lamp was stabilized after the ignition, to notify the change during weekly operation of the lamp

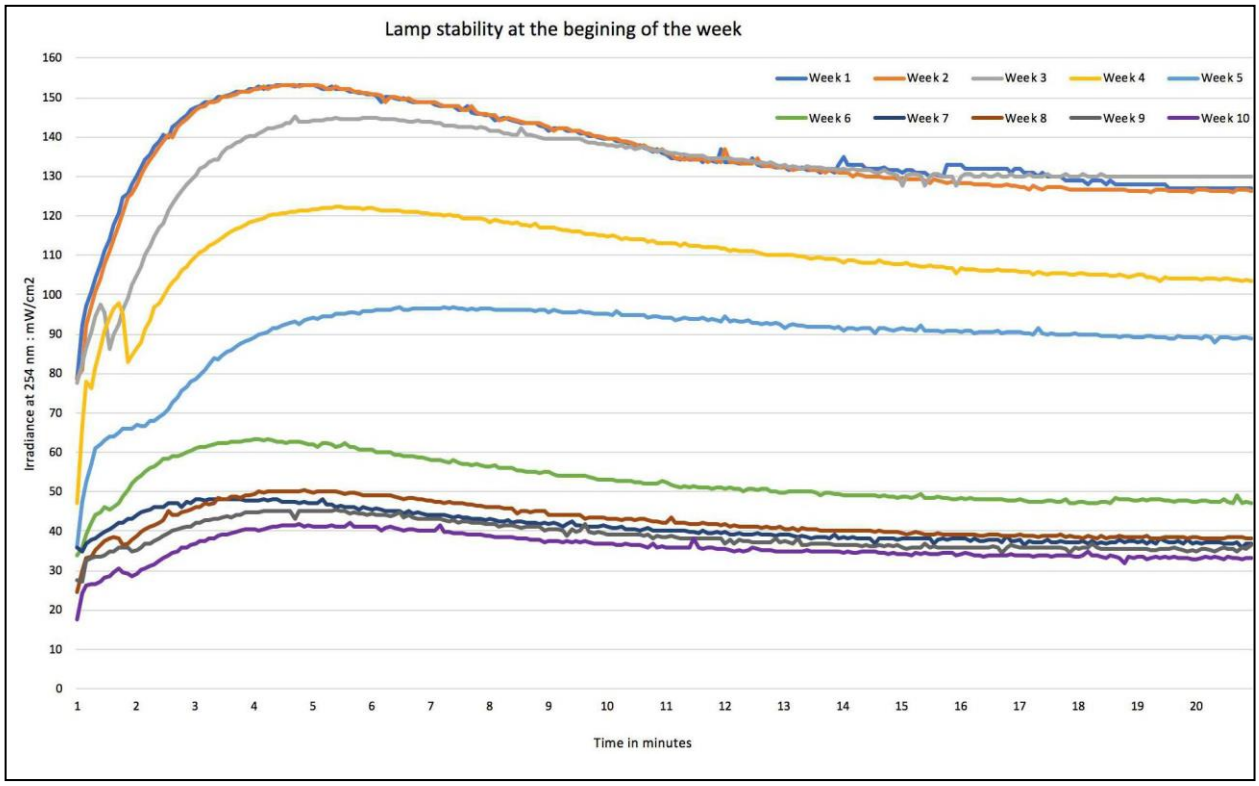

Figure 4. 15 UV output peak and stability at the beginning of every week

Initially when LP lamp was new, the UV output at position 0.00 cm was extremely high, when compared to the UV output at later stages as see in figure 4.15. During week 1, week 2 and week 3, the lamp output was extremely high and was able to stabilize at the higher output when compared to the later experimental stages during lamp operation. However, after week 3, the UV output consistently decreased for position 0.00 cm. Furthermore, in earlier figures 4.1, 4.2 and 4.3 the darkening near the lamp electrode has reported, which can be a considerable reason for reduced output at position 0.00 cm due to an obstruction to UVT.

The appearance of the electrode darkening was first noticed during week 4 of the lamp operation, which became more denser during week 7, as can be seen in figure 4.2. After week 7, the lamp output at position 0.00 cm was decreased by 70% based on the output obtained when the lamp was new, and output obtained after week7. As can be seen in figure 4.15, after the lamp ignition, the UV output reached its peak, and after that, it consistently decreased towards a stable output range. Initially, the peak value of the lamp output at position 0.00 was extremely high during week 1 and week 2. However, as the lamp was operated further, the peak output value decreased, so does the value at which lamp was able to stabilize. As mentioned previously, the reason behind this drastic decrease in output is the non-uniform ageing phenomenon of the lamp which can be confirmed based on the following figure, in which darkening of the lamp electrodes can be spotted, which is prevalent than any other section of the lamp sleeve.

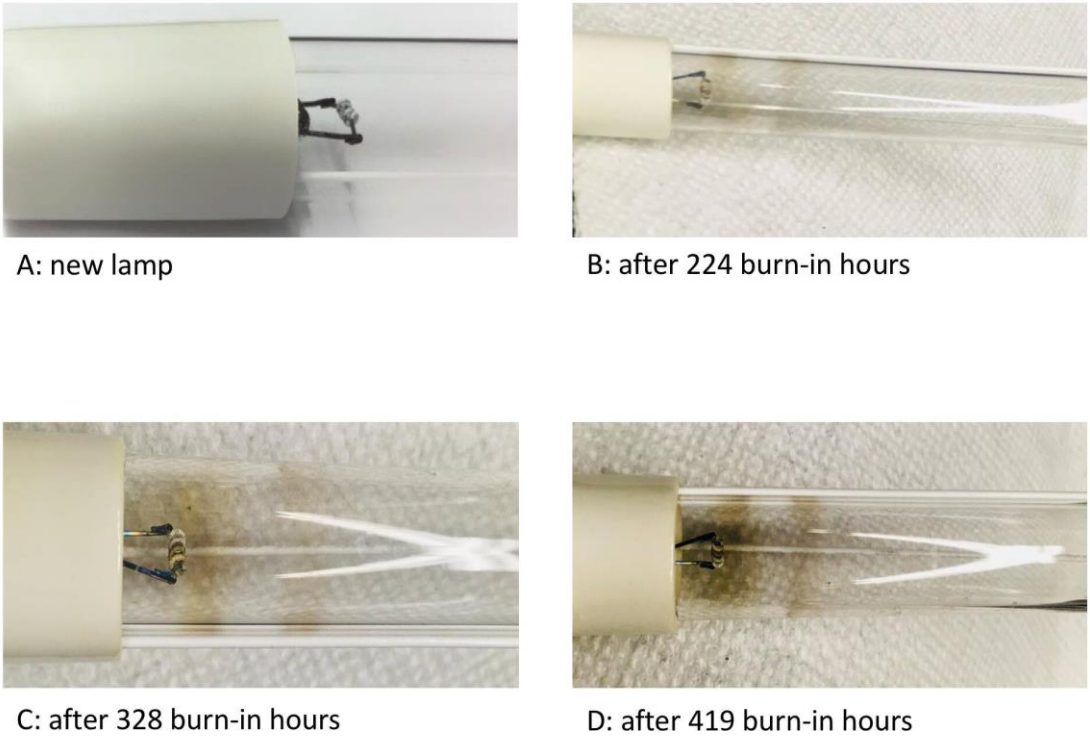

Figure 4. 16 Lamp end darkening

The following table demonstrates the weekly variable lamp output and corresponding peak and stability range at position 0 (0.00 cm).

Table 4. 1 Weekly peak and stable output at the beginning of the week for position 0.00 cm

Week	Burn-in hours at the time of curve plot	Peak irradiance at 254 nm mW/cm^2	Stable output at 254 nm mW/cm^2
Week 1	~5	153	127
Week 2	19	153	126
Week 3	64	145	130
Week 4	109	122	104
Week 5	154	97	89
Week 6	200	63	47
Week 7	269	46	37
Week 8	328	51	38
Week 9	370	45	37
Week 10	419	42	33

The graph shown in figure 4.17 was plotted at the end of every week to observe weekly variation at scheduled intervals to notify a change in the output stability of the UV LP lamp at fixed position 0 (0.00 cm).

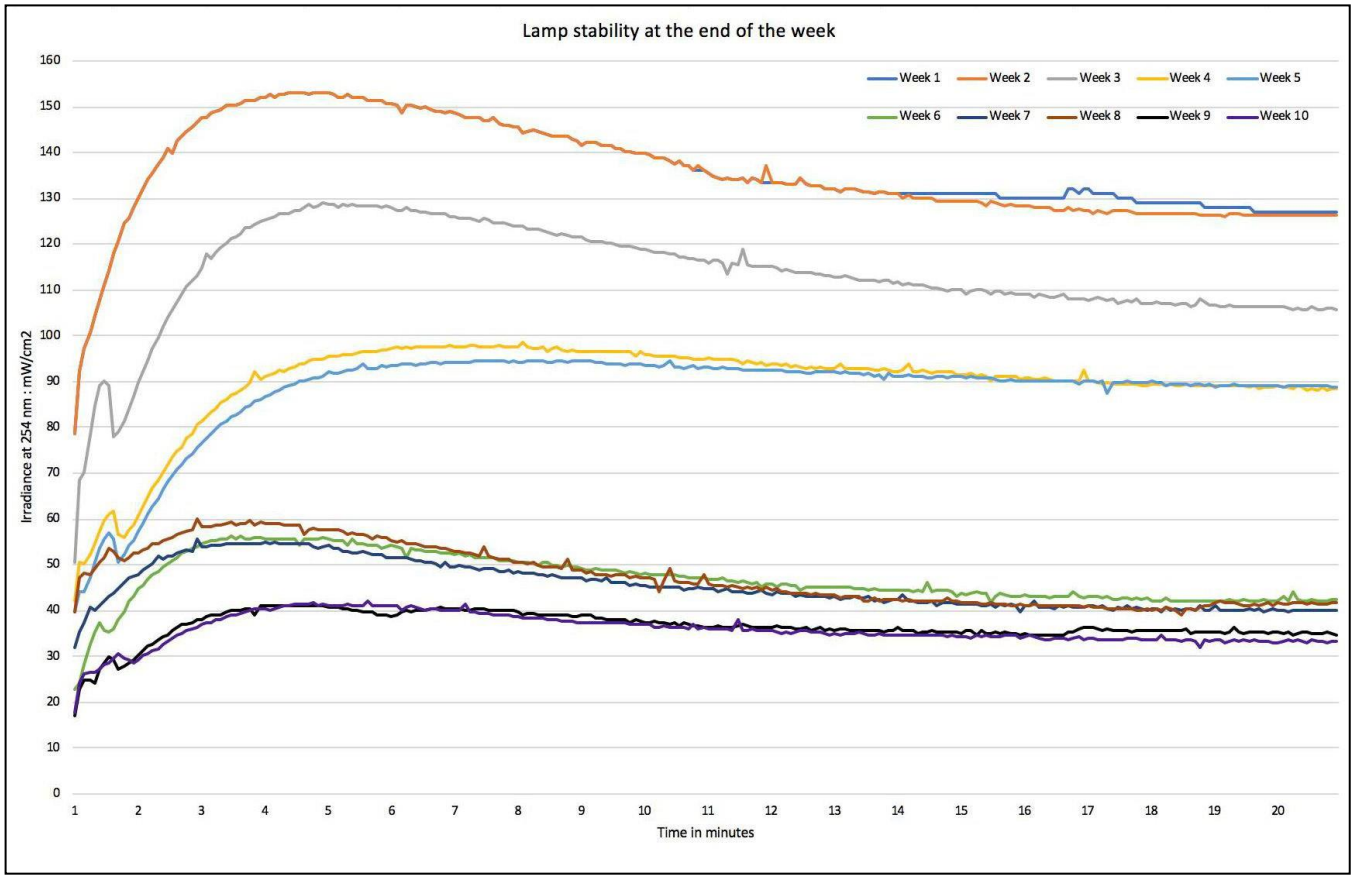

Figure 4. 17 UV output stability test during lamp warm up phase after lamp ignition

During week 1 and week 2, when the lamp had less than 50 burn-in hours lamp performed exceptionally well, with peak UV irradiance up to 150 mW/cm2. The output was outstanding with less fluctuating UV stability and stable output after reaching the maximum UV output during the warm-up phase at the corresponding lamp operating cycle (refer figure 4.19 and 4.20). During week 3 (i.e. after 109 burn-in hours) the output of UV lamp decreased, compared to the previous week's output. Also, the peak irradiance, which preliminary was able to reach to 150 mW/cm2 decreased to 129 mW/cm2 and was able to reach stability at 100 mW/cm2 irradiance.

After week 3, the UV output at position 0.00 cm consistently dropped as can been seen the figure 4.17. After week 5 (i.e., during 224 burn-in hours) extreme drop in UV irradiance at position 0.00 cm can be seen as a result of the darkening at the electrode on the lamp sleeve as shown in figure 4.1. Furthermore, the drop in UV irradiance at position 0.00 cm continued, and afterwards when the lamp was operated for 328 hours the darkening at the electrode become predominant; consequently, it affected UVT at 0.00 cm location when compared to the other location across the length of the lamp. Figure 4.2 displays the denser darken layer at position 0.00 cm as the influence of non-uniform lamp ageing. By the end of 328 burn-in hours, the lamp UV lamp stability for position 0.00 was 50 mW/cm^2 with peak intensity at 65 mW/cm^2 during the warm-up phase.

The consistent decrease in the UV intensity continued, and by the end of the scheduled experimental phase (i.e. at 450 hours) the peak UV output during warm-up phase was 40 mW/cm^2 and after the warm-up phase lamp was able to stable output at 40 mW/cm2. The reason behind this extreme drop in UV output at 0.00 cm position is the darken lamp area at the electrode which had affected the UV transmittance of the quartz sleeve. The darkening of the quartz sleeve near electrode has shown in the following figure 4.18

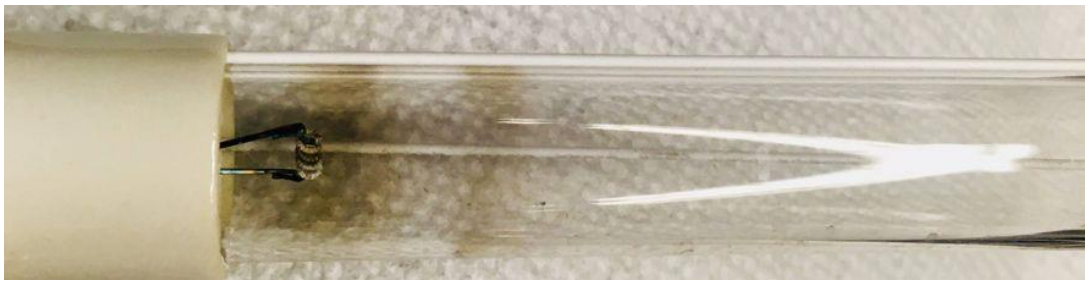

Figure 4. 18 Darken area around the lamp electrode during week 9

Furthermore, initially the lamp was able to stabilize with almost null fluctuations in the output; however, as the lamp aged and darkening appeared at the end of the lamp near electrodes, the UV output has shown slight fluctuations, which can be perceived from figure 4.15, line graph for week 7, week 8, week 9, and week 10.

The following table summarises the UV lamp output during the stability test for peak intensity after lamp ignition (for corresponding lamp operating cycle) and the UV output value at which lamp irradiance was stabilized.

Table 4. 2 Weekly peak and stable output at the end of the week for position 0.00 cm

Week	Burn-in hours at the time curve plot	Peak irradiance at 254 nm mW/cm^2	Stable output at 254 nm mW/cm^2
Week 1	19	153	127
Week 2	64	153	126
Week 3	109	129	106
Week 4	154	98	89
Week 5	200	95	89
Week 6	269	56	43
Week 7	328	55	40
Week 8	370	60	42
Week 9	419	42	35
Week 10	450	42	33

4.4 UV lamp irradiance at 254 nm along the length of the lamp

Irradiance at 254 nm was measured along the length of the lamp by 2000 µm increment in one radial direction of the lamp. The purpose behind focusing only one radial direction during the entire experimental phase was to keep lamp components undisturbed as disturbance could have affected filled mercury and inert gas. The experiment was initiated, after the UV lamp output was stabilized, which was verified through computer program generated textual file as well as through the radiometer readout, as shown in figure 3.13 in the previous chapter. The procedure and sequences of the steps followed for this experimental analysis has described in section 3.6. This section elaborates the changes occurred in the UV output every week. Furthermore, it contents the particular measurements results at when the visible ageing sign of the UV lamp was observed, i.e. spots and scaling on the lamp sleeve.

4.4.1 UV output of new lamp

The figure 4.19 shows the spectral output of the new lamp at 254 nm. Initially, the UV output from the new LP lamp was extremely high, even more than the desired intensity, required to inactivate the microorganism. The optimum range of UV output is >0.1 W/cm2 or >100 µW/cm^2.

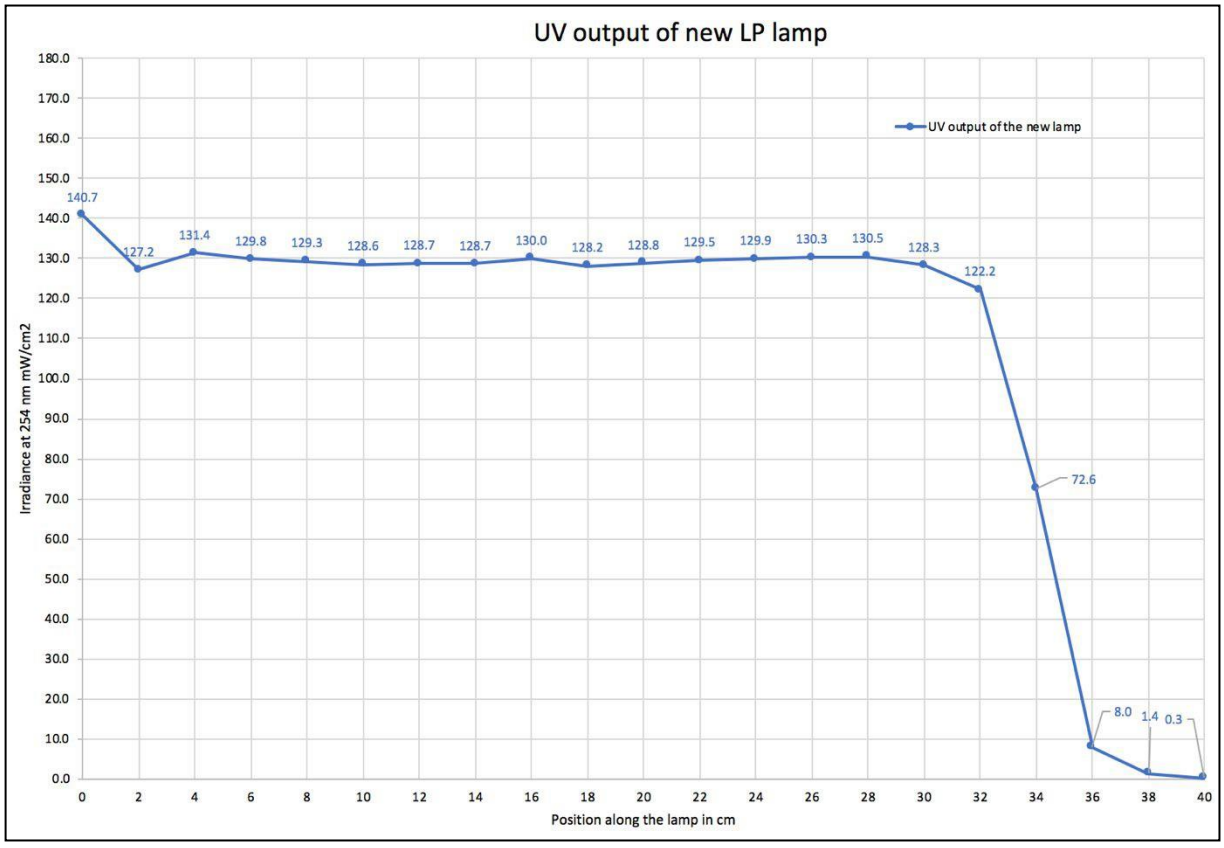

Figure 4. 19 UV output of the new lamp at 254 nm

The LP lamp was new with ~5 burn hours, and the line graph shown in figure 4.19 was generated prior to 100 burn-in hours . Although the lamp was new with less than 100 burn-in hours, the lamp had a non-uniform output with unexpected peak and dune formation. The lamp output was increased rapidly from the low output at lamp ends at position 0 and 40, with peak output at position 16, 22, 26.

4.4.2 UV output variation during week 1 and 2

As mentioned earlier (in section 4.1), the experimentation was performed daily, and results were prepared based on the averaging method. Figure 4.20 illustrates the UV output at 254nm along the length of the lamp during week 1 and week 2.

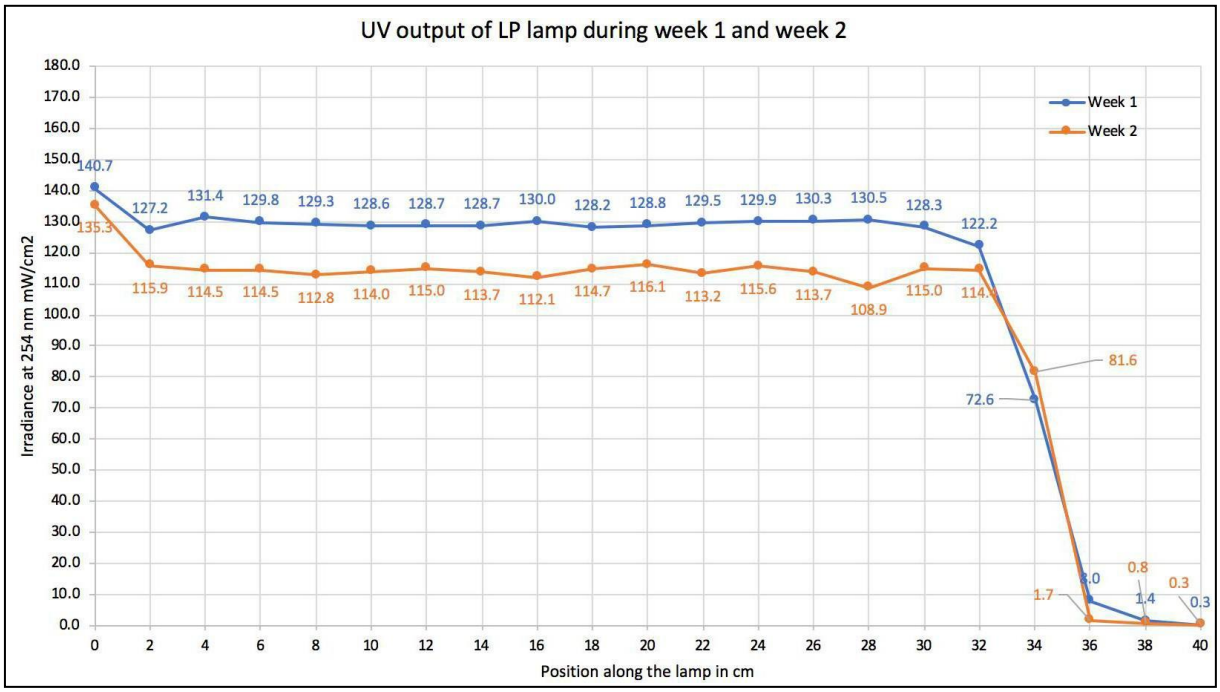

Figure 4. 20 UV output at 254nm along the length of the lamp during week 1 and 2

As can be seen in figure 4.20, the lamp output during week 1 was almost stable, providing uniform output across the length of the lamp, with slight variation due to varying voltage and electric feed. During week 1of experimentation, the lamp was relatively new (~ 5 hours) the graph data shows the average of ~19 hours (+ warm-up time). During week 1, slight output peak formation at position 16 and 28 was observed output dune or drop at position 2 was consistent. The lamp was 40 cm long; however, position 36, 38 and, 40 were partially covered by the support structure and electric feed (refer figure 3.3 and 3.5 for setup arrangement). The UV output at electrode dropped by 3% while, at the central part of the lamp UV output dropped by 13% when compared among the week 1 and week 2 data.

Later, during week 2, the UV output was dropped, which can be verified by the week 2 line graph from figure 4.20. During week 2, the lamp was operated for 64 burn-in hours. As can be seen in figure 4.20, the drop formation at position 2 continued, furthermore the peak formation was shifted towards the position 20 from position 6, and from position 22 to position 24. This lamp behaviour can be accountable for the tendency of the non-uniform UV output as a consequence of variable interaction of the lamp operating parameters, i.e. in-constant voltage, speed of mercury activation and photochemical reaction between the mercury atoms and electrons).

4.4.3 UV output variation during week 3 and 4

Figure 4.21 illustrates the LP lamp output during week 3 and week 4. As can be seen in figure 4.21, the line graph of week 3 and week 4, shows a non-uniform output, although the experimentation was performed after the UV lamp was stabilized after the warm-up phase. The results obtained during week 3 and week 4 were unexpected. The graph plotted for the week 4 data shows the extreme drop at position 12, though the lamp was operated for the same operating conditions.

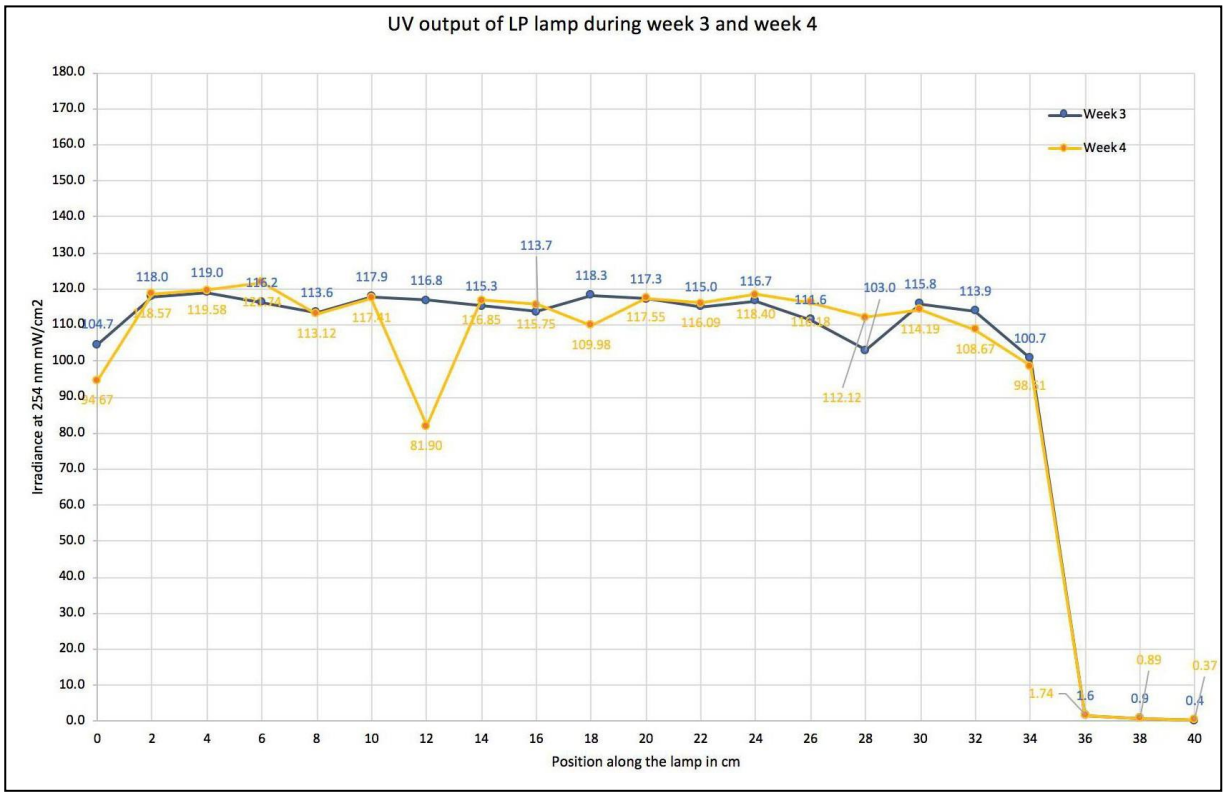

Figure 4. 21 UV output at 254nm along the length of the lamp during week 3 and 4

The week 3 graph (109 burn-in hours+ warm-up time) shows 25% reduction in the UV output and week 4 (154 burn-in hours + warm-up time) shows 32% reduction in UV output at position 0 near the electrode, when compared with the data obtained for the newer lamp (refer figure 4.20). Furthermore, during week 3, output drop was formed at position 28; however, during week 4, the output drop disappeared. There is no precise explanation available because the LP lamp was operated under the same conditions, and the thermal camera was implemented after the 4th week

of lamp operation. The extreme drop at position 12 in a line graph of week 4 appeared after 118 burn-in hours, which held steady drop position during week 4 (for ~ 45 continual operating hours). The extreme drop at position 12 shows 36.36% reduced output when compared with the output than was measured in week 1 (5 burn-in hours) for position 12. The drop at position 12 was consistent, and its consistency was verified by examining the UV output measurements after 118,127,136,145 and 154 burn-in hours. Moreover, the output drop that was confirmed at position 28 during week 3 shows 8.74% increase during week 4 for the same position.

The drop that can be seen at position 28 during week 3 of lamp operation remained consistent during the entire week, and it was confirmed by verifying the measurements after 73,82,91,100 and, 109 burn-in hours.

4.4.4 UV output variation during week 5 and 6 and consistent drop at position 12

Figure 4. 22 shows the variation in UV output of LP lamp during week 5 and week 6. As can be seen in the line graph for week 5, the output drop at position 12 was consistent for ~ 98 hours span, with the slightest increase in the UV output at position 12, i.e. by 11.1 % during week 6. However, it had 29.13 % decreased output, when compared with week 1 data. As previously observed, the output drop at position 12 was unmoving, and its consistency was verified again after 163,170 and 177 burn-in hours during week 5. However, the drop at position 12 started to be disappeared after 188 burn-in hours during week 5, with slightest peak formation after 200 burn-in hours, and after 212 burn-in hours, the drop at position 12 was disappeared entirely, and formation of the peak was observed.

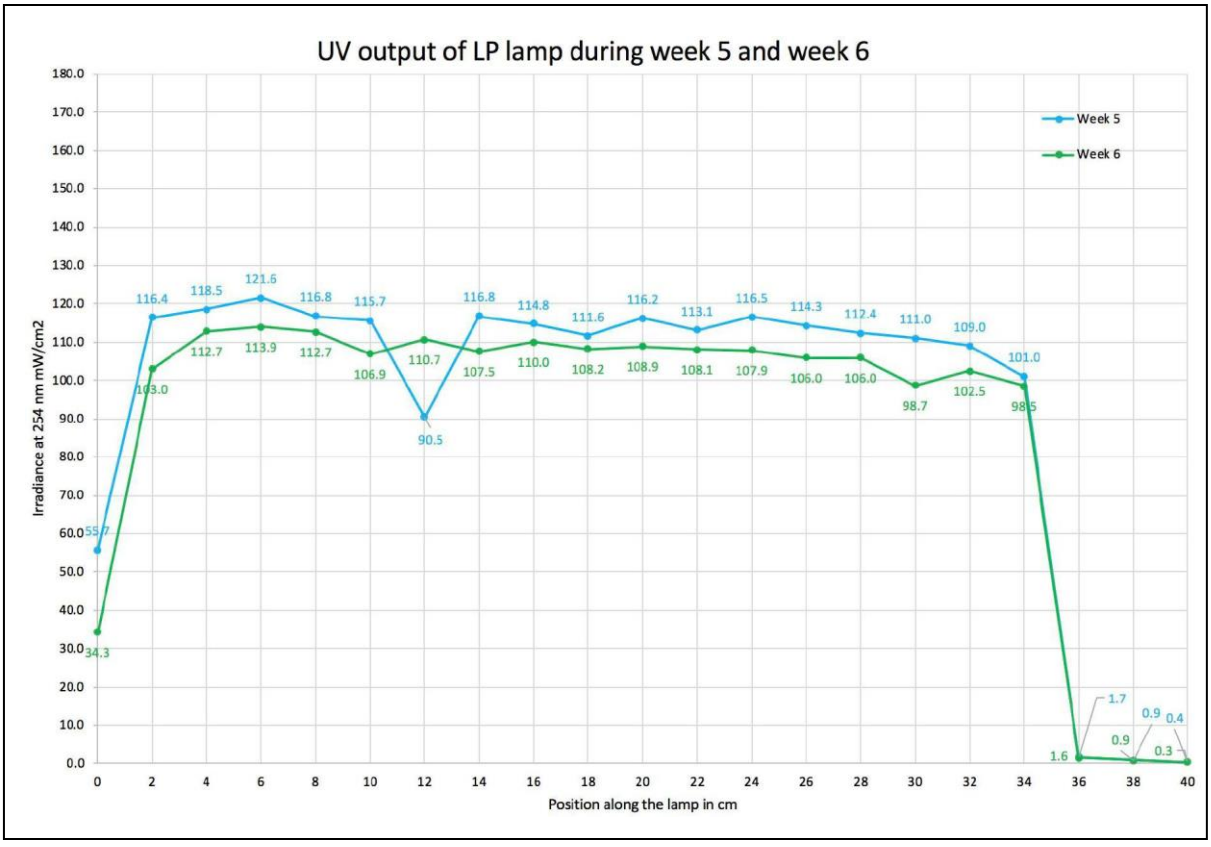

Figure 4. 22 UV output at 254nm along the length of the lamp during week 5 and 6

But, if graph of week 5 and week 6 are compared, the drop at position 12, which was consistently observe before (i.e. during week 3, week 4 and week 5) has disappeared and has merged and upheld the rise in the output by 22.2 % , when compared with the previous week's output (i.e., week 5). Though, the output at position 12 was still 15.38% less compared to week 1 output. Moreover, another output drop, which was spotted during week 3 and week 4 at position 28, has been disappeared during week 5 and week 6. However, its disappearance did not increase UV output significantly at position 28.

The experimental analysis was able to notice a non-uniform output pattern along the length of the UV lamp, which disclosed a decrease in UV output for all position when compared with the data obtained during week 1. Another observation that can be seen in the above graph is a shift in the position of the output drop; the drop at position 12 disappeared with the formation of another output drop at position 10. Likewise, output drop at position 28 disappeared, with the formation of another drop position at 30. There is no justifiable answer to this phenomenon. However, this non-uniform output pattern can relate to the temperature gradient along the length of the lamp, as mentioned by the Schmalwieser et al. (2014).

Figure 4. 23 displays the temperature profile for specific locations. Figure 4.23 shows a thermal image taken by a FLIR thermal imaging camera. In thermal image small colder spot was observed, which had a different temperature than the rest of the locations along with the lamp, and it can be accountable for the consistent drop at position 12. Furthermore, the thermal image confirms the partial part of the lamp had a non-uniform temperature profile. Moreover, the temperature profile along the length of the lamp became intensively uneven as the lamp was operated for further burn-in hours (after ~350 burn-in hours).

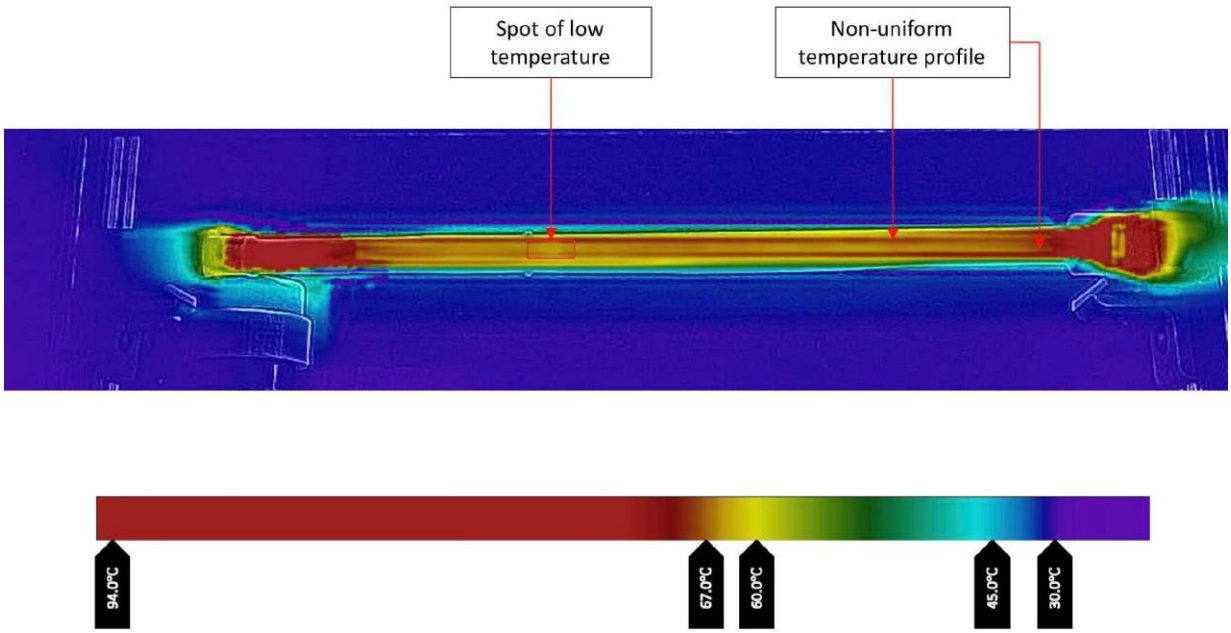

Figure 4. 23 Thermal image showing cold spot formation position 12

4.4.5 UV output variation during week 7 and 8

Figure 4.24 shows the UV output of LP lamp during week 7 and week 8. The graph for week 7 and week 8 has a significant resemblance. However, based on the comparison between UV output results of week 7 and week 8 with an earlier result (i.e., when lamp had considerably less burn-in hours), we can recognize decreased UV output as well as non-uniform output pattern along the length of the lamp. Earlier, during week 3, week 4 and, week 5, formation of the intense drop at position 12 was noticed, which has disappeared during week 6 experimental measurements, and as can be seen in the line graph of week 7 and week 8, the peak formed at the position 12 and position 28 remained continual throughout the week. Figure 4.26 confirms the disappearance of the cold spot at position 12 as output at position 12 was back to required output range, which was noticed during week 6.

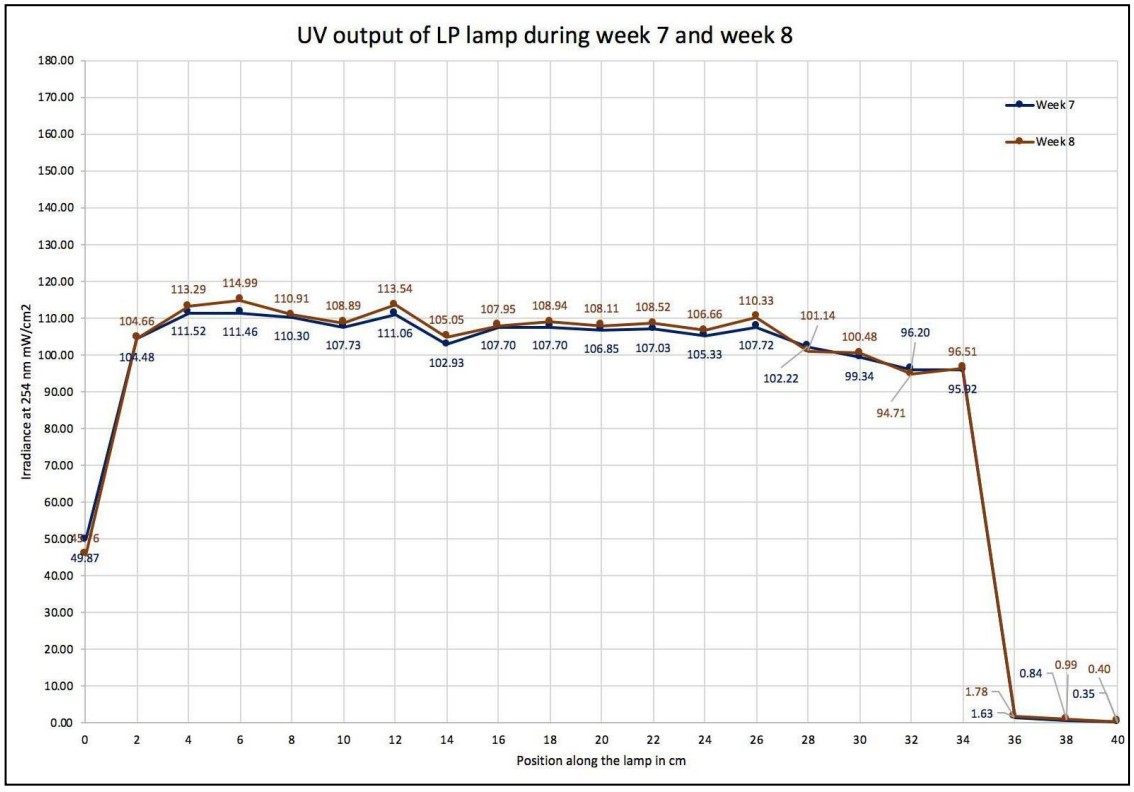

Figure 4. 24 UV output at 254 nm along the length of the lamp during week 7 and 8

Previously, in another study by Schmalwieser et al.(2014), it has mentioned that the UV output along the length of the lamp rapidly increase from the lamp ends and then reaching towards the maxima at 2 locations along the length of the lamp, and in between these two maxima lamp output has sharp drop; however it is appropriate for the lamps with amalgam spots. However, the LP lamp that was used for this experimental analysis has showed formation of the peak at position 12 and 28, and lamp output held the peak output at these spots during week 6, week 7, and week 8; though there was a new drop formation in a line graph at position 14 and position 24. The lamp output along the length of the lamp did not have significant change; however, the lamp output was continually reducing.

During week 7 and week 8, the UV output along the lamp length was significantly similar, however, if the results are compared with earlier measurement results, the non-uniform output pattern along the length of the lamp can be confirmed. During week 6, week 7 and, week 8 UV output at positions 16,18,20,22 and, 24 has not changed. In a line graph of week 7 and week 8, the drop in the UV output for positions 28,30,32 and, 34 can be seen, which can be a result of scaling formed on the lamp sleeve as previously mentioned in section 4.2.2 and as shown in figure 4. 25.

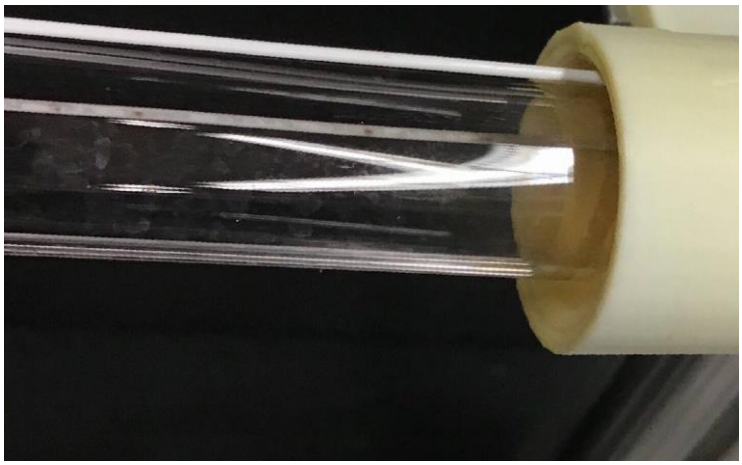

Figure 4. 25 Scaling of the lamp sleeve during week 7

Figure 4.26 displays the non-uniform temperature profile along the length of the lamp, clarifying the inconstant temperature at the affected areas along the length of the lamp. The inconstant temperature profile can be considered as another reason for the affected mercury ionization and generation of the photon energy, ultimately affecting the UV output. As can be noticed in the thermal image below, the temperature at the lamp area near 24 cm to 30 cm had a variable temperature; the lamp sleeve was ~25°C cooler than the inside lamp temperature. This variation in temperature profile can cause mercury condensation at lamp sleeve, which affects mercury ionization as well as the entire process of UV radiation generation (recapped from section 2.6.4.2 and 4.2.2).

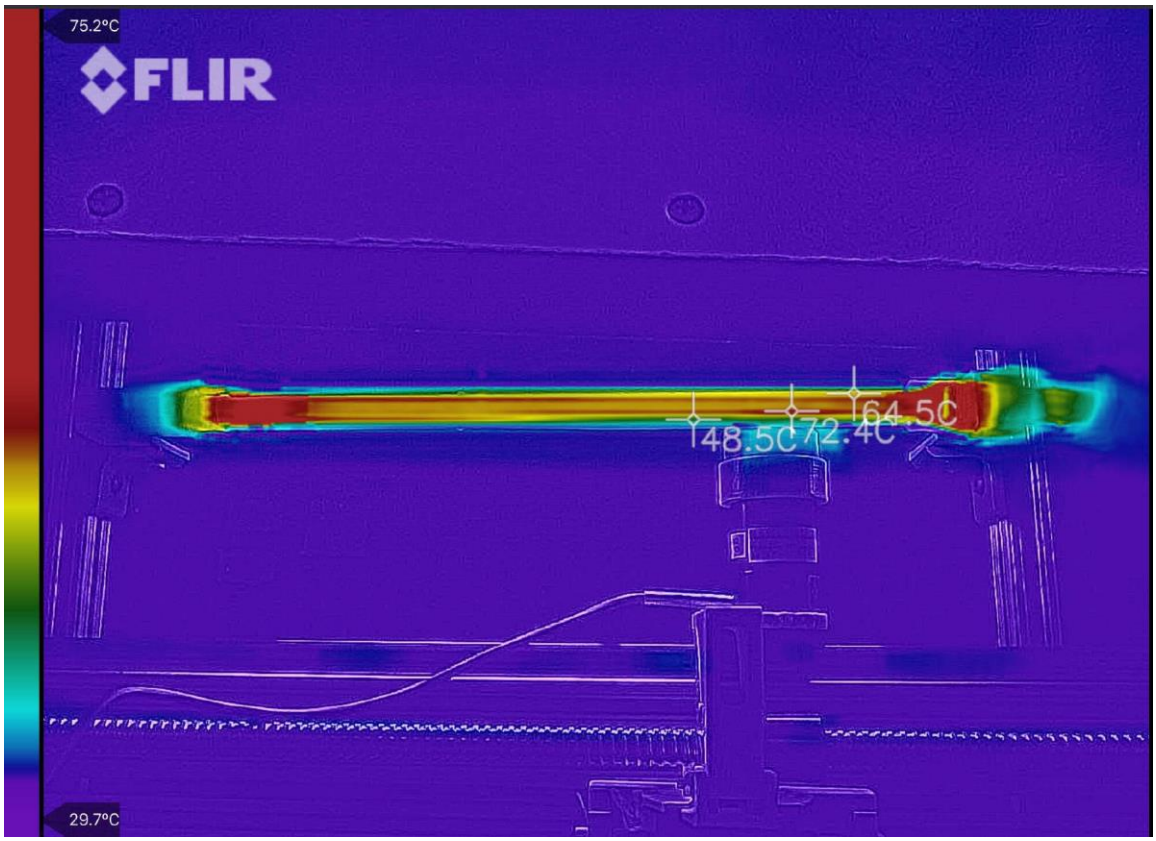

Figure 4. 26 Thermal image showing inconstant temperature profile at lamp area

4.4.6 UV output for variation during week 9 and 10

Figure 4.27 shows the UV lamp output along the length of the lamp during week 9 and week 10. As can be observed in the line graph for week 9 and week 10, the UV output of the lamp along its length, followed significantly similar output pattern, but with decreased output during week 10 (450 hours + warm-up time) than the output, observed during week 9 (419 + warm up time).

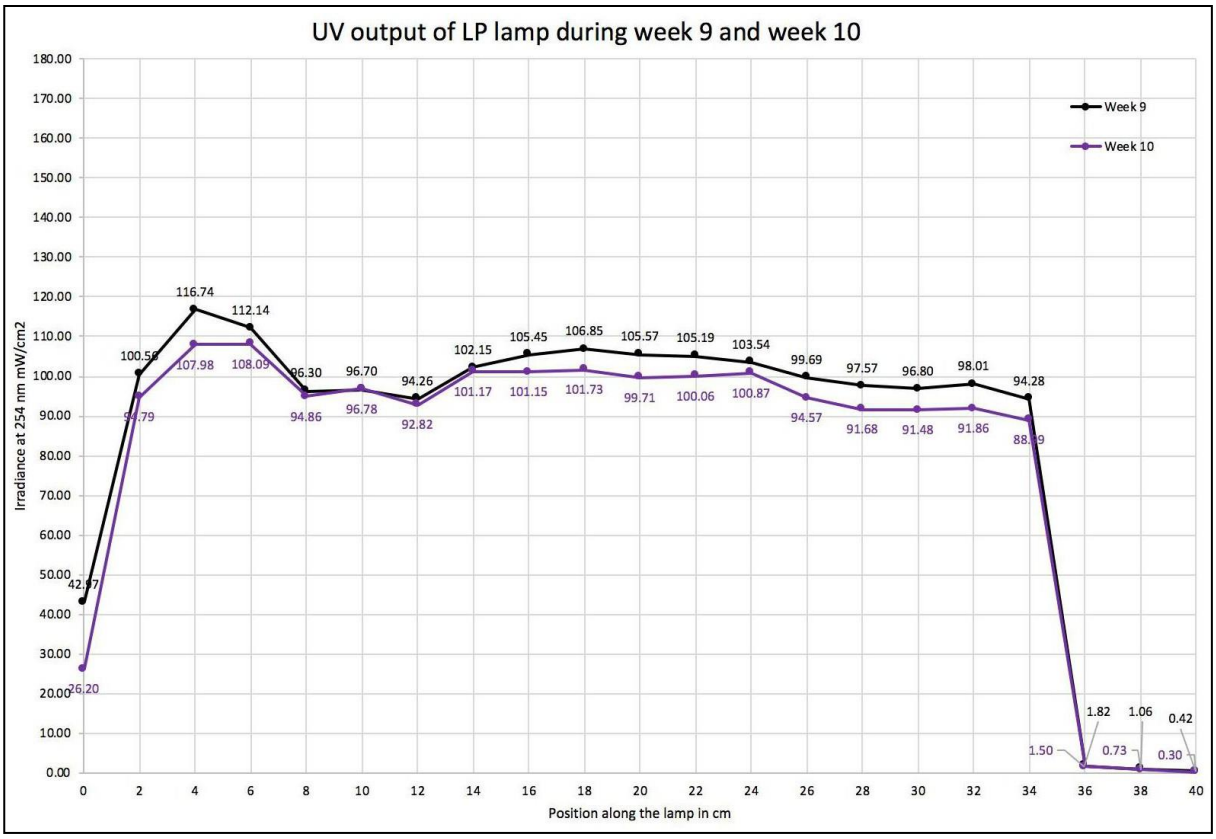

Figure 4. 27 UV output at 254 nm along the length of the lamp during week 9 and 10

If , UV output results of the LP lamp during week 9 and week 10 are compared, with the UV output results obtained during the week 7 and week 8, the change in the output pattern can be identified. Earlier, during the week 7 and week 8 measurement, the UV output for position 8, 10 and, 12 was ~12.73% higher than the output, that was observed during the week 9 and week 10. The non-uniform UV output, observed at position 8,10, and 12 can be an effect of the scaling spots formed on the lamp sleeve from the inside, as shown in figure 4.28.

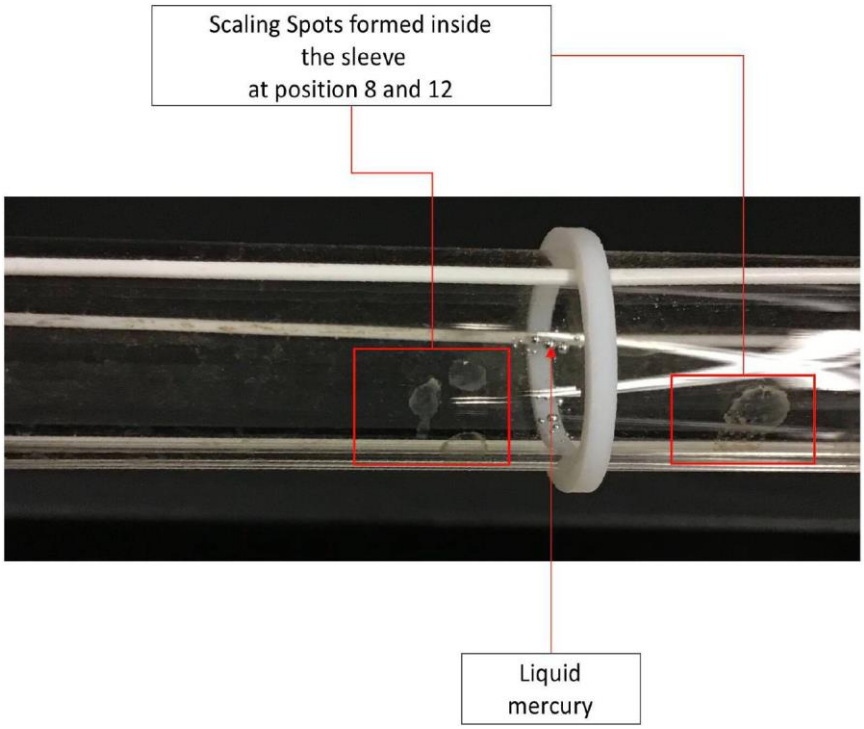

Figure 4. 28 Scaling spots at position 8 and 12 after 370 burn-in hours

Though the UV output was disturbed at the position as mentioned earlier, the UV output at position 14,16,18,20,22 and, 24 was indistinctly uniform with a slight decrease by 1.8% at position 18, 20 and, 22. Furthermore, for position 4 and 6, the UV output slightly increased (1.2%) than it was reported during the previous week's measurements. The UV output at position 2,4, and, 6 was not changed drastically during week 3 to week 8; however, it had patterned decrease in output as lamp was consistently operated. The reason behind the non-uniform output pattern can be considered as an effect of uneven discoloration and lamp sleeve fouling due to mineral deposition from electrode sputtering; it can be observed in figure 4. 29.

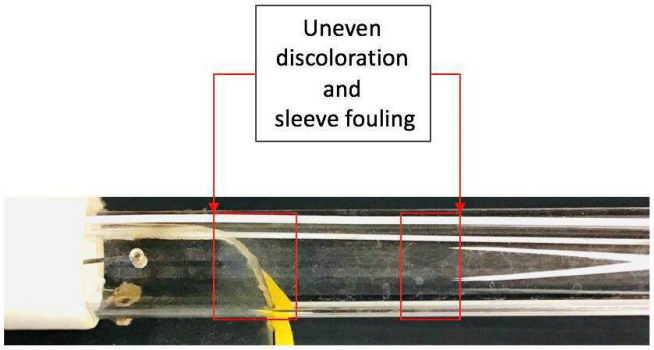

Figure 4. 29 Uneven discoloration and sleeve fouling after 419 burn-in hours

During week 7 and week 8, decrease in the UV output at position 28,30,32 and 34 was spotted, which was persistent during week 9 and week 8 as can be verified in the figure 4.27. During week 7 and week 8 UV output for position 28,30,32 and, 34 was significantly equivalent, however during week 9 the UV output for a position as mentioned above decreased by ~ 4%) and by week 10 the UV output decreased by 10% (when compared to the week 7 and week 8). When results were compared to the UV output that was obtained during week 1, 25% reduction for week 9 and 28.9% reduction in the UV output for week 10 results for position 28,30,32 and 34 was observed.

Figure 4.9 displays the scaling of the lamp sleeve at position 28,30,32 and, 34, which can trigger the non-uniform output by obstructing the transmittance of the UV radiation from the sleeve. However, the output measured during week 9 shows 70% decreases in UV output at position 0 (near electrode) and 81.3 % reduced output at position 0 during week 10. This extreme drop in UV output is due to a darkening of the lamp sleeve at the electrode. The initial darkening signs appeared after 224 burn-in hours and became denser later. The persistent spread of the darken lamp sleeve near the electrode can be in figure 4.16

4.4.7 UV lamp output after 450th burn-in hour

Figure 4.30, displays, two-line graphs of the UV lamp output along the length of the lamp after 5 hours of operation and after 450 hours of operation. As can be seen in figure 4.30, the UV output of the LP lamp has considerably changed since the beginning of the experimentation. At the end of the planned experimental phase, i.e. after 450 burn-in hours, the analysis confirmed the last drop at position 0 (lamp electrode) due to premature lamp ageing. Furthermore, lamp ageing was confirmed with the persistent darkening of the sleeve near the electrode as can be seen in the figure 4.16, which was affecting the UVT from the lamp sleeve, though the LP lamp was able to operate properly. The UV output at position 0 was dropped by 86.9% after 450 hours of operation due to darkening of the lamp sleeve near the electrode.

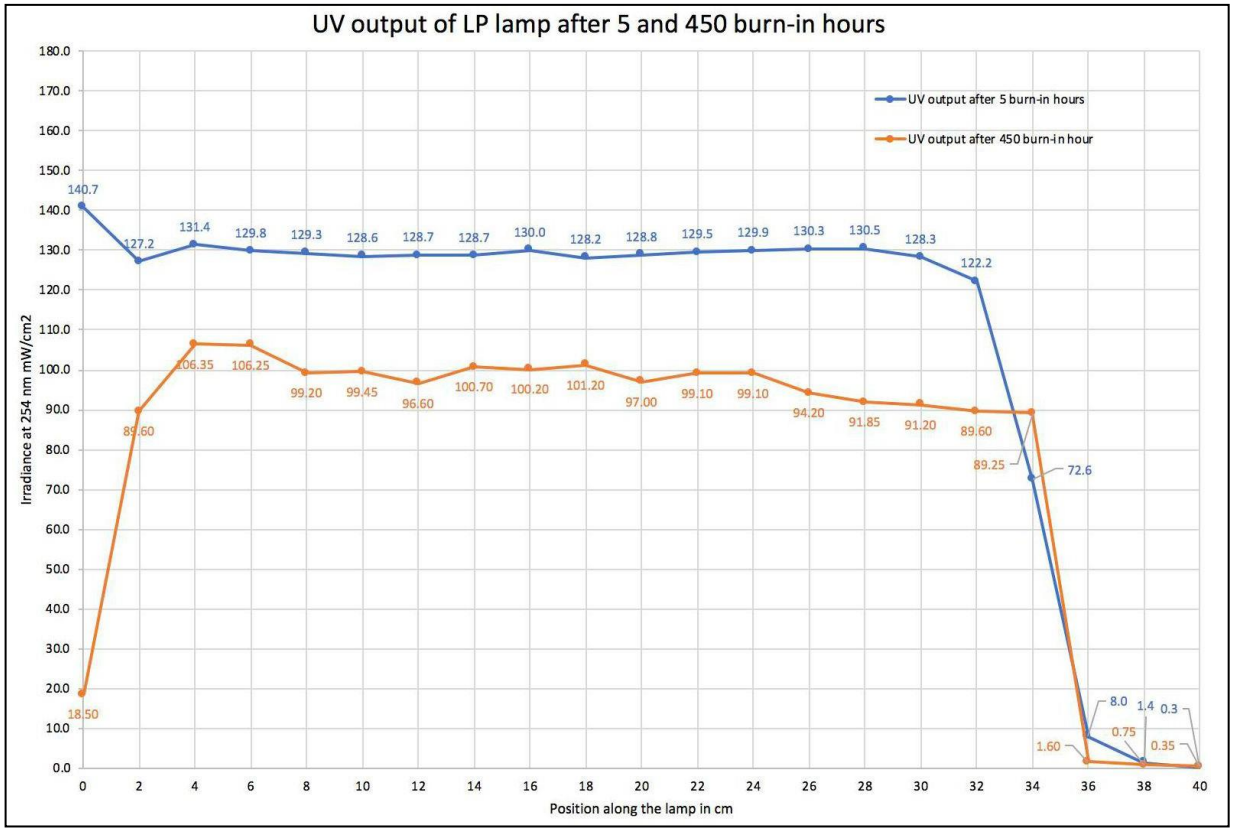

Figure 4. 30 UV lamp output after 5 and 450 burn-in hours

The UV output for position 2 and 4 was decreased by 18.9% at the end of the experimentation as a result of sleeve fouling and scaling patches formed on the sleeve, as shown in figure 4.29.

Likewise, the UV output at position 8,10 and 12 dropped by 22.66% due to the scaling spots appeared during week 9 after 419 burn-in hours. The UV output at position 14,16,18,20,22 and, 24 were less affected and did not show any intense signs of the disturbance in the UV output. Although, the output at these locations was dropped by ~21.88%, and analysis did not show intense scaling and discolouration similar to the positions mentioned earlier.

Furthermore, the experimental analysis confirmed a non-uniform UV output pattern for position 26,28,30 and, 32 with a sudden drop at position 28 during week 3. However, it disappeared during week 4 but reappeared during week 9 and 10. The analysis noticed fouling of the lamp sleeve at position 26,28,30,32, and, 34 after 298 burn-in hours (figure 4.7), which became more visible by 450 burn-in hours (figure 4.9) The UV output for position 26,28 and, 30 dropped by 30.8% when compared to the UV output measured when the lamp was new. Likewise, for position 32, the UV output dropped by 27%. For position 34, an unexpected result was observed because the UV output at position 34 increased by 4% than it was reported at the beginning of the experimental analysis (i.e. after 5 burn-in hours) thought the lamp was operated under the same condition throughout the entire experimental phase.

Overall, UV output along the length the lamp was consistent when the lamp was new. However, as the lamp was operated consistently, the UV output along the length of the lamp has changed. The changes occurred in the UV output were a consequence of the non-uniform ageing pattern, the discoloration and scaling formed on the lamp sleeve (figure 4.28, figure 4.8, figure 4.9), affecting the UVT of the lamp sleeve and considerably affecting UV output detected by the UV sensor. Furthermore, another reason for non-uniform UV output along the length of the lamp is uneven temperature profiles giving rise to cold spots (figure 4.23), which affects the overall temperature profile of the lamp sleeve, due to different temperature gradient along the lamp sleeve (figure 4.26), mercury condenses on the lamp sleeve from inside, which triggers the imbalanced mercury atom and electron collision responsible for the generation of the UV light and eventually affecting the UV output.

4.5 Temperature profile of the lamp

The non-uniform output of the UV lamp was observed with the direct measurement set-up, using radiometer-sensor configuration. Likewise, a non-uniform temperature profile along the length of the lamp was observed using a FLIR thermal imaging IR camera (figure 3.18). During experimental analysis, thermal images were collected at hourly basis to observe lamp temperature profile. During one lamp operating cycle, ~10 experimental runs were performed, and ~ 10 images were captured for every lamp operating cycle during the measurements. Figure 4.31 displays the temperature profile along the length of the lamp during one experimental run, at the time of the thermal image collection lamp had 370 to 381 operating hours.

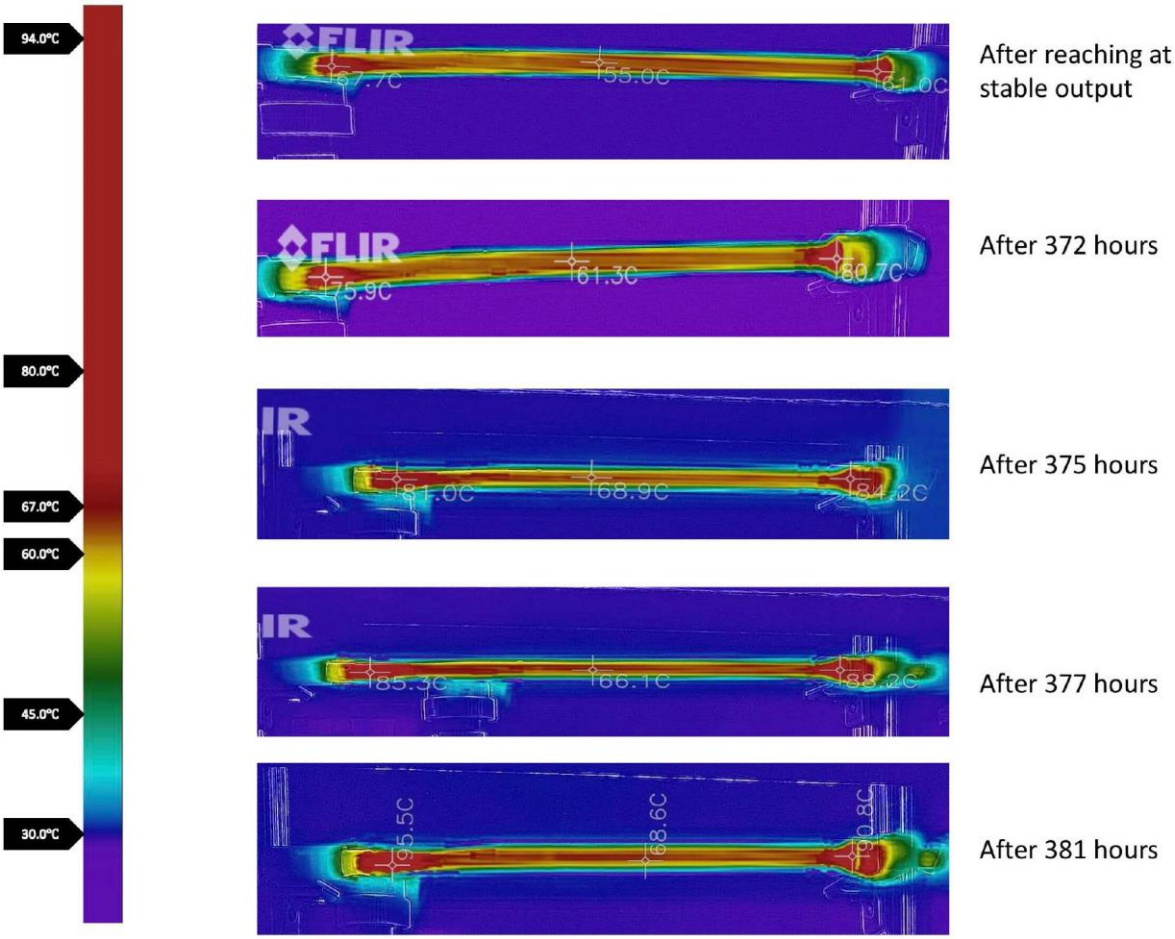

Figure 4. 31 Thermal image of the lamp during 370 to 381 operating hours

As can be seen in figure 4.30 at the beginning of the experiment lamp had a lower temperature; however, as the experiment was conducted further, the rise in temperature can be seen.
During initial 0 to 4 hours of lamp operation, the lamp electrodes were at lower temperature ~ 60°C to 70 °C, however as the experiment proceeded, we can observe, the lamp electrode showed a significant temperature rise to 90°C than the central part of the electrode. Especially the electrode on the left side (opposite to electric feed) always had a higher temperature than the rest of the lamp. The thermal images displayed in figure 4.31, were taken during the same experimental analysis while lamp had~370 burn-in hours.

The electrode on the left side in figure 4.31, has shown significant sleeve darkening than any other area on quartz sleeve, it can be seen in figure 4.16. Mainly, the temperature at both the electrode was almost the same as can be seen in figure 4.32. However, the right-sided electrode was partially coved with the by the electric feed configuration and support structure. The image shown in figure 4.32 was taken by a different angle to verify the temperature profile at both electrodes. The IR scale at the time of image click was fixed show temperature at 98°C.

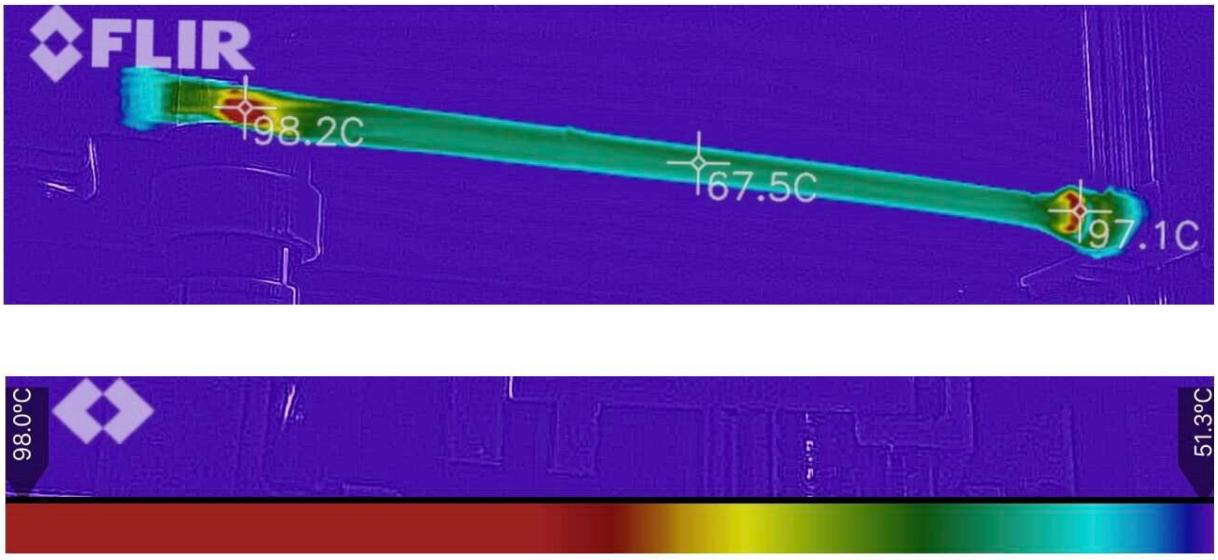

Figure 4. 32 Temperature profile at lamp electrodes (after 385 operating hours)

Furthermore, during 419 to 450 hours of lamp operation, the analysis reported temperature rise to ~103°C for the quartz sleeve at the left electrode, while the middle part of the lamp had ~70° temperature.

The reason behind temperature rise can be an outcome of heat absorption by the darken area near the electrode, which results in the overheating of the quartz sleeve near the electrode (refer figure 4.19). Figure 4.33 displays the temperature profile of the amp after 450 hours of operation.

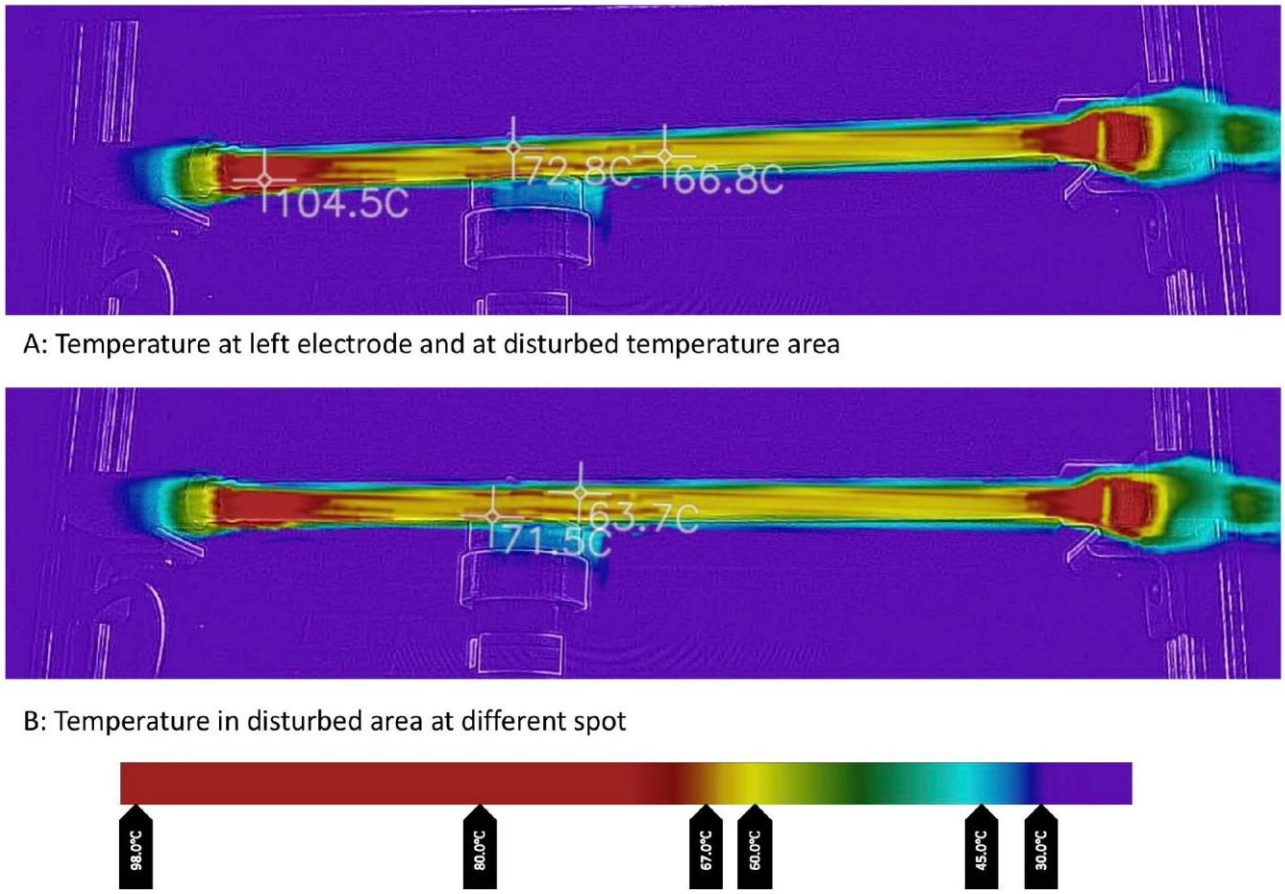

Figure 4. 33 Temperature profile of the lamp after 450 operating hours between 8 to 14 cm

The image clicked by the thermal camera confirms that, as the lamp was aged, the temperature at electrode was increasing, while the temperature at partial half part of the LP lamp remained unaffected and had uniform temperature profile as can be seen in the figure 4.34.

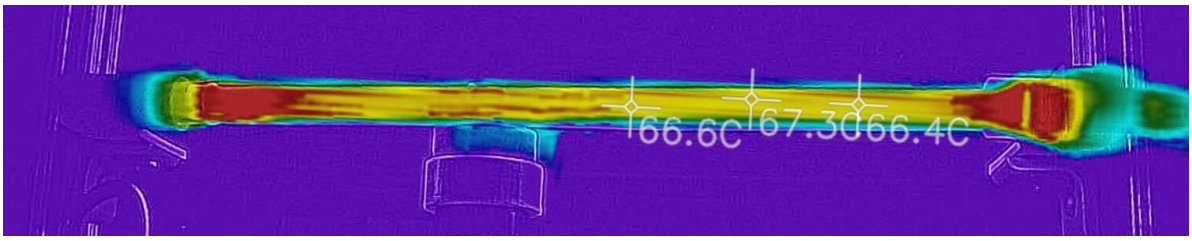

Figure 4. 34 Temperature profile of the lamp after 450 operating hours between 18 to 32 cm

Moreover, analysis verified visual ageing sign of the lamp, i.e. darkening of the quartz sleeve near electrode than the central part of the quartz sleeve , the changes detected in the UV output through the direct measurement set-up, and an imbalanced temperature profile observed by thermal camera and image analysis confirmed the lamp's non-uniform ageing profile, which predominates the area near lamp electrode than the central part of the lamp (refer figure 4.30). Furthermore, decreased UV output at the lamp electrode was a result of the darken quartz sleeve, which was obstructing the UV transmittance form the quartz. LP lamp has shown premature ageing signs at the electrode (i.e. darkening) and at certain areas across the quartz sleeve (i.e. fouling and scaling), which has disturbed the UV transmittance at a darken and fouled area at the lamp sleeve. Ultimately, it has reduced UV output detected by the UV sensor as a result of obstruction to UV transmittances at affected areas along the length of the lamp.

4.6 References

Awwa Research Foundation (Awwa RF), & New York State Energy Research and Development Authority (NYSERDA). (2007). Optimization of UV Disinfection (NYSERDA Report Number 07-07 1P-4C-91184-11/07-NH). Retrieved from https://www.nyserda.ny.gov/About/...and.../Optimization-of-UV-Disinfection

E Calculator Soup. (2011, February 18). Percentage Change Calculator. Retrieved June 11, 2019, from https://www.calculatorsoup.com/calculators/algebra/percent-change-calculator.php

FLIR ONE Pro. (2019). Retrieved May 14, 2019, from https://www.flir.ca/products/flir-one-pro/

Franke, S., Lange, H., Schoepp, H., & Witzke, H. (2006). Temperature dependence of VUV transmission of synthetic fused silica. Journal of Physics D: Applied Physics, 39(14), 3042-3046. doi:10.1088/0022-3727/39/14/025

Hypercable. (n.d.). Conversion chart. Retrieved June 10, 2019, from https://www.hypercable.fr/images/stories/Conversion_Chart_dbm_v_m.pdf

National Instruments. (2006, September 6). Improving Accuracy through Averaging. Retrieved May 30, 2019, from http://www.ni.com/product-documentation/3488/en/

Schmalwieser, A. W., Wright, H., Cabaj, A., Heath, M., Mackay, E., & Schauberger, G. (2014). Aging of low-pressure amalgam lamps and UV dose delivery. Journal of Environmental Engineering and Science, 9(2), 113-124. doi:10.1680/jees.13.00009.

Schöpp, H., & Steffen, F. (2016). Mercury Vapour Lamps. In R. Karlicek, C. Sun, G. Zissis, & R. Ma (Eds.), Handbook of Advanced Lighting Technology (pp. 1080-1093). doi:10.1007/978-3-319-00176-0

NOTES

CHAPTER 5

CONCLUSIONS AND RECOMMENDATION

This chapter concludes the research findings based on the experimental analysis, performed during 45 lamp operating cycles on the LP UV lamp throughout the preliminary ~5% life span. Additionally, this section provides a brief description of the possible modification to the setup.

5.1 Conclusion

This study demonstrated the direct measurement technique to analyze the UV output of the LP lamp along the axial length of the lamp in one radial direction. Furthermore, this study enhanced the experimental analysis by utilizing the thermal imaging camera to perceive temperature profile along the length of the lamp. In previously reported studies by other researchers, the non-uniform output pattern of the UV lamp was considered as a result of the imbalanced temperature gradient across the quartz sleeve; however, none of the referred studies actually performed thermal analysis by implementing the thermal camera This research was principally focused on the experimental findings of the lamp output, and changes occurred in the UV lamp output during 450 hours of lamp operation for a single lamp. The results were generated firmly based on the 450 hours of operation, which helped to notify and compare output changes occurred in the lamp's UV intensity as a function of time for 0 hours to 450 hours of lamp operation.

5.1.1 Conclusion related to lamp ageing and UV output

Aforementioned direct measurement technique (refer chapter 3), allowed to study the lamp ageing phenomenon as a function of time. The research outcomes of the experimental analysis performed on LP lamp confirmed, that the lamp's UV output was not homogeneous. The study observed non-uniform UV output profile along the length of the lamp with the persistent rise and drop at certain areas across the quartz sleeve. The lamp used for this experimental analysis was new, however as it has undergone multiple operating cycles, the premature ageing signs were more visible, such as darkening at the electrode, formation of the scaling spots and fouling of the lamp sleeve during lamp's initial 5% life span. Among visual ageing signs, the prominent ageing sign

was the darkening of the lamp electrode, which has affected UVT of the quartz sleeve. The study was able to provide firm justification about the darkening of the lamp electrode as a result of the overheated quartz sleeve area at the electrode with the help of the thermal imaging camera. Also, the study was able to spot the non-uniform temperature profile, which had affected UV output along the length of the lamp.

5.1.2 Conclusions related to the experimental setup

This research had a goal to provide, completely established and optimized experimental setup to Thunder Bay WPCP, which will enable them to test and evaluate the UV lamp performance, the relation between the lamp performance and operating hours, and accurate expectancy of the lamp life based on the operational conditions, to verify lamp characteristics with lamp statistics provided by the corresponding lamp manufacturer. Also, this setup will enable them to monitor the random lamps if they wish to evaluate the lamp performance of currently installed lamp at the disinfection unit. This research was able to devolve such experimental setup with automated control thought Arduino-LabVIEW interfaced program, which provides experimental observation in a textual file which can be segregated and graphically arranged as needed. Furthermore, this research has implemented a thermal imaging camera to enhance the direct measurement technique, which allows the evaluation of the temperature profile of the lamp. The research has fulfilled all of the objectives planned to complete this thesis as well as the research has accomplished the final goal of the thesis (refer section 1.4).

5.2 Recommendation for future work

This research has demonstrated a practical, optimized experimental setup which can be used to evaluate UV lamp performance along the length of the lamp or at a single measurement point. The direct measurement approach applied for the experimental analysis can be modified and enhanced further.

5.2.1 Recommendation for future experimental analysis

The experimental analysis was performed to study UV output of the lamp during preliminary 5% life span of the LP lamp, basically to perform in-house testing of the setup operation to ensure setup components are working properly prior to giving the experimental setup to the Thunder Bay WPCP. The experimental setup was operated properly with seamless collaboration among the mechanical and electric components of the setup. The setup idea can be used to evaluate the UV output of a lamp during lamp's expected lifespan ~10000 hours.

5.2.2 Recommendation for setup modification

The setup that was developed to performed direct measurement of the UV lamp output along the length of a lamp was designed to conduct measurement in one radial direction. The experiment could have been conducted in four radial directions, as shown in figure 5.1.

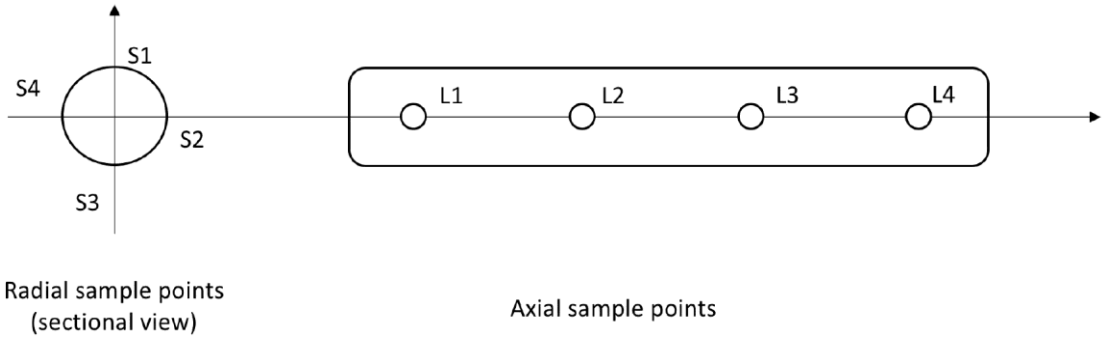

Figure 5. 1 Radial and axial sample points

However, to do so the UV lamp needs to be turned on and off after each measurement run and has to be rotated by 90° until the lamp has been scanned along its length in each radial direction. Moreover, if the lamp has been tested for each radial direction, the lamp has to be turned off before it could be removed, then rotated by 90° and then it should be turned on for the corresponding measurement run. This procedure allows to study lamp behaviour in four radial directions of the lamp; however, to do so the lamp has to be undergone for four operating cycles just for one experimental run. Due to consistent disturbance to the lamp, it disturbs mercury and inert gas mixture, which can affect the photochemical reaction and eventually the UV output. Hence, the experimental analysis performed during this research, comprising of only one operating cycle and lamp was undisturbed during the entire experimental phase.

If the lamp has to be tested for four radial directions, it could be done by improving the setup design. Instead of removing and rotating the lamp at 90° after each experimental run, the sensor can be rotated by 90° along the circumference of the lamp. However, it will need a modified and complex structure of the adapter housing, on which sensor has been mounted, which could be rotated to 90° through a computer command by adjusting the computer program code.

NOTES